

AD-A043 382

SPECTROLAB INC SYLMAR CALIF
HIGH EFFICIENCY SOLAR PANEL (HESP). (U)

F/G 10/2

JUL 77 J SCOTT-MONCK, C GAY, P STELLA, F UNO

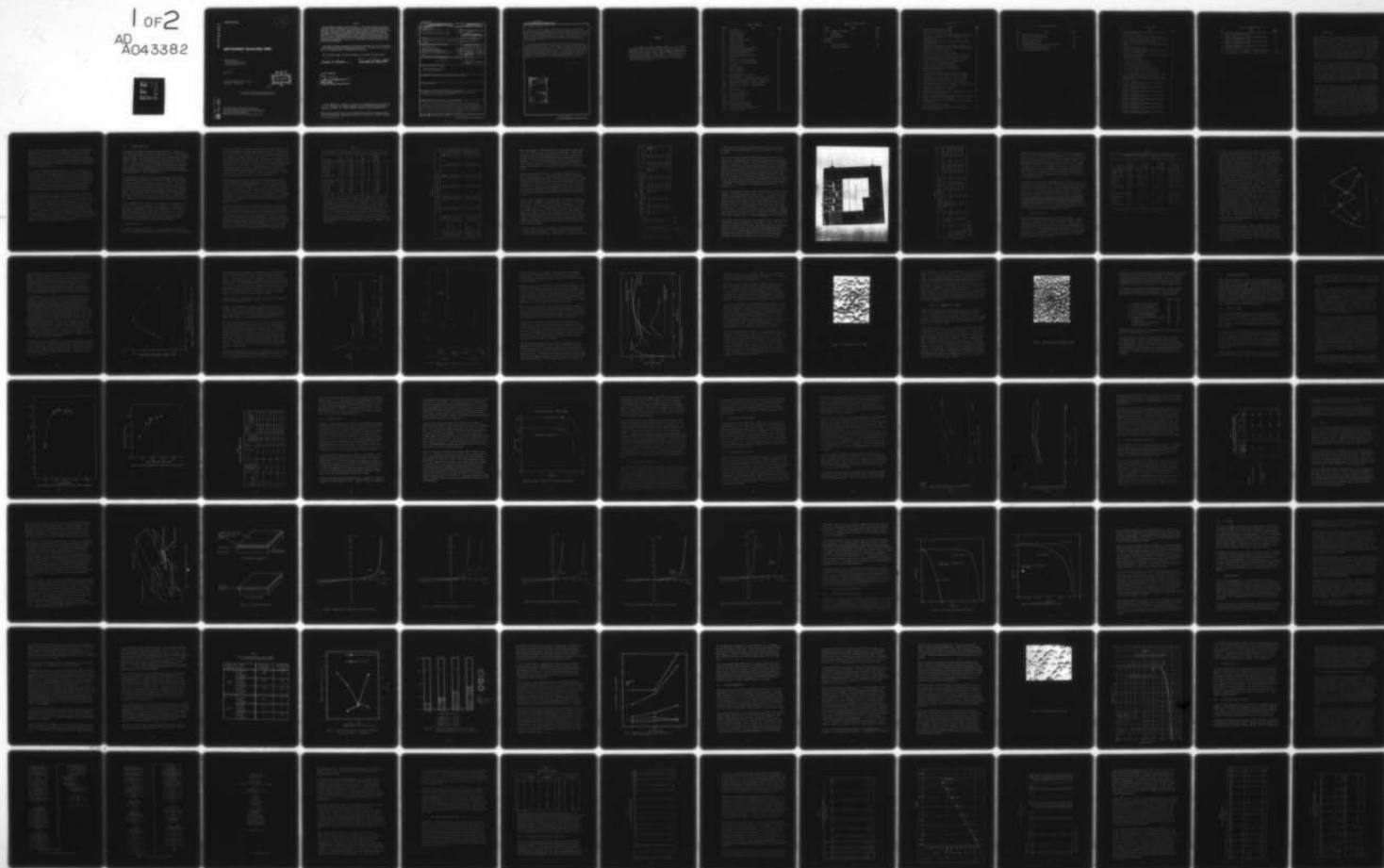
F33615-75-C-2028

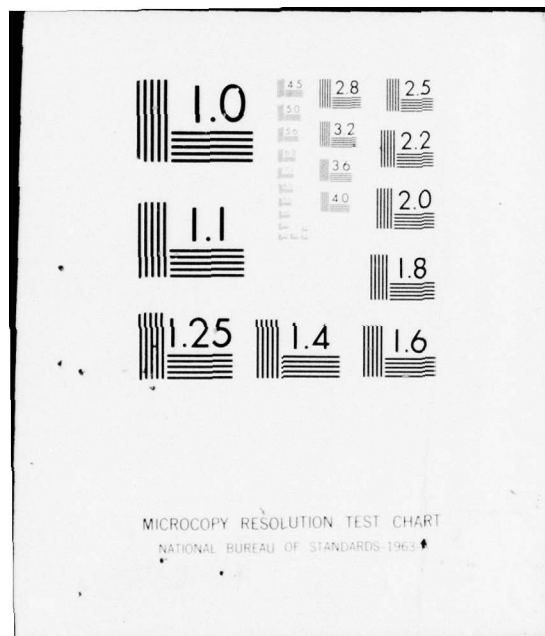
UNCLASSIFIED

AFAPL-TR-77-36

NL

1 of 2
AD
A043382





AD A 043382

AFAPL-TR-77-36

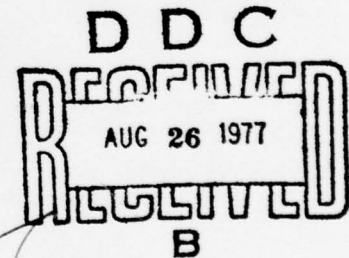
12

HIGH EFFICIENCY SOLAR PANEL (HESP)

*SPECTROLAB, INC.
12500 GLADSTONE AVENUE
SYLMAR, CALIFORNIA 91342*

JULY 1977

TECHNICAL REPORT AFAPL-TR-77-36
1 June 1975 - 15 June 1977



Approved for public release; distribution unlimited.

DDC FILE COPY

AIR FORCE AERO PROPULSION LABORATORY
AIR FORCE WRIGHT AERONAUTICAL LABORATORIES
AIR FORCE SYSTEMS COMMAND
WRIGHT-PATTERSON AIR FORCE BASE, OHIO 45433

NOTICE

When Government drawings, specifications, or other data are used for any purpose other than in connection with a definitely related Government procurement operation, the United States Government thereby incurs no responsibility nor any obligation whatsoever; and the fact that the government may have formulated, furnished, or in any way supplied the said drawings, specifications, or other data, is not to be regarded by implication or otherwise as in any manner licensing the holder or any other person or corporation, or conveying any rights or permission to manufacture, use, or sell any patented invention that may in any way be related thereto.

This report has been reviewed by the Information Office (OI) and is releasable to the National Technical Information Service (NTIS). At NTIS, it will be available to the general public, including foreign nations.

This technical report has been reviewed and is approved for publication.

Lowell D. Massie

Donald P. Martell

FOR THE COMMANDER


JAMES D. REAMS
Actg Chief, Aerospace Power Division

"If your address has changed, if you wish to be removed from our mailing list, or if the addressee is no longer employed by your organization please notify POE-2, W-PAFB, OH 45433 to help us maintain a current mailing list".

Copies of this report should not be returned unless return is required by security considerations, contractual obligations, or notice on a specific document.

UNCLASSIFIED

SECURITY CLASSIFICATION OF THIS PAGE (When Data Entered)

REPORT DOCUMENTATION PAGE		READ INSTRUCTIONS BEFORE COMPLETING FORM
1. REPORT NUMBER AFAPL-TR-77-36	2. GOVT ACCESSION NO.	3. RECIPIENT'S CATALOG NUMBER
4. TITLE (and Subtitle) HIGH EFFICIENCY SOLAR PANEL (HESP)	5. TYPE OF REPORT & PERIOD COVERED Final Report, June 1975 - June 1977	6. PERFORMING ORG. REPORT NUMBER
7. AUTHOR(s) John/Scott-Monck, Charles/Gay, Paul/Stella and Frank/Uno	8. CONTRACT OR GRANT NUMBER(s) F33615-75-C-2028	
9. PERFORMING ORGANIZATION NAME AND ADDRESS Spectrolab, Inc. 12500 Gladstone Avenue Sylmar, California 91342	10. PROGRAM ELEMENT PROJECT TASK AREA & WORK UNIT NUMBERS P.E. 63401F, Project 682J Task 682J04, Work Unit 682J0401	
11. CONTROLLING OFFICE NAME AND ADDRESS Air Force Aero Propulsion Laboratory POE-2 Wright Patterson AFB, Ohio 45433	12. REPORT DATE 1 July 1977	13. NUMBER OF PAGES 146
14. MONITORING AGENCY NAME & ADDRESS (if different from Controlling Office)	15. SECURITY CLASS. (of this report) Unclassified	15a. DECLASSIFICATION DOWNGRADING SCHEDULE
16. DISTRIBUTION STATEMENT (of this Report) APPROVED FOR PUBLIC RELEASE; DISTRIBUTION UNLIMITED		
17. DISTRIBUTION STATEMENT (of the abstract entered in Block 20, if different from Report)		
18. SUPPLEMENTARY NOTES		
19. KEY WORDS (Continue on reverse side if necessary and identify by block number) Advanced Silicon Solar Cells, Solar Energy Conversion, Space Power, Radiation Effects, Temperature Coefficient		
20. ABSTRACT (Continue on reverse side if necessary and identify by block number) A family of high efficiency, weldable silicon solar cells, incorporating every feature of advanced technology developed in the past four years, was produced and subjected to space qualification testing. This matrix contained both field and non-field cells ranging in thickness from 0.10 mm (0.04) to 0.30 mm (0.12), and in base resistivity from nominal two to one hundred ohm-cm. Initial power outputs as high as 20 mW/cm ² (14.8% AMO efficiency) were produced by certain cell types within this group. → 59 cm.		

DD FORM 1 JAN 73 1473

EDITION OF 1 NOV 65 IS OBSOLETE

UNCLASSIFIED

SECURITY CLASSIFICATION OF THIS PAGE (When Data Entered)

330 250

LB

UNCLASSIFIED

SECURITY CLASSIFICATION OF THIS PAGE(When Data Entered)

Continuation of Block No. 20

All these cells had certain common features; a selectively etched front surface which reduced reflection losses, tantalum-palladium-silver front contacts, chromium-palladium-silver back contacts, junction depths of $\sim 0.10 \mu\text{m}$, and a tantalum pentoxide antireflection coating. For the field cells, acceptor doping was accomplished using a screen printed aluminum paste source. The baseline cell, which was 0.23 mm thick, nominal two ohm-cm, non-field type was produced in three sizes, 2 x 2 cm, 2 x 4 cm and 2 x 6 cm, the others in 2 x 2 cm form.

The 2 x 2 cm baseline cell underwent a complete space qualification test cycle including all the typical environmental requirements such as temperature-humidity and thermal cycling. The baseline cell and eleven other types were tested to electron fluence levels of 1×10^{16} equivalent 1 MeV electrons/cm², fission spectrum neutron fluence levels of 1×10^{13} equivalent 1 MeV neutrons/cm², and were characterized with respect to their radiometric properties. In addition, thermal coefficients of current, voltage and power were obtained for all twelve cell types over the temperature range from -20°C to +100°C as a function of electron fluence to 1×10^{16} equivalent 1 MeV electrons.

ACCESSION for	
NTIS	Write Section <input checked="" type="checkbox"/>
DDC	B. fi Section <input type="checkbox"/>
UNANNOUNCED	<input type="checkbox"/>
JUS	
DISSEMINATION/AVAILABILITY CODES	
or SPECIAL	
A	

UNCLASSIFIED

SECURITY CLASSIFICATION OF THIS PAGE(When Data Entered)

2

FOREWORD

This final report was submitted by Spectrolab, Inc. under F33615-75-C-2028. The effort was sponsored by the Air Force Aero Propulsion Laboratory, Air Force Systems Command, Wright-Patterson AFB, Ohio under Project No. 682J, Task No. 682J04 and Work Unit No. 682J0401 with Lowell D. Massie (POE-2) as Project Engineer In Charge. John Scott-Monck of Spectrolab, Inc. was technically responsible for the work. The work covered the time period of June 1975 through June 1977.

TABLE OF CONTENTS

<u>Section</u>	<u>Title</u>	<u>Page</u>
1.0	Introduction	1
2.0	Technical Discussion	3
2.1	Silicon Evaluation	3
2.2	Selective Etching	12
2.3	Shallow Junction Studies	28
2.3.1	Diffusion Studies	28
2.3.2	Oxidation Studies	33
2.3.3	Textured Surface Junction Studies	36
2.4	Back Surface Field Development	37
2.4.1	Evaporated Aluminum Source	37
2.4.2	Nonvacuum Aluminum Field Source	41
2.5	Contacts	43
2.6	Antireflection Coating and Filter	52
2.6.1	Antireflection Coating Evaluation	52
2.6.2	Coverglass	56
2.7	Welding Evaluation	56
2.8	Process Integration	65
2.9	Pilot Production	70
2.9.1	Manufacturing Control Document	70
2.9.2	HESP Assembly Fabrication Process-Baseline Cells	71
2.9.3	HESP Assembly Fabrication Process - Hybrid Cells	76
2.9.4	Production Test Results - Baseline HESP Cells	77
2.9.5	Production Test Results - Hybrid HESP Cells	87
2.9.6	Filtering	89
2.9.7	Module Fabrication	90
2.10	Qualification Testing	92
2.10.1	Temperature-Humidity Test	92
2.10.2	Temperature Cycling	94
2.10.3	Radiation Testing	96
2.10.3.1	Electron Radiation Testing	96
2.10.3.2	Neutron Radiation Testing	97
2.10.4	Temperature Coefficient Measurements	100
2.10.4.1	Analysis of Results	102

TABLE OF CONTENTS (CONT'D)

<u>Section</u>	<u>Title</u>	<u>Page</u>
2.10.5	Radiometric Properties	119
3.0	Conclusions	124
3.0	Recommendations	126
References		128
APPENDICES		
A	Cell Specifications	129
B	System Safety Analysis	137

LIST OF FIGURES

<u>No.</u>	<u>Title</u>	<u>Page</u>
1	Photon Redegradation Testing Setup	10
2	VMJ Aspect of Etched Surface Cell	15
3	Etch Rate as a Function of Sodium Hydroxide Concentration	17
4	Etch Rate of Saw-Cut and Chemically Polished 2 ohm-cm Silicon Wafers	19
5	Etching Ratio of Solutions of Different Concentrations and Temperatures	20
6	Short Circuit Current vs. Etching Time for Different Concentrations and Temperatures of NaOH Etching Solution	22
7	Typical Etched Surface, 2000X	24
8	Improved Surface Texturization, 2000X	26
9	Short Circuit Current as a Function of Sheet Resistance	30
10	Spectral Response as a Function of Sheet Resistance	31
11	Effect of Thick Oxide on Cell I-V Characteristic	35
12	2-Step P+ Diffusion Then Alloy Method	39
13	2-Step P+ Alloy Then Diffusion Method	40
14	Heater Assembly Enclosed in Vacuum Chamber	45
15	Test Sample Preparation	46
16	Tantalum-Silver Contacts Heated to 600°C in Vacuum	47
17	Vanadium-Silver Contacts Heated to 600°C in Vacuum	48
18	Zirconium-Silver Contacts Heated to 600°C in Vacuum	49
19	Niobium-Silver Contacts Heated to 600°C in Vacuum	50
20	Tantalum-Palladium-Silver Contacts Heated to 600°C in Vacuum	51
21	Vacuum Baked Titanium-Silver Contacts	53
22	Vacuum Baked Tantalum-Silver Contacts	54
23	Trade-Off of Strength vs. Electrical Degradation for Cells Welded with 10 μ Plated Tabs	61
24	Effect of Decreasing Welding Voltage on Weld Strength and Failure Rate Using 10 μ Plated Tabs	62
25	Degradation of Cells with Various Diffusion Depths Using 15 μ Plated Tabs	64
26	Gridline Metallization Fringes	68
27	Short Circuit Output Difference Between Weld Pad and Ohmic Bar Configuration	69

LIST OF FIGURES (CONT'D)

<u>No.</u>	<u>Title</u>	<u>Page</u>
28	Crystal/Mechanical Processing	72
29	Diffusion and Final Processing	73 & 74
30	Yield vs. Average Power	81
31	Assembled Sample Modules	91
32	Temperature-Humidity Qualification Flow Chart	93
33	Cell Temperature Testing Chamber	103
34	Complete Temperature Testing Setup	104

LIST OF TABLES

<u>No.</u>	<u>Title</u>	<u>Page</u>
1	Pre-Irradiation Electrical Characteristics of First Screening Test Cells	5
2	Initial Post Irradiation Electrical Test Data	6
3	Photon Redegradation of Irradiated Silicon Solar Cells	8
4	Post Irradiation Illumination Test Data	11
5	Room Temperature Annealing of Irradiated Silicon Solar Cells	13
6	Polished Cell Characteristics	32
7	Effect of Thickness of Deposited Aluminum on Electrical Character of 2 ohm P+ Cells	42
8	Effect of Tab Metallization on Weld Strength and Failure Rate for Two Cell Groups	60
9	HESP Hybrid Cell Matrix	77
10	2 x 2 HESP Pilot Production Data	78
11	2 x 2 HESP Electrical Distribution	80
12	Contact Integrity Test Results (2 x 2 cm)	82
13	2 x 4 and 2 x 6 HESP Pilot Production Data	84
14	2 x 4 and 2 x 6 HESP Electrical Distribution	85
15	Contact Integrity Test Results (2 x 4 and 2 x 6 cm)	86
16	2 x 2 Hybrid HESP Electrical Syntheses (Unfiltered)	88
17	Maximum Power as a Function of 1 MeV Fission Spectrum Neutron Fluence	99
18	Electrical Properties vs. Temperature and Electron Fluence - Baseline HESP Cell	105
19	Electrical Properties vs. Temperature and Electron Fluence - HESP Hybrid Type 1	106
20	Electrical Properties vs. Temperature and Electron Fluence - HESP Hybrid Type 2	107
21	Electrical Properties vs. Temperature and Electron Fluence - HESP Hybrid Type 3	108
22	Electrical Properties vs. Temperature and Electron Fluence - HESP Hybrid Type 4	109
23	Electrical Properties vs. Temperature and Electron Fluence - HESP Hybrid Type 5	110
24	Electrical Properties vs. Temperature and Electron Fluence - HESP Hybrid Type 6	111
25	Electrical Properties vs. Temperature and Electron Fluence - HESP Hybrid Type 7	112

LIST OF TABLES (CONT'D)

<u>No.</u>	<u>Title</u>	<u>Page</u>
26	Electrical Properties vs. Temperature and Electron Fluence - HESP Hybrid Type 8	113
27	Electrical Properties vs. Temperature and Electron Fluence - HESP Hybrid Type 9	114
28	Electrical Properties vs. Temperature and Electron Fluence - HESP Hybrid Type 10	115
29	Electrical Properties vs. Temperature and Electron Fluence - HESP Hybrid Type 11	116
30	Solar Absorptance and Emittance of HESP Assemblies	121
31	Solar Absorptance and Emittance of HESP Hybrid Assys	122 & 123

1.0 INTRODUCTION

Since 1972 there have been a number of significant developments in the field of silicon solar cells which have shown that high efficiency (14.5 percent AMO) radiation resistant (15 mW/cm^2 at 1×10^{15} equivalent 1 MeV electrons/ cm^2) devices can be achieved. These facts coupled with future Air Force requirements acted as a stimulus for the High Efficiency Solar Panel (HESP) program. The purpose of this effort was to develop the new laboratory derived technology to the point that a hardened, space qualified, silicon solar cell which possessed very high initial efficiency and superior performance in both natural and threat induced radiation environments, was production ready.

During the life of this program the emphasis on developing a single cell that would meet all the contract goals was reduced. The initial phase did concentrate on applying the new technology to a baseline or "standard" HESP cell, but as more information was obtained from screening tests it became apparent that the single cell concept had to be expanded in order to achieve all the program objectives. Inclusion of the HESP "hybrid" cells provided the additional technology that enabled the initial power goal of 14.5 percent air mass zero (AMO) efficiency to be achieved.

This work can be divided into three distinct phases. The first concentrated on developing, testing and evaluating those various technical advancements such as shallow junction work, new contact materials and selective etch technology which would be included in the finalized version of the HESP solar cell. The second phase was involved with integrating those portions of technology into a process scheme that was suitable for high volume production, and implementing this process by means of formal documentation and control. The final phase demonstrated that the prior work was valid. In this portion of the contract, pilot line production of both the baseline and "hybrid" HESP solar cells was demonstrated. Not only were significant numbers of cells produced in a manufacturing environment, but these parts were required to pass those tests mandated for space qualified cells.

In the final, or qualification phase a wealth of technical information was made available. To the best of our knowledge this is the most systematic attempt to collect the basic solar cell information required by panel designers for their activity. Not only does this report present pilot line manufacturing data, but it also includes such vital information as electrical performance as a function of temperature and various radiation environments as well as radiometric data.

The success of this program can be measured in two ways, what has been achieved and of even more importance, what new directions have been pointed out for future work. At the conclusion of this contract there existed six cell types that were capable of meeting the initial power performance goals. Of these there were at least three types which came within a few percent of meeting the radiation performance goals. The basic technology employed to produce the HESP cell family was fully demonstrated under typical space flight manufacturing conditions using standard production equipment.

The original HESP cell was to have been 0.20mm (.008") thick, but this was revised to 0.30mm due to configuration restraints (2 x 6 cm cells). As a result of our work on HESP "hybrids," prototype cells 0.10mm (.004") thick with AMO efficiencies exceeding 14 percent were produced. These cells have the best electrical performance under natural and "artificial" radiation environments of any cell type evaluated. Based on the knowledge derived from this program it is possible to project a sixteen percent HESP silicon solar cell that will be thin (less than 0.20mm thick), hardened and capable of producing in excess of 15 mW/cm^2 after 1×10^{15} equivalent 1 MeV electrons/cm². This cell will merely build on the technology now reduced to manufacturing practice and thus will be suitable for mass production.

2.0 TECHNICAL DISCUSSION

As mentioned previously, this program was divided into three phases with the initial phase concentrating on technology application. It was originally planned to combine shallow junctions, a more efficient grid collector pattern, selective etching, and a high index antireflection coating with float zone silicon in order to achieve the beginning of life power goals of this contract. At this time back surface field (BSF) technology was not considered since preliminary evidence indicated that until the cell was made thinner than 0.20mm there was no improvement in electrical performance after moderate radiation fluences (1×10^{14} electrons/cm²).

The program began by isolating the various advancements being considered and optimizing each independently of the others. Therefore selective etch work was done separately from shallow junction activities. In the case of the shallow junction it was necessary to combine this with efforts aimed at producing a more efficient contact collector pattern since the increased series resistance from a shallow junction demanded the optimized collector pattern. The evaluation of float zone silicon was done in conjunction with the shallow junction studies because the standard float zone material did not possess the correct crystal orientation for our selective etch technology.

As the development effort matured and it became apparent that no single cell type would satisfy all the HESP goals it was decided to investigate the possibility of employing back surface field technology. This work will be described in this discussion of the initial contract phase. It should be noted that the baseline HESP cell was developed without any consideration being given to the application of the BSF effect. However many of the "hybrid" HESP types employed back surface field technology.

2.1 Silicon Evaluation

Achievement of high initial efficiency in conjunction with superior radiation resistance was predicated in part on the belief that float zone silicon possessed

better initial minority carrier lifetime and also was less sensitive to the effects of penetrating radiation than crucible grown silicon. According to the literature, solar cells made from float zone silicon have higher initial power outputs as compared to crucible grown silicon⁽¹⁾ which is used for all cells manufactured for space flight use in this country. In addition it had been predicted that two ohm-cm float zone silicon cells would degrade by only fifteen percent in power after $\sim 3 \times 10^{14}$ equivalent 1 MeV electrons/cm²⁽²⁾ as compared to twenty percent for crucible grown silicon solar cells.⁽³⁾ Experimental evidence showed that in the case of high efficiency cells, the float zone silicon devices delivered \sim five percent more power at 3×10^{14} e/cm² than similar cells made from crucible grown material.⁽⁴⁾

However the observation that two ohm-cm float zone silicon solar cells exhibited significant additional degradation in output power when exposed to photons after electron radiation⁽⁵⁾ was a cause for concern. Since all European cell material has a common source, it was possible that the problem was due to a processing variable in that particular silicon growth method rather than intrinsic to float zone silicon. Accordingly float zone silicon was purchased from a United States source (Texas Instruments). This material was nominal two ohm-cm with (111) orientation which did not allow us to selectively etch it.

A matrix was formed consisting of 0.20mm thick cells made from both float zone and crucible grown silicon. Crucible grown silicon was used to fabricate traditional deep junction as well as shallow junction evaluation cells. In addition selectively etched (textured) front surface and back surface field cells were included in the evaluation matrix. Shallow junction and back surface field cells were produced from float zone silicon for comparison. Table 1 is a summary of the electrical performance for each cell group included in this test measured at 25°C under AMO intensity. These samples were then subjected to 1 MeV electrons using the JPL Dynamitron facility.

TABLE 1

Pre-Irradiation Electrical Characteristics of First Screening Test Cells				
Cell Type	I_{sc} (mA)	V_{oc} (mV)	P_{max} (mW)	Planned Fluence (e/cm^2)
Conventional (CG)	130.1	586.4	58.2	3×10^{14}
Shallow (CG)	142.2	583.8	64.4	3×10^{14}
Shallow (FZ)	143.5	590.5	66.9	3×10^{14}
BSF (CG)	149.2	598.0	67.4	3×10^{14}
BSF (FZ)	147.6	603.8	68.2	3×10^{14}
Textured (CG)	157.6	591.8	71.8	3×10^{14}
Conventional (CG)	126.3	588.0	56.4	1×10^{15}
Shallow (CG)	140.3	580.0	64.2	1×10^{15}
Shallow (FZ)	144.3	592.0	65.7	1×10^{15}
BSF (CG)	148.5	601.0	67.7	1×10^{15}
BSF (FZ)	146.3	602.5	67.9	1×10^{15}
Textured (CG)	156.2	590.3	70.9	1×10^{15}

These cells were mounted onto an aluminum plate using Apiezon grease and the plate in turn was mounted to a water cooled block. The cell plate was covered with a thin aluminum foil to attenuate the electron beam. The radiation was performed under vacuum using a fluence rate of 1×10^{11} 1 MeV electrons/ cm^2 /sec with the cells held at a temperature of between 25 and 30°C. In all, three cell plates were tested, two to 3×10^{14} e/cm^2 and the third to 1×10^{15} e/cm^2 . After the irradiations the cells were taken to Spectrolab and initial post irradiation electrical measurements were obtained within six hours after the electron screening. Table 2 is a summary of this initial data.

TABLE 2

Cell Type	I_{sc} (mA)	$\frac{I}{I_o}$	V_{oc} (mV)	$\frac{V}{V_o}$	P_{max} (mW)	$\frac{P}{P_o}$	$\frac{\phi}{e/cm^2}$
Conventional (CG)	114.8	.88	552.8	.94	48.6	.835	3×10^{14}
Shallow (CG)	126.0	.885	555.0	.95	53.2	.825	3×10^{14}
Shallow (FZ)	129.8	.905	564.0	.955	57.2	.855	3×10^{14}
BSF (CG)	126.0	.845	551.3	.92	53.3	.79	3×10^{14}
BSF (FZ)	127.2	.86	559.8	.925	54.7	.80	3×10^{14}
Textured (CG)	140.9	.895	556.8	.94	60.4	.84	3×10^{14}
Conventional (CG)	99.4	.785	534.0	.91	40.5	.72	1×10^{15}
Shallow (CG)	115.0	.82	537.0	.925	47.8	.745	1×10^{15}
Shallow (FZ)	118.0	.82	542.7	.915	49.0	.745	1×10^{15}
BSF (CG)	113.1	.76	534.0	.89	46.5	.685	1×10^{15}
BSF (FZ)	116.4	.795	541.5	.90	48.3	.71	1×10^{15}
Textured (CG)	127.6	.815	537.0	.91	52.4	.74	1×10^{15}

There are a number of observations that can be made from the initial data. At $3 \times 10^{14} \text{ e/cm}^2$ the float zone silicon does appear to be less sensitive to radiation than the crucible grown silicon solar cells. However, the textured CG silicon solar cells delivered the most power which was to be expected. At $1 \times 10^{15} \text{ e/cm}^2$ the difference was not as apparent between the two types of silicon, but the textured cells continued to display a significant superiority in output power when compared to any other cell type tested.

After the initial electrical tests, a four cell test matrix was placed under a xenon simulator set to AMO (135.3 mW/cm^2) in order to investigate photon induced degradation effects. The four cells consisted of a CG shallow diffused cell irradiated to $1 \times 10^{15} \text{ e/cm}^2$, two FZ shallow diffused cells irradiated to $1 \times 10^{15} \text{ e/cm}^2$ and one FZ shallow diffused cell irradiated to $3 \times 10^{14} \text{ e/cm}^2$. One of the heavily irradiated FZ cells was placed under a load voltage corresponding to its maximum power voltage point. The cells were mounted on a water cooled block held at 25°C along with a monitoring sensor.

The four cells were measured at various times for evidence of photon degradation. Table 3 summarizes the test data for the four cells. Four trends were obvious: (1) the CG cell showed no sign of degradation; (2) the FZ cell irradiated to 1×10^{15} showed a major decrease in output power; (3) the FZ cell irradiated to 3×10^{14} showed a less, but still significant reduction in output; (4) the FZ cell irradiated to 1×10^{15} and loaded, showed some slight degradation but has stabilized after 24 hours. Spectral response measurements of these cells taken after 60 hours exposure showed significant reduction in long wavelength response indicating a bulk rather than a surface phenomenon.

In view of these results, a second electron screening test was performed to further examine the influence of light on irradiated float zone and crucible grown silicon solar cells. The samples tested consisted of eighteen

TABLE 3

Time (hrs)	Photon Redegradation of Irradiated Silicon Solar Cells											
	CG (1×10^{15})			FZ (3×10^{14})			FZ (1×10^{15})			FZ* (1×10^{15})		
	I_{sc} (mA)	V_{oc} (mV)	P_{max} (mW)	I_{sc} (mA)	V_{oc} (mV)	P_{max} (mW)	I_{sc} (mA)	V_{oc} (mV)	P_{max} (mW)	I_{sc} (mA)	V_{oc} (mV)	P_{max} (mW)
0	114.5	538	47.7	128.8	565	56.6	119.1	544	48.6	117.0	543	48.8
24	114.5	538	47.7	122.0	552	52.5	111.5	530	44.9	116.0	540	47.3
90	115.3	538	-	121.5	552	-	109.4	528	-	116.5	541	-
90	114.8	538	-	121.1	551	-	108.6	527	-	116.5	541	-
160	114.2	538	-	120.2	551	-	107.5	527	-	116.0	542	-
250	-	-	-	-	-	-	108.0*	527*	-	116.5 [†]	541 [†]	-

* Held under load at 450 mV

[†] Not loaded

2 ohm-cm cells, three CG and fifteen made from FZ silicon. The cells were irradiated at the JPL Dynamitron to 1×10^{15} electrons/cm² using 1 MeV electrons.

The cells were measured under AMO conditions within three hours after irradiation. Following this, the fifteen FZ cells were divided into three groups. Tabs had been attached to ten of the FZ cells prior to irradiation in order to allow them to be loaded or shorted while the post irradiation light test was being performed. One group was tested with no external load, a second group was shorted so that they were in the short circuit current mode, and the third group was loaded with fixed 8 ohm resistors so that they were operating in the vicinity of the maximum power point. The three CG control samples had no external load. The samples were fixed to a water cooled plate using apiezon grease and exposed to tungsten illumination of $\sim 100 \text{ mW/cm}^2$. (See Figure 1.) The block temperature was held at $\sim 27^\circ\text{C}$ during the test.

The cells were periodically removed from the plate and I-V curves were taken. A summary of the data obtained is given in Table 4. In this test FZ cells that were loaded degraded to the same level as the groups that were operated either in the open circuit or short circuit mode. The rate of light induced degradation was different for the groups during the initial time increments, but after a total exposure of ninety hours, there was little difference in their electrical performance. The CG control cells displayed the same behavior as previously reported, namely a slight amount of degradation during the first twenty-four hours, followed by a recovery that brought them to their original outputs as measured immediately after irradiation.

There is one difference between the test conditions, here a tungsten source was employed in order to illuminate a large sample of cells. The first screening test data was obtained under xenon illumination which more closely matches the solar spectrum. However the spectral response measurements indicated that the long wavelength response of the irradiated cells was changed and thus tungsten illumination which has a very strong long wavelength component would probably not be an influential variable.

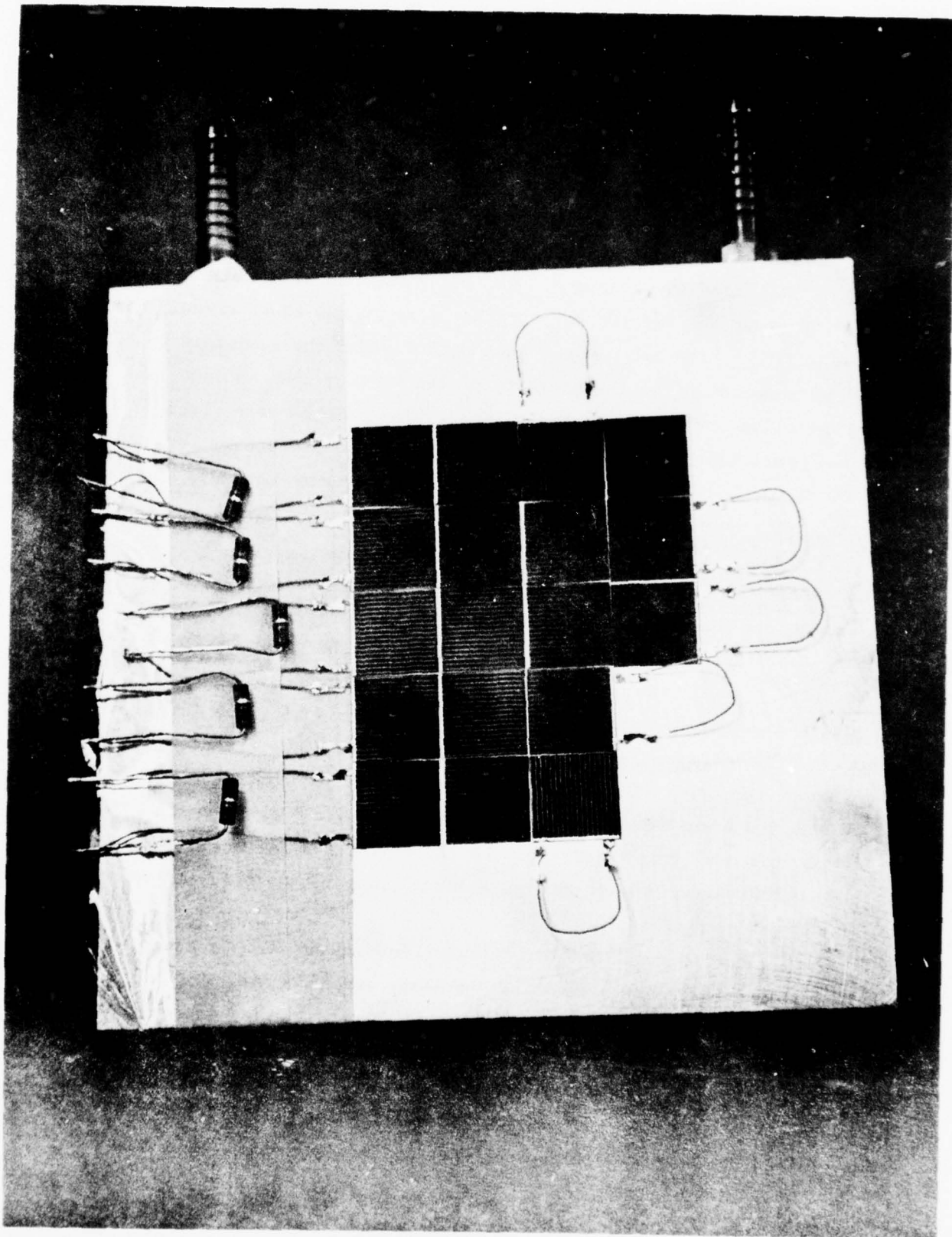


TABLE 4

Post Irradiation Illumination Test Data					
Group	P_{\max} $\phi = 0$	P_{\max}^{15} $\phi = 10^{15}$ $t = 0$	P_{\max} (P/P') $t = 4$ hrs	P_{\max} (P/P') $t = 24$ hrs	P_{\max} (P/P') $t = 90$ hrs
CG (V_{oc})	65.1	47.6	46.8 (.983)	47.8 (1.00)	47.7 (1.00)
FZ (V_{oc})	64.9	49.9	46.8 (.938)	44.9 (.900)	44.2 (.886)
FZ (I_{sc})	65.9	50.1	48.7 (.972)	45.8 (.914)	44.8 (.894)
FZ (P_{\max})	66.3	50.6	49.5 (.978)	46.1 (.911)	44.8 (.885)

$P' \phi = 10^{15}, t = 0$

Another observation that was made from the first electron screening test involved the post irradiation annealing behavior of crucible and float zone silicon solar cells. Those cells that were not examined for photon induced degradation were remeasured after forty days under ambient conditions of temperature and humidity. During this period the cells were not exposed to ambient light. Table 5 is a summary of this data. In all cases the crucible grown silicon cells showed gains of from one to three percent in output power after irradiation, while those cells made from float zone silicon displayed at best no improvement in output power as the result of room temperature annealing.

As a result of the photon induced redegradation effect observed in cells made from float zone silicon it was decided to employ crucible grown silicon for the HESP cell development effort. Even though immediately after radiation testing the float zone cells were superior, subsequent exposure to either xenon or tungsten illumination reduced the output to well below those values obtained from crucible grown silicon cells. The net effect was that cells made from two ohm-cm crucible grown silicon were superior to cells made from float zone silicon if the photon redegradation effect was taken into consideration. Since the use of float zone material was considered one of the key factors in achieving the program goals, the potential for success was considerably reduced at this point.

2.2 Selective Etching

One of the more significant innovations that has been applied to silicon solar cells has been the use of orientation dependent etches to reduce reflection losses from the front surface of the cell. Compounds such as hydrazine catechol, potassium hydroxide and sodium hydroxide exhibit markedly different etch rates along the main crystallographic planes of single crystal silicon. As an example it has been shown that for potassium hydroxide (KOH), the etch rate is at least thirty times greater in the $\langle 100 \rangle$ direction than in the $\langle 111 \rangle$ direction.

TABLE 5

Room Temperature Annealing of Irradiated Silicon Solar Cells							
Cell Type	I_{sc} (mA)	%	V_{oc} (mV)	%	P_{max} (mW)	%	ϕ (e/cm^2)
Conventional (CG)	2.0	1.7	4	0.7	1.3	2.7	3×10^{14}
Shallow (CG)	1.4	1.1	4	0.7	1.4	2.6	3×10^{14}
Shallow (FZ)	(0.4)	(0.3)	0	0	0	0	3×10^{14}
BSF (CG)	1.7	1.3	4	0.7	0.6	1.1	3×10^{14}
BSF (FZ)	(1.0)	(0.8)	0	0	0	0	3×10^{14}
Textured (CG)	1.5	1.1	5	0.9	1.2	2.0	3×10^{14}
Conventional (CG)	2.1	2.1	4	0.7	1.1	2.7	1×10^{15}
Shallow (CG)	0.7	0.6	3	0.6	0.6	1.3	1×10^{15}
BSF (CG)	2.7	2.4	5	0.9	1.5	3.2	1×10^{15}
Textured (CG)	1.9	1.5	5	0.9	1.2	2.3	1×10^{15}

By etching (100) oriented silicon in either KOH or sodium hydroxide (NaOH), the rapid attack of the (100) orientation surface selectively exposes the (111) planes forming tetrahedrons on the surface. These tetrahedrons are formed at an angle of $\sim 55^\circ$ to the normal at the surface. When light impinges on this surface, multiple interactions with the silicon occurs and thus the amount of light reflected is significantly reduced. For example, a bare silicon surface which would normally reflect 35 percent of the impinging radiation will reflect only 12 percent after a second reflection thereby providing a large increase in absorption. Furthermore the reflectance reduction is maintained across the spectrum unlike an AR coating which tends to be more peaked at a particular wavelength. Although in theory an AR coating can be broadened through the use of multiple coatings it is unlikely to equal the "black" surface broad band spectral characteristic. However this is not intended to suggest that AR coatings are not needed on etched surface cells since they do bring about additional reflectance reduction. The possibility of also increasing the device collection efficiency by means of a semi vertical multi junction effect is shown in Figure 2. Here incident radiation is depicted as entering the cell in part at position A and in part at position B. Carriers are generated in accordance with the conventional exponential relationships. As can be seen for carriers generated through absorption at positions "a" and "b", the distance to the junction is considerably less than their absorption lengths A_a , and B_b , respectively. Although not all carriers will be generated so close to a junction it is apparent that carrier generation distances will vary between a value equal to the absorption distance and an insignificant fraction of it (best case). This reduction in path length to the junction will be most pronounced for long wavelength radiation, thereby increasing long wavelength collection efficiency.

As bulk region diffusion length is reduced by radiation damage the reduced effective path length would enable a textured surface device to maintain more of the long wavelength response than a comparable smooth cell. Hence higher efficiencies could be obtained throughout the device's operating lifetime not only due to increased short wavelength response (less reflection) but also enhanced long wavelength response (less reflection and shorter collection distances).

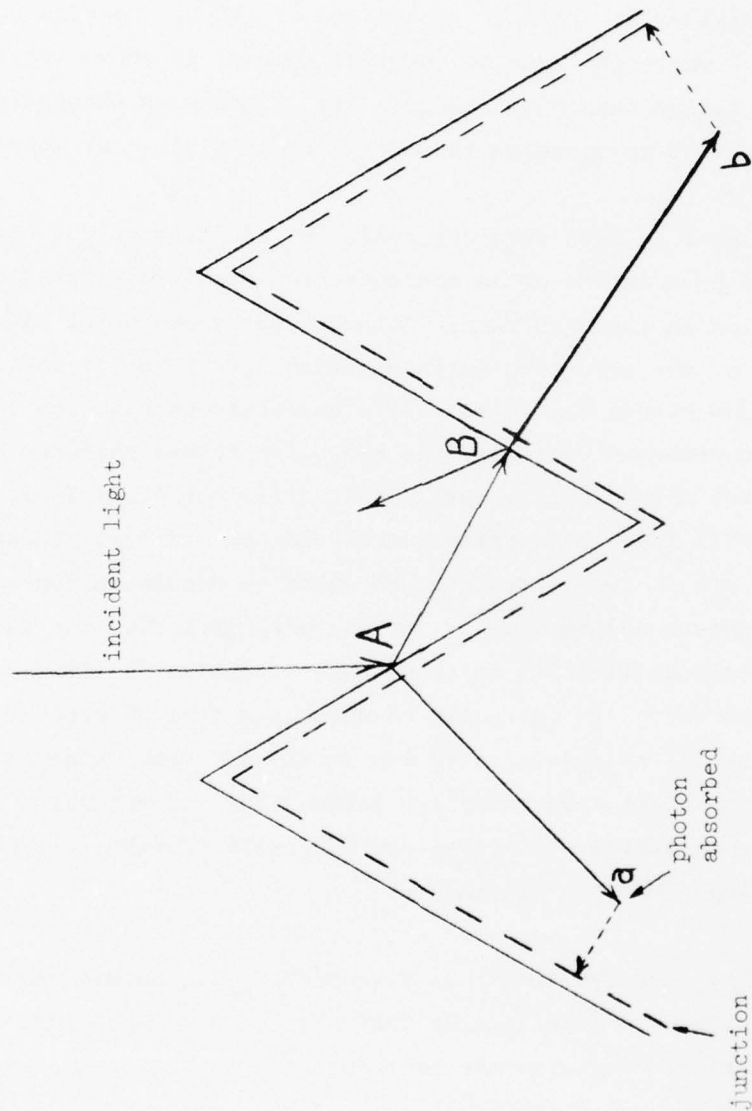


Figure 2. VMJ Aspect of Etched Surface Cell

FIGURE 2

Sodium hydroxide was chosen for investigation based on cost, safety and the ability to be used in high volume production. Experiments were performed using as-cut (100) orientation two ohm-cm silicon, examining etched surface structure and etch rates (both thickness and width) for various sodium hydroxide concentrations at a fixed temperature of 100°C. Results are plotted in Figure 3 where the rate of material removal is shown for two surfaces as an overall dimensional change. Etch rates were integrated over a 20 minute time period to minimize the impact of initial wafer condition.

A rather definite peak in etch rate occurs in the vicinity of 30% concentration, with a 50 percent change in concentration providing approximately 20 percent reduction in the etch rate. Although not shown here, microscope examination of the resulting surfaces (with approximately 150 μ of silicon removed) did reveal a physical difference between high and low NaOH concentration etches. Typically the hydroxide etched surface, because it attacks different crystal plane surfaces at different rates (i.e., etches anisotropically) will leave a non-planar semipolished surface. These anisotropic etch rates are in turn a function of solution concentration so that the resulting structure can be varied. At the peak etch rate the surface appears to be covered by large (\sim mm in extent) irregular "pillows." As the solution concentration is increased or decreased from 30 percent the "pillow" size decreases so that at very low (\sim 2%) and very large (\sim 60%) concentrations, very small structures are formed (<20 μ in extent). At high concentrations the resulting structures are typically rectangular, whereas at low concentrations they are tetrahedral.

An average etch rate (for two sides) of 9.7 μ m/min \pm 0.3 μ m/min was determined at 100°C for 30% NaOH. Considering the variables of concentration, temperature and wafer surface condition the reproducibility is good and the relatively slow etch rate, compared with the usual acid etches, indicates a potential for good process control. Varying the wafer resistivity showed no effect on the etch rates reported.

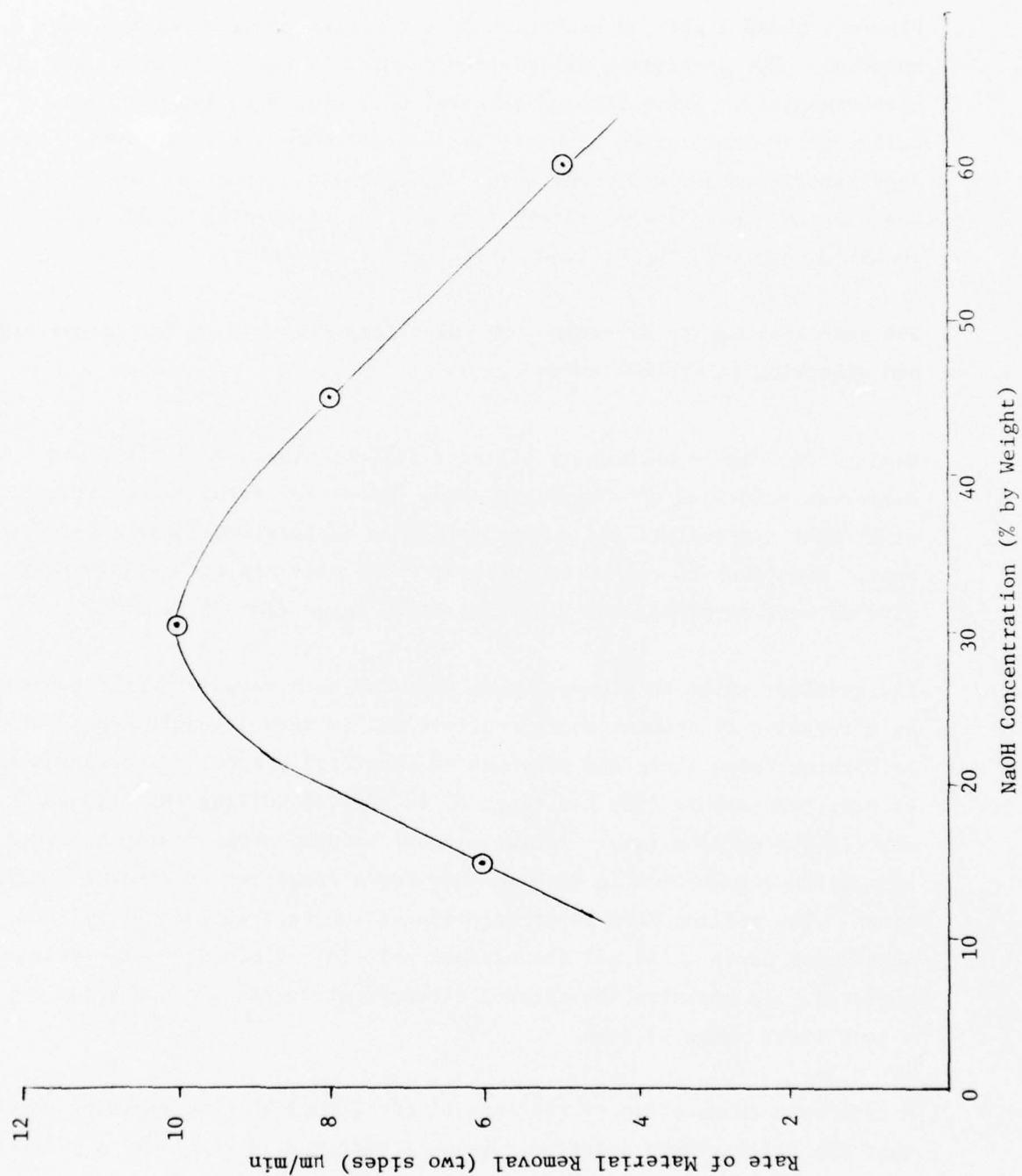


Figure 3. Etch Rate as a Function of Sodium Hydroxide Concentration

An experiment was then performed to determine how much time was required for an initial 30% NaOH etch to remove the surface-damaged material. Figure 4 shows a plot of etch rate as a function of time for two ohm-cm material. For comparison damage free chemically polished cells were etched simultaneously. Since damaged material will etch more rapidly the etch rate will come to equilibrium once all the damaged material is removed. Undamaged material (chemically polished) will display a constant etch rate. Based on this data approximately five minutes of etching in 30% NaOH is required to remove the silicon damage caused by cutting.

The next step was to determine the parameters required to form a uniform nonreflecting (textured) surface.

Nominal two ohm-cm chemically polished silicon blanks were etched in different solutions of sodium hydroxide (NaOH) to evaluate the influence of etchant temperature and concentration on surface tetrahedron development. Solutions of one to two percent NaOH, with and without isopropyl alcohol were examined over the temperature range from 75 to 95°C.

The results, given in Figure 5 show that the etch rate is nearly constant as a function of etchant concentration, but is very strongly dependent on etching temperature and presence of isopropyl alcohol. Increasing the etching temperature from the range 80 to 85°C to boiling (95°C), nearly doubled the etching rate. Adding alcohol brought about nearly an order of magnitude reduction in etching rate for a given set of etching conditions. The boiling NaOH solution produced the best surface of all the nonalcohol cases while all the alcohol solutions yielded nearly optimized surfaces. In addition the alcohol etchants produced this condition over a much wider range of time.

Microscopic examination of the selectively etched silicon surfaces showed that the boiling NaOH solution developed tetrahedrons of varying sizes with small areas of undeveloped surface between them. The lower temperature

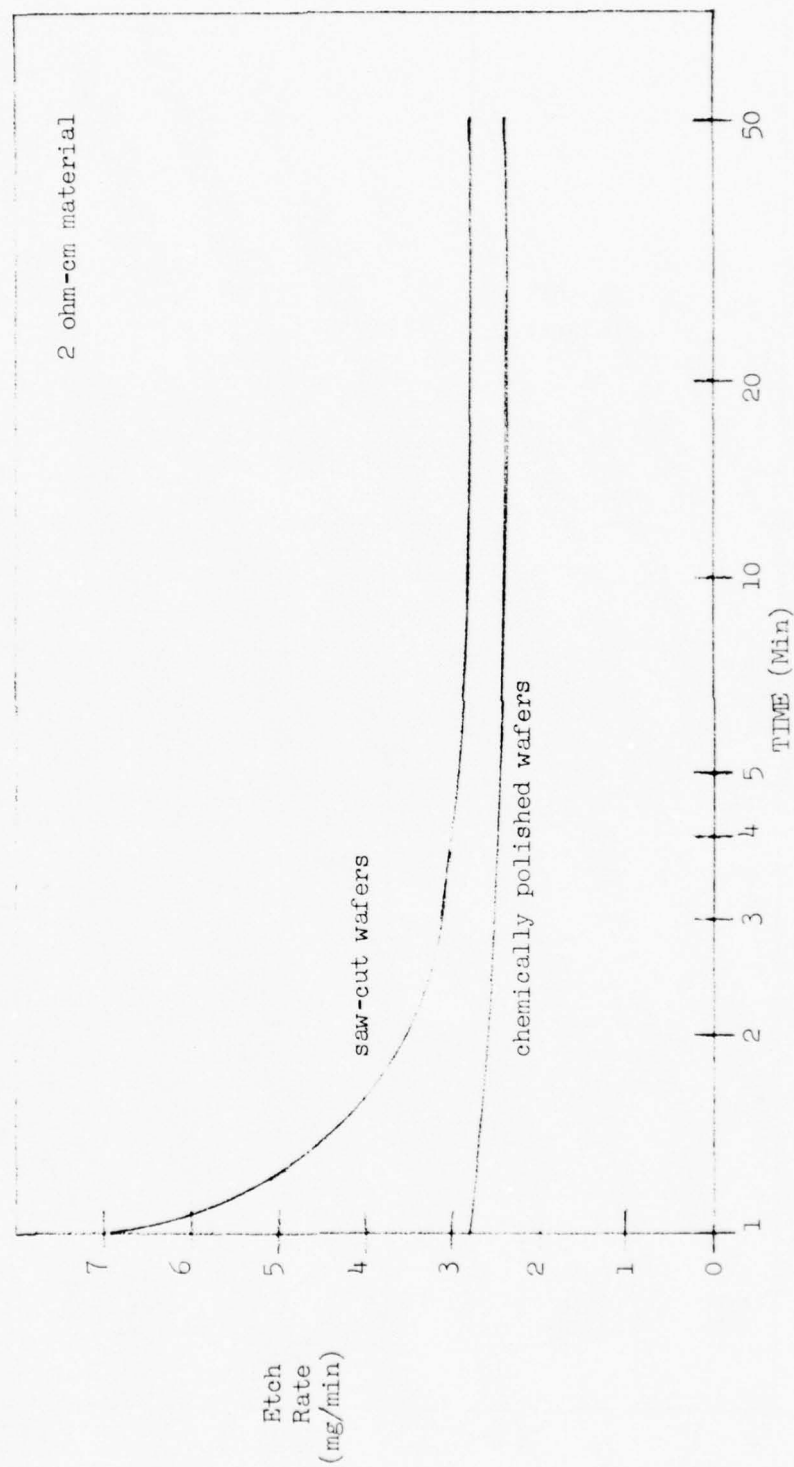


Figure 4. Etch Rate of Saw-Cut and Chemically Polished 2 ohm-cm Silicon Wafers

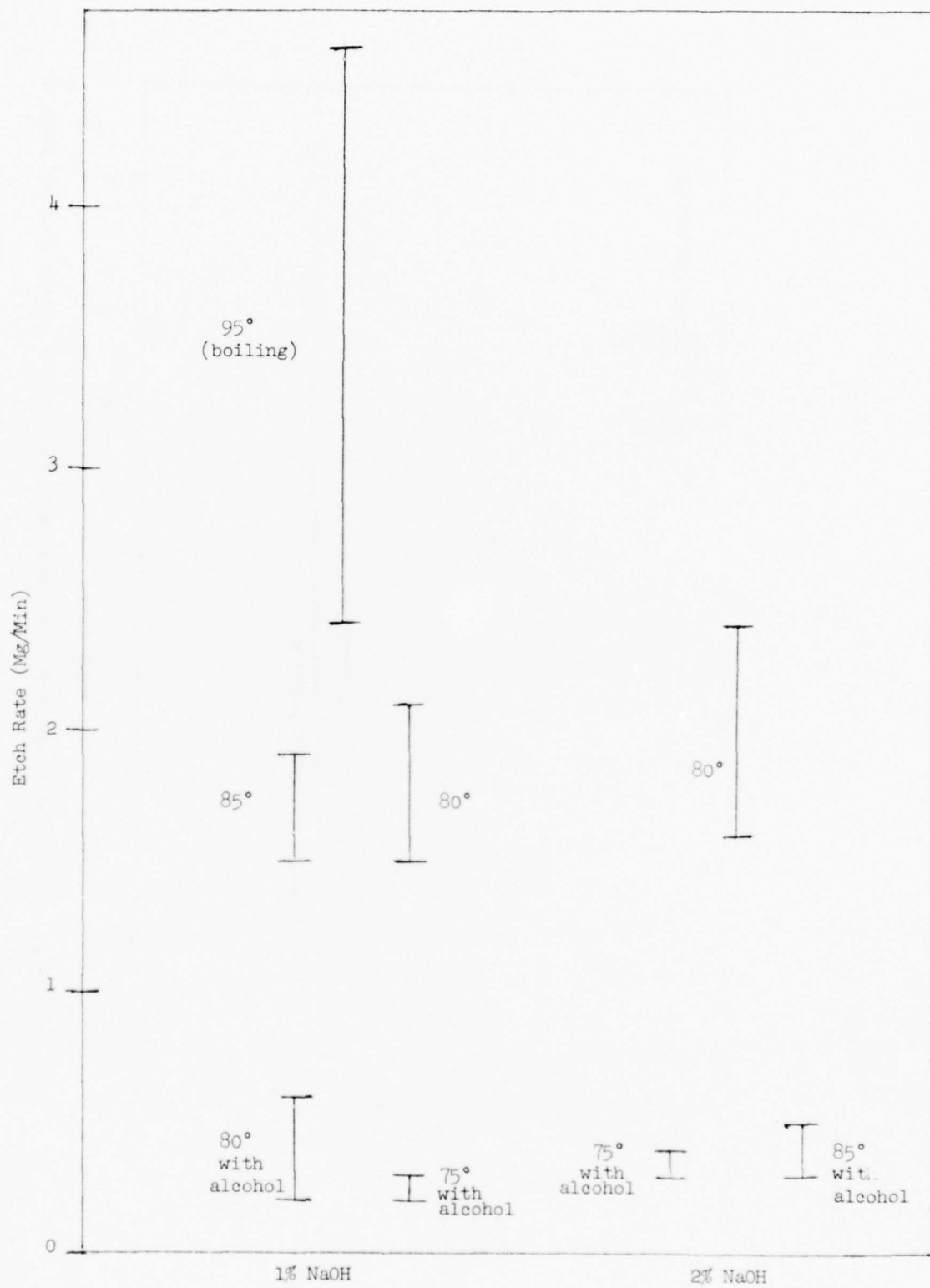


Figure 5. Etching Ratio of Solutions of Different Concentrations and Temperatures

(80-85°C) nonalcohol etches developed fewer tetrahedrons separated by larger regions of undeveloped surface. In contrast, the alcohol etches produced completely etched surfaces with no evidence of undeveloped regions between tetrahedrons.

Macroscopically, the nonalcohol etches produced surfaces with small regions of nearly smooth silicon, probably resulting from bubbles of liberated gas (H_2) which cling to the surface of the blanks and inhibit further etching action. The alcohol etchants yielded surfaces with little if any evidence of this condition, consistent with the fact that any gas bubbles formed during the etching reaction do not cling to the silicon surface, but almost immediately flow off, allowing a more uniform etch to occur.

Not only are the etching rates much lower for solutions using alcohol, the amount of material that must be removed to develop an optimized surface is less for the alcohol based solutions. Approximately .001" of silicon must be removed using alcohol while from .002" to .003" of silicon must be etched away to develop the surface in the case of NaOH only solutions.

Figure 6 plots the short circuit current of the cells as a function of etching time for the various conditions studied. Included is the current obtained from chemically polished control cells as well as the calculated value for perfect double reflection. All cells were initially .013" thick, but naturally for progressively longer etch times they became thinner and therefore all current values shown are corrected to a .013" thickness using appropriate data from the literature.

All groups showed a general pattern of rising to a maximum value, then dropping, with the nonalcohol boiling etchant exhibiting a very narrow optimum range, while the alcohol etches displayed fairly broad ranges in time, not unexpected since the etch rates were very low with respect to the nonalcohol etches. The nonalcohol low temperature etches gave broad ranges also, but the maximum current output was much lower due to the poor quality of the developed surface. The best groups proved to be the boiling one

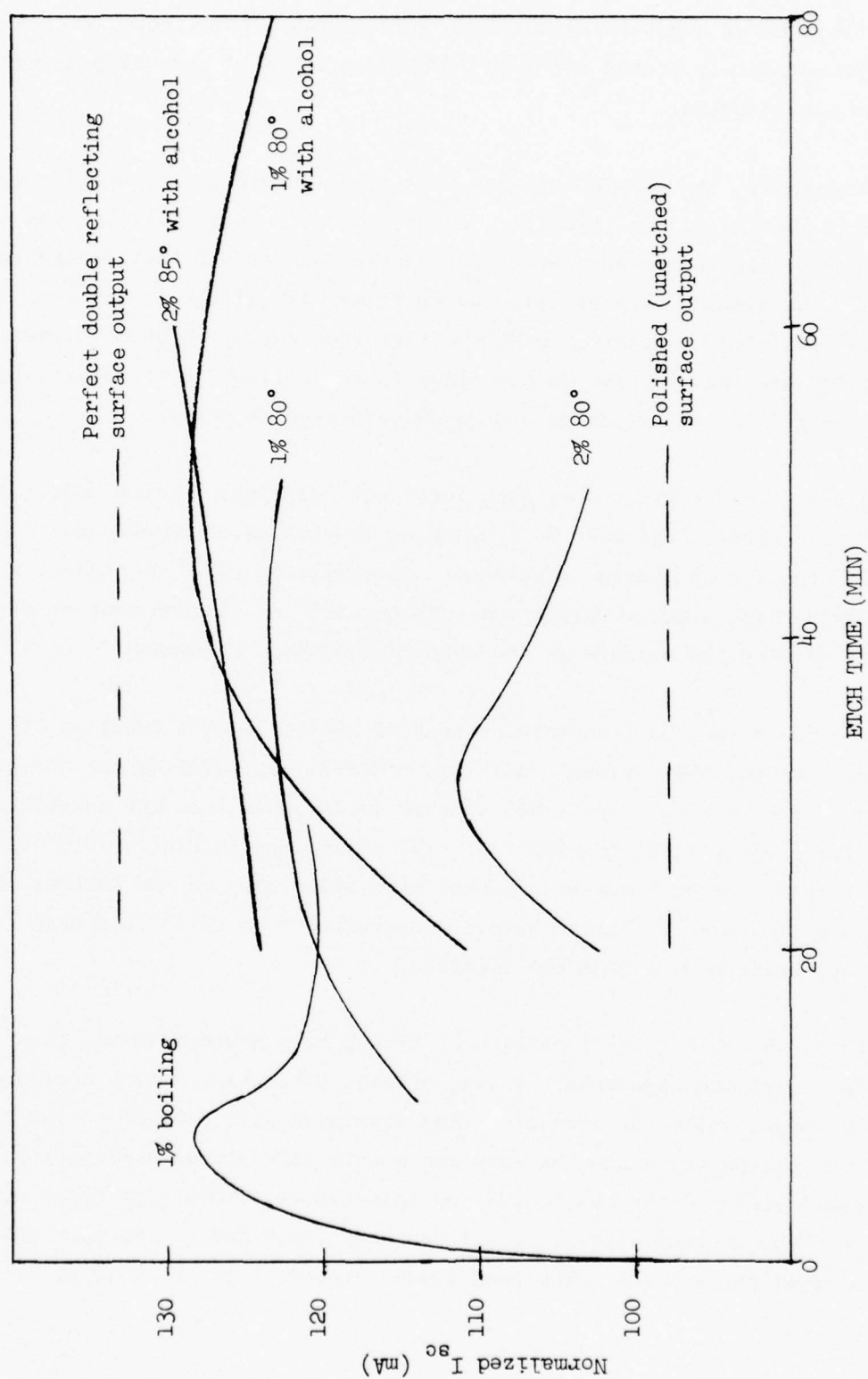


Figure 6. Short Circuit Current vs. Etching Time for Different Concentrations and Temperatures of NaOH Etching Solution

percent NaOH solution, and the two alcohol etches, cells from each group yielding current values approximately ninety-seven percent of the calculated value for ideal double reflecting surfaces.

Based on this work it is concluded that the presence of alcohol in the NaOH etching solution results in a process that has a high potential for control. This occurs because the amount of time required to form an optimized surface is long, and the developed surface is less susceptible to over-etching. In addition the alcohol solutions produce a more optimized surface with less material removed. This is important since the outside dimensions of the blank must generally conform to rather tight tolerances.

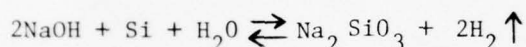
A water solution containing 2% sodium hydroxide and 35% isopropyl alcohol maintained at 80°C for 50 minutes was selected as the optimum set of parameters for obtaining a textured surface. This technique creates the surface shown in Figure 7. This SEM micrograph taken at 2000 magnification shows structures ranging in size from approximately two to four microns. Since the basic procedure had to be established to obtain this surface, work was performed to understand the actual chemistry involved. The impetus for this being the definition of important process variables and further etch optimization such as a smaller size pyramid with less scatter in height, permitting a higher density of double-reflecting surfaces.

Two areas of investigation were pursued: 1) the nature of the silicon surface prior to reaction with the etchant and 2) the factors influencing the formation of tetrahedra during the actual hydroxide etch. In order to obtain uniform tetrahedra the silicon surface should be of equivalent chemical reactivity with localized points of non-nucleating or slower reacting nature being desirable. This is necessary because the actual silicon etch proceeds into the silicon wafer forming an indented pyramid. The three dimensional intersection of these tetrahedral recesses leaves upright pyramids of varying size. The dimensions are directly proportional to the original size and overlapping of indentations.



Figure 7. Typical Etched Surface, 2000X

To see if the apex of a pyramid resulted from some nonreactive site originally present on the silicon surface, a variety of pre-etch treatments were performed. These included pre-stressing, lapping, 3-1-2 (HNO_3 -HF- CH_3COOH) chem polishing, 60-40 (HNO_3 -HF) chem polishing and chem-mech polishing. Also oxidation in peroxide, air, aqua regia and nitric acid was tried to convert the hydrophobic silicon wafer with surface layer Si-F or Si-O bonds to Si-OH bonds which are hydrophilic. After hydroxide etching, all of these wafers were equivalent with the exception of the lapped wafers which showed unusually large tetrahedra. The final etch obtained was found to be independent of the original silicon surface. From this one must conclude that the localization of slower-reacting points must be obtained during the hydroxide etch. The actual reaction involved is:



Sodium silicate (Na_2SiO_3) is partially soluble in water, but insoluble in alcohols and certain ketones. Our etching solution contains isopropyl alcohol to precipitate the silicate and leave a more uniform surface. Since one needs the variation in surface reactivity, the alcohol performs optimally when the silicate precipitates onto the Si wafer and remains there though the reaction is necessarily slowed.

To test this hypothesis a layer of a long chain carboxylic acid was applied to silicon wafers. Stearic acid was typically employed. It is only partially soluble in water and alcohol and as a consequence is porous to the hydroxide but helps to maintain a high viscosity layer on the cell surface. Figure 8 shows the result of such a treatment. This is a 2000X SEM micrograph of a wafer etched while coated with a very thin layer of carboxylic acid. The results are quite dramatic and point out the necessity for maintaining a viscous diffusion layer between the silicon wafer and the alkaline etchant. As a further test, the diffusion layer was removed by continuous agitation, vigorous boiling or the addition of a surfactant. In all cases the attempted etch resulted in the formation of only a few tetrahedra and numerous rounded shapes with little definition.

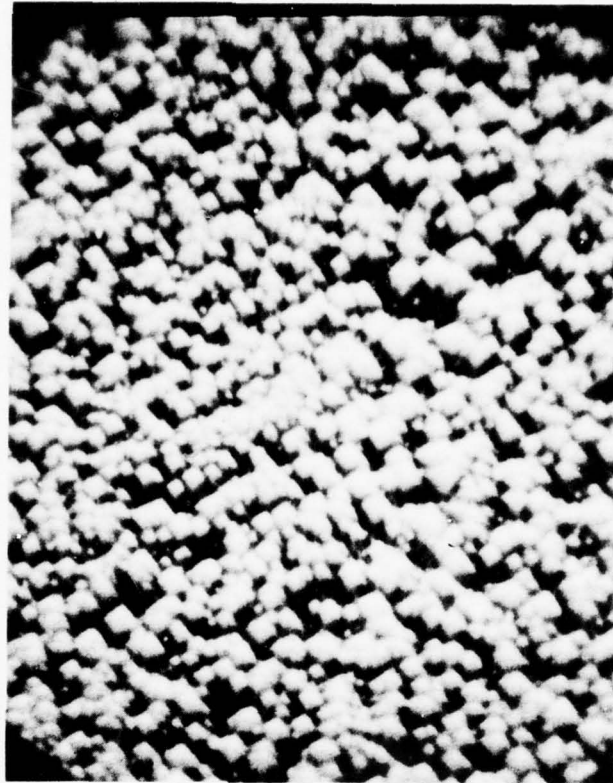


Figure 8. Improved Surface Texturization, 2000X

The effect of a precipitating agent was next studied using methanol, n-propyl alcohol, methyl ethyl ketone and isopropyl alcohol. There was a definite trend which correlated with steric hindrance in the solvent. The more sterically hindered isopropyl alcohol gave the best results. This piece of information fits well with the usefulness of a viscous diffusion layer.

To correlate the optimum etch with maximum efficiency, etching parameters were varied to obtain seven basic etch patterns. The following results were obtained for 2 ohm-cm material diffused for 15 minutes at 825°C.

	<u>E_{oc}, mV</u>	<u>I_{sc}, mA</u>
1 μ tetrahedra, 90% packing density*	601	155
1 μ matted, 80% packing density	603	154
1 μ tetrahedra, 50% packing density	598	153
3 μ tetrahedra, 20% packing density	598	153
6 μ matted, 100% packing density	601	152
6 μ tetrahedra, 20% packing density, uneven	597	152
polished control	601	147
Standard density etch solution, 3 μ tetrahedra 80% packing	600	154

*Packing density is defined as the percentage of the silicon surface that possesses this particular etch pattern.

The output efficiency clearly follows the trend in density of double reflecting surfaces. The only surprising result was the good output of a matted surface in which the tetrahedra are not pointed, but rounded. From this data one can conclude that the etch conditions previously selected as optimum do in fact provide nearly ideal outputs without the need for extensive care in surface preparation required to achieve smaller size tetrahedra.

2.3 Shallow Junction Studies

Solar cell junction depth is a critical factor in obtaining both improved initial efficiency as well as enhanced behavior after being exposed to the typical space radiation environment. The high efficiency cell being developed for HESP required an optimized junction depth that would yield maximum short wavelength response without compromising the curve fill factor of the device. In order to obtain this two approaches were taken. The first method involved adjusting the diffusion parameters of time and temperature to form a shallow junction. The second approach was to deliberately grow a post diffusion oxide layer which would take up a certain portion of the silicon junction, and then to dissolve this layer using hydrofluoric acid.

2.3.1 Diffusion Studies

The electrical performance of nominal two ohm cm polish-etched surface silicon solar cells was determined as a function of diffusion depth. Although this type of effort had been conducted previously on nominal ten ohm cm silicon it was felt that this parametric study should be made again due to changes in process technology implemented after the original work had been done.

Seven groups of cells were made with sheet resistance values ranging from 45 to 160 ohms /sq. Since the surface concentration of phosphorous in silicon is independent of diffusion temperature over the region investigated, the value for sheet resistance, ρ_s , can be correlated directly to junction depth. Half of the diffused wafers from each group were held aside for the oxidation work which will be described in the next section of this report.

The cells fabricated for this investigation were crucible grown, nominal 0.30mm thick and were 2 x 2 cm in area. Silver-titanium contacts were

evaporated through bimetallic masks to provide a collector pattern that was optimized for very shallow junctions. For the preliminary electrical and spectral response measurements the cells were tested without antireflection coatings.

Figure 9 shows a plot of cell short circuit current (I_{sc}) as a function of sheet resistance (ρ_s) which is inversely proportional to junction depth. Figure 10 plots cell response at 400 nm as a function of ρ_s for the seven groups. Electrical measurements were made at 28°C using a Model 1206 Spectrosun^R solar simulator set for the air mass zero (AM0) spectrum. There is a significant increase in short circuit current and short wavelength response as the junction depth is reduced from $\sim 0.35\mu\text{m}$ ($\rho_s \sim 40$) to $0.20\mu\text{m}$ ($\rho_s \sim 70$). Beyond this point there is a minimal change in cell current and short wavelength response. This trend has been previously observed in the case of ten ohm cm silicon.

In order to evaluate the amount of response available from the shallow junction cells at short wavelengths, antireflection coatings of tantalum pentoxide (Ta_2O_5) optically peaked for the AM0 spectrum (580-600 nm) and the short wavelength region (450-480 nm) were deposited on cells from each element of the matrix. At 400 nm the AM0 peaked coatings improved response from 24 to 42 percent with the average increase for all groups being 32 percent. The short peaked coatings improved 400 nm response from 60 to 72 percent with the increase for all groups averaging 66 percent. Table 6 is a summary of the spectral and electrical data obtained. As would be expected the "short" coatings yielded lower total I_{sc} values since there was significant reflection in the more active regions of the AM0 spectrum. The significance of this data is apparent when the work on producing nonreflecting silicon surfaces by orientation dependent etching is considered (Section 2.2).

Cells made with normal Ta_2O_5 coatings gave power outputs, at 28°C under AM0 test conditions, between 61 mW (deepest junction) and 68 mW (junction depth $\sim 0.2\mu\text{m}$). These cells were not covered with quartz covers so they were

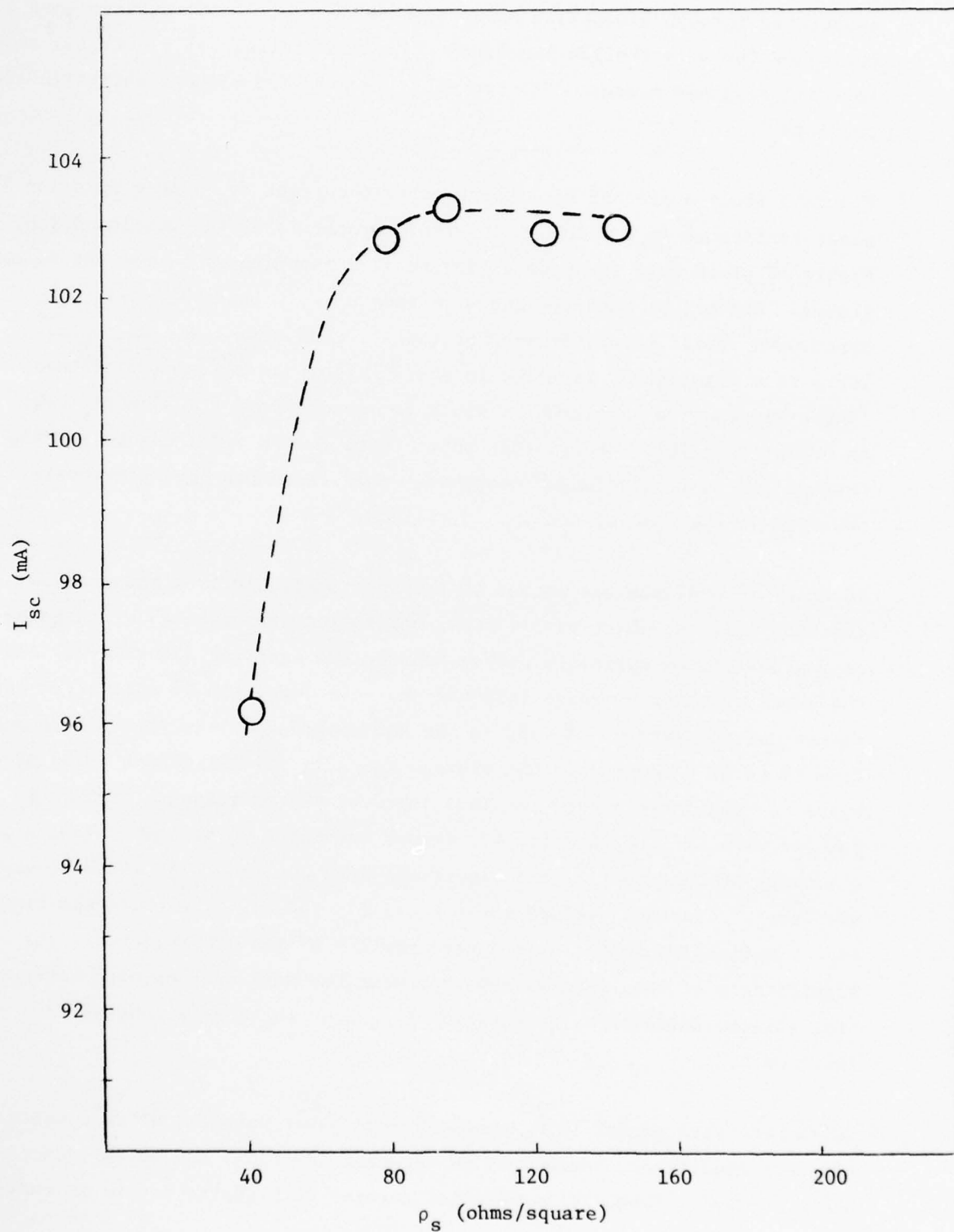


Figure 9. Short Circuit Current as a Function of Sheet Resistance

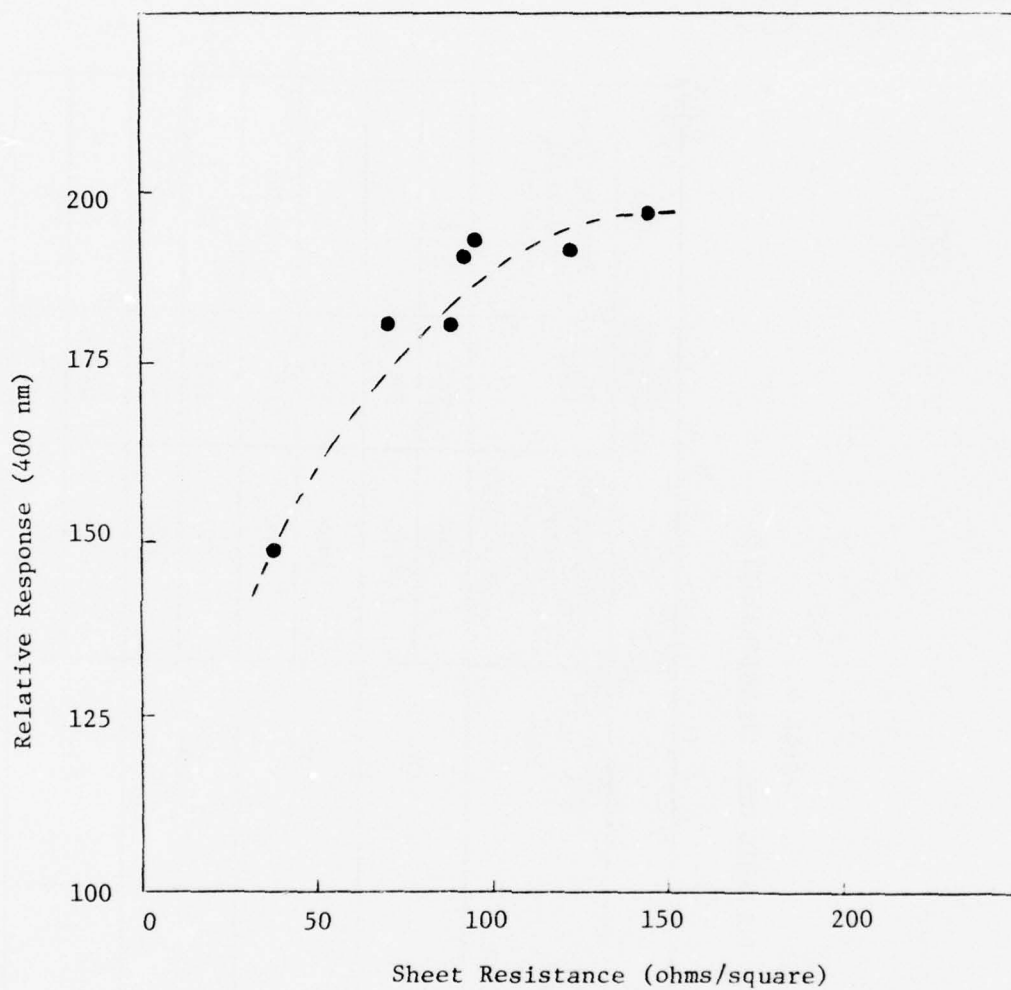


Figure 10. Spectral Response as a Function of Sheet Resistance

TABLE 6
POLISHED CELL CHARACTERISTICS

Sheet resistance ohms/square	BARE		AR COATED			
	Relative Spectral Response .4 micron	I _{sc} (mA)	Relative Spectral Response .4 micron	I _{sc}	Coating Type N= normal S= short	
40	155	99	195	138	N	
			250	122	S	
95	180	103	250	143	N	
			310	126	S	
125	195	104	255	145	N	
			325	125	S	
145	200	105	265	143	N	
			330	126	S	

actually between one and two percent better, since Ta_2O_5 is not optically matched to air ($n = 1$). The 18 gridline contact configuration was adequate over the entire junction depth range that was studied. This was verified by series resistance measurements and fill factor calculations. Series resistance was nearly constant for all junction depths, ~ 0.11 to $0.15 \mu m$; fill factors from .75 to .78 were obtained, with the highest value coming from a cell with a junction depth of $\sim 0.20 \mu m$.

2.3.2 Oxidation Studies

Although the shallow junction work indicated that significant improvement in response could be obtained, the question of whether this approach completely removes the zero concentration gradient region in the junction remained unresolved. The purpose of the oxide-etch phase was to examine this question more thoroughly. During oxidation, a certain amount of silicon is converted to silicon oxide (SiO_x). By deliberately growing relatively thick oxide layers (.05 to .10 μm) and etching them away using hydrofluoric acid, the top portion of the junction can be removed in a controllable fashion. This should result in an increase in short wavelength response since the impact of surface recombination velocity will be decreased because the zero gradient region will have been removed.

To provide an ambient condition most conducive to oxide growth, a quartz steam generator was designed and built. The generator was attached to the inlet joint of the furnace and wrapped with a heater tape. Double distilled water was used as the steam source to minimize the introduction of contaminants during the oxide process. The water was introduced into the top of the generator via a Teflon sealed glass joint and the water reservoir in the generator was carefully metered to allow only steam to enter the furnace tube along with a carrier gas of oxygen.

Using the steam oxide apparatus oxides were grown on samples for a range of temperatures varying from 850 to 700°C. Growing an oxide on a phosphorous

diffused wafer should increase the phosphorous concentration in the silicon at the oxide-silicon interface. As the oxide takes up silicon during its growth the segregation coefficient for the phosphorous leads to a net movement of phosphorous out of the glass and into the silicon. This increased phosphorous concentration should, by increasing the gradient near the surface, provide a larger electric field to aid the diffusion of minority carriers toward the junction. This will then manifest itself as an increased short wavelength response in the finished cell.

Samples for the oxide test sequence were obtained from the diffusion optimization experiments. In those experiments extra wafers were diffused and then held out, without further processing, to be used in the oxide study. In this manner the diffusion optimization sample cells would serve as controls for the oxide experiment. Prior to the steam oxidation, diffused samples were immersed in HF acid to remove any diffusion glass and leave a relatively clean surface. The samples were then placed in the furnace, oxidized, and removed. The oxide grown was then removed in HF acid, sheet resistances measured, and cells were fabricated for electrical tests consisting of I-V curves and spectral response.

Since each oxidation used wafers with diffusion depths varying from 0.3μ to 0.1μ a large number of diffusion variables could be examined quickly. On the first oxidations, which produced thick oxides, sheet resistance measurements were difficult to obtain. They varied considerably (factors of 2-3) with changes in current polarity and current magnitude, although in general they were always higher than the unoxidized wafer's value. This indicated some local breakdown or nonuniformity in the diffusion region, which was subsequently verified on the fabricated solar cell samples, which exhibited severe voltage suppression (up to 100 mV) and lower short circuit current (see Figure 11). Spectral response measurements indicated that the current loss was at long wavelengths, indicative of lifetime degradation.

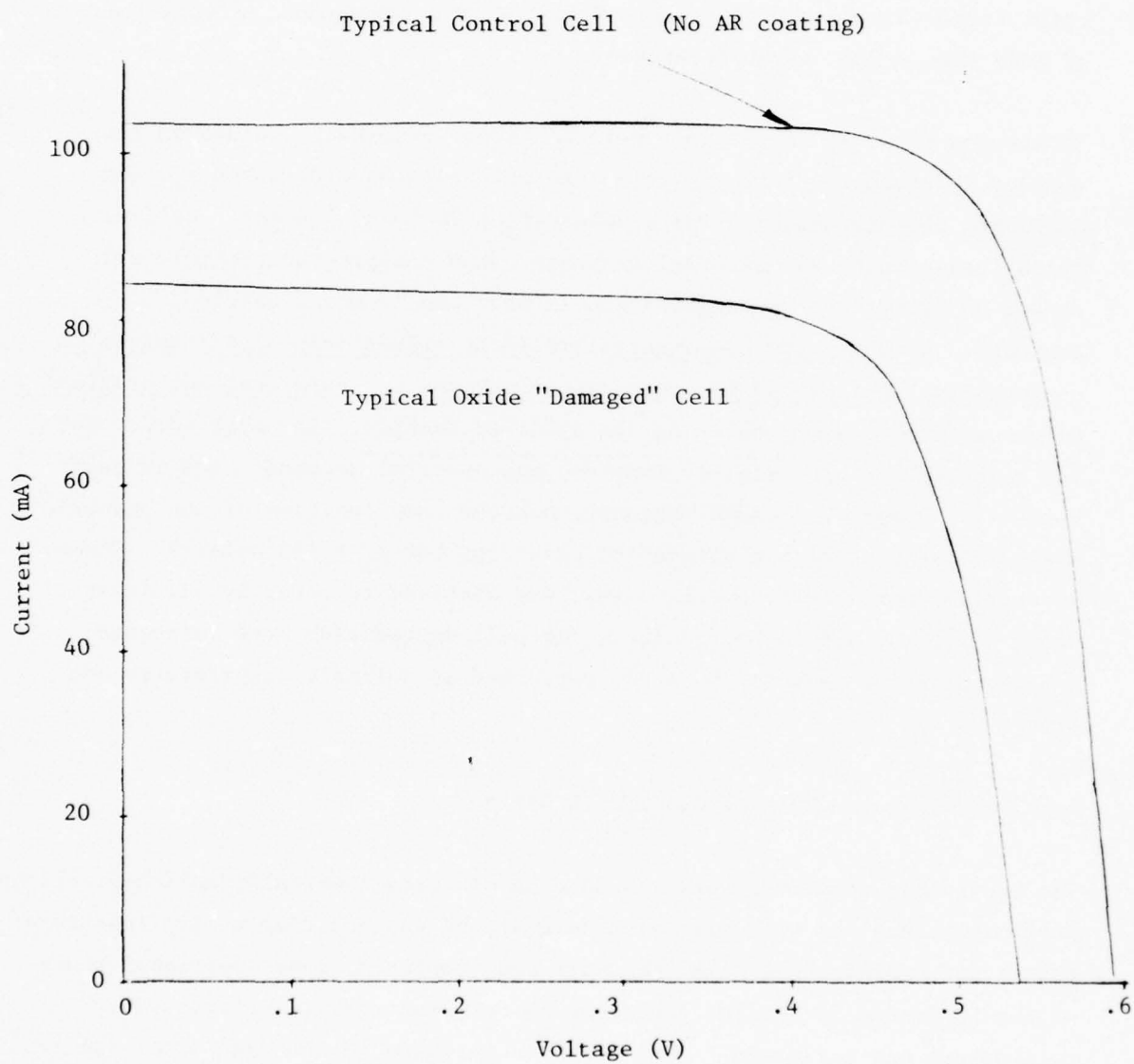


Figure 11. Effect of Thick Oxide on Cell I-V Characteristic

In an attempt to eliminate this damage, oxide growth time and temperatures were rapidly reduced in subsequent experiments. As this was done deep diffused wafers first showed a lack of damage and as oxide thicknesses were decreased further the shallower diffused samples were not damaged. Ultimately at temperatures of 700-750°C and an oxidation time of approximately ten minutes, samples were typically a brownish color, indicating a total oxide thickness of less than 0.04 μ , with a subsequent silicon loss of less than 0.02 μ after HF etching.

It was now possible to obtain consistent sheet resistance values on the samples which showed that typically the oxidation had increased ρ_s , (or decreased the diffusion depth) anywhere from 20 to 50 percent. Cell electrical performance and spectral response, when compared to control cells, showed no electrical degradation and an increase in short wavelength response. However, the new spectral response values were also found to be essentially identical to the response of samples not oxidized, but originally diffused to the same ρ_s value as the oxidized samples. In other words, both for oxidized and non-oxidized samples, the spectral response, and in particular, the short wavelength response, was the same function of the measured sheet resistance, with a saturation occurring for $\rho_s \geq 140$ ohms/sq. Consequently no improvement in cell output was observed to occur by oxidizing silicon wafers, and in fact chances for cell degradation were increased by the oxidation process, when not performed at suitable temperatures and times.

2.3.3 Textured Surface Junction Studies

The previously described work was done on standard chemically polished silicon surfaces, since the selective etch development was not completely finished at this time. However when the etch work was completed, some additional study of the influence of shallow junctions on textured surface silicon solar cell output was performed. This work was not done in the same detail as the original studies, but the results obtained generally corroborated those observed on chemically polished surfaces. At this stage of the program it was not possible to utilize diffused textured silicon cells with sheet resistances greater than 90 ohms/square due to curve shape problems. This will

be discussed in detail in Section 2.8 of this report. Once this difficulty was resolved the optimized sheet resistance for textured surface diffused cells was found to be the same $\sim 125\text{--}150$ ohms/square as for chemically polished surfaces. This is not unexpected since the texturizing process reduces reflection across the entire useful spectrum of the silicon solar cell's response.

2.4 Back Surface Field Development

The baseline HESP cell is a non-field two ohm-cm device. However as this program matured it became evident that no single cell could be fabricated that would satisfy all the goals of this contract. There are many missions which are very dependent on the radiation performance of the silicon solar cells. However there are other mission classes which require cells with maximum initial output power. The development of back surface field (BSF) cells on this program was oriented toward the latter mission class, although as will be shown in a later section, the back surface field cell proved to be quite radiation tolerant provided the thickness and the bulk resistivity of the silicon were properly chosen.

2.4.1 Evaporated Aluminum Source

Evaporated aluminum had been almost exclusively used as the acceptor doping source for the formation of BSF solar cells. Aluminum can produce excellent results at diffusion temperatures of $800\text{--}850^{\circ}\text{C}$ which are comparable to those used for front junction formation, and therefore will not degrade the minority carrier lifetime below that which results from the junction diffusion step. Two basic processing concepts can be employed for field cell fabrication, both have produced good results. The first approach employs a simultaneous field and junction formation diffusion. However this method places a limitation on the minimum junction depth that can be achieved. To avoid this constraint, a two-step process was developed consisting of separate junction and field formation diffusions.

Both methods can provide thin high efficiency cells provided the base resistivity is no less than nominal ten ohm-cm. Lower resistivity BSF cells do display the increased short circuit current and open circuit voltage, but the fill factor is reduced to the point that two ohm-cm non-field cells produce more power than the field cells. Since some missions would require low resistivity BSF cells, a serious effort was initiated to solve the fill factor problem in two ohm-cm BSF cells.

The majority of this work employed the two step process, either forming the junction, then the field defined as method 1, or the reverse, defined as method 2. Small groups of wafers were processed following the above methods using different aluminum diffusion temperatures (825° , 850° , 875° , 900°) and times (15 seconds, 30 seconds, and 15 minutes). The results for current at load are shown in Figures 12 and 13. (The data is for cells with no antireflective coating.) The longer diffusion time groups are superior for the junction then field method (1), while the 30 second heating appears best for the field then junction method (2). The best enhancement of the long wavelength response (at 1050 nm) occurred in the cells from the junction then field method done at 825°C for 15 minutes. After AR coating, this group had the highest open circuit voltage and maximum power, 607 mV and 72 mW respectively.

Most of the method 1 groups were plagued by poor fill factors while the method 2 groups had low short circuit currents (I_{sc}). Twice attempts were made to reproduce the favorable results of the method 1 group field diffusion at 825° for 15 minutes. Both times the cells had low E_{oc} values (7-16 mV lower than the first experiment) and/or poor fill factors ($\sim .73$ compared to $\sim .77$ for the first experiment).

Two additional variables which were examined, were (1) deposited aluminum thickness and (2) rate of alloy warm-up and cool-off. In one experiment cells with aluminum thicknesses of 1.5 μm , 3-4 μm , 8 μm , and 17 μm , were

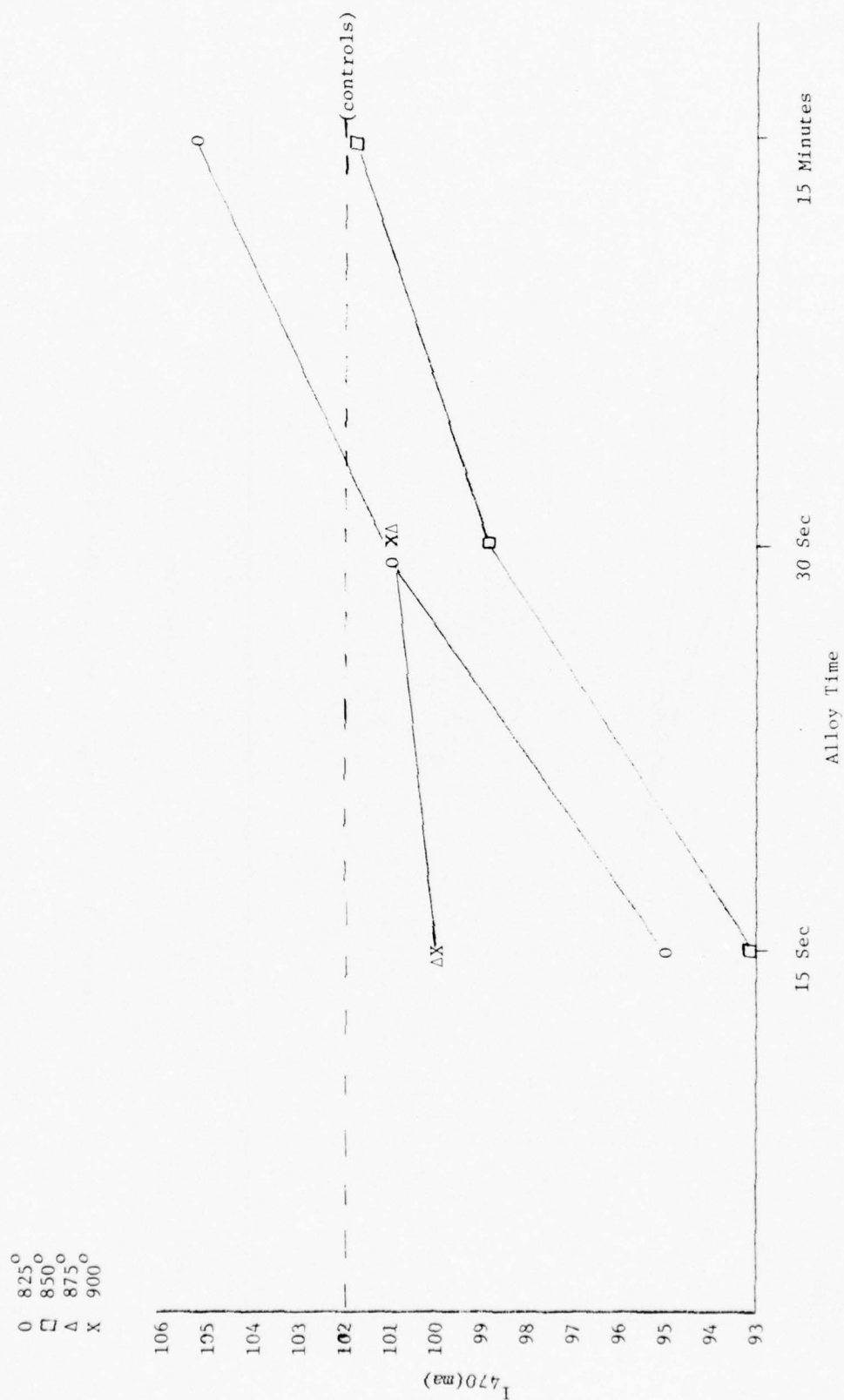


Figure 12. 2 Step P+ Diffusion Then Alloy Method

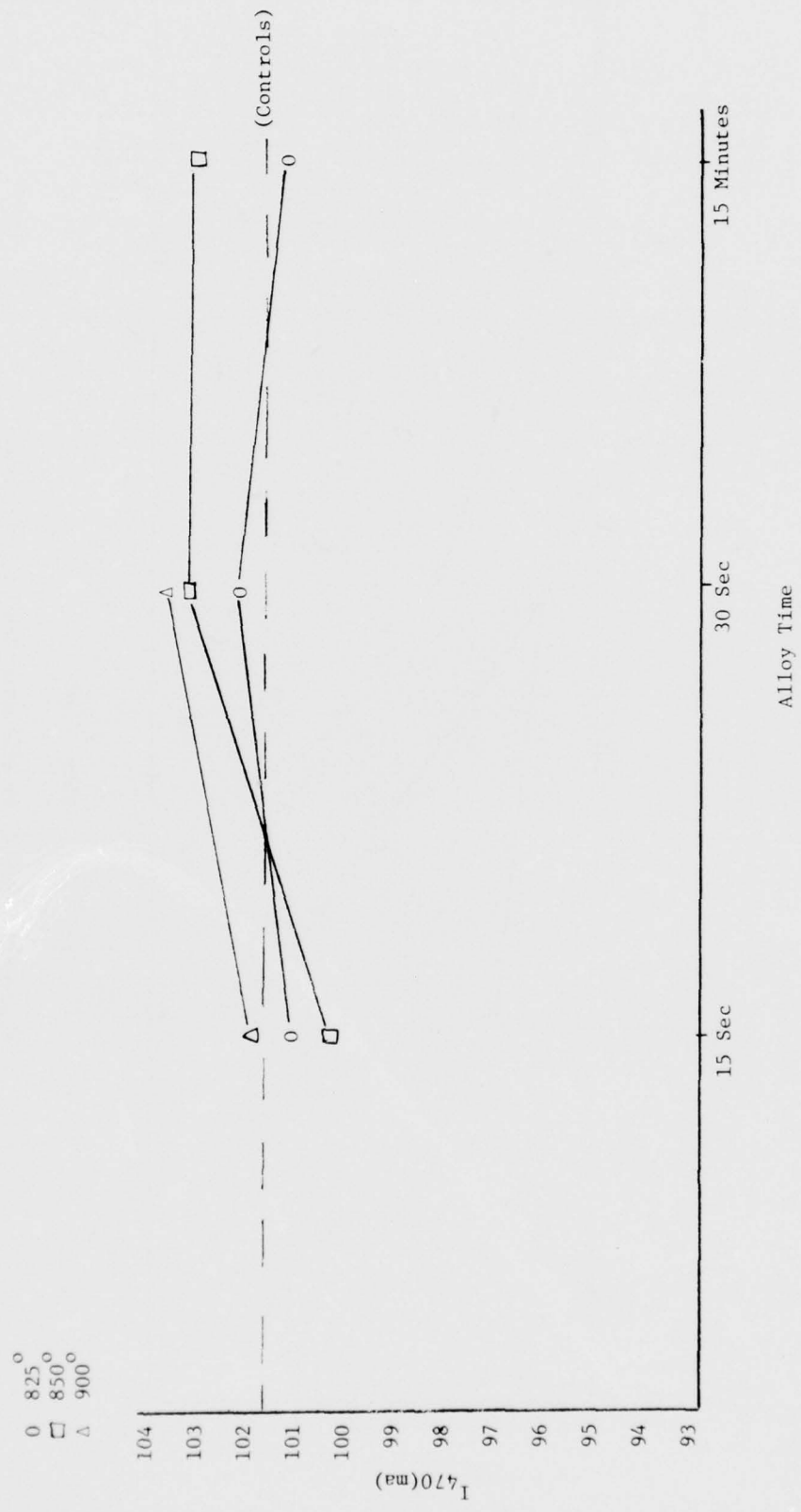


Figure 13. 2 Step P+ Alloy Then Diffusion Method

processed according to method 1 and field diffused at 825°C for 15 minutes. The results are shown in Table 7. The best power was from the 8 μ group, although as the I_{sc} increased with aluminum thickness, the fill factor and E_{oc} decreased.

In another experiment, cells were processed according to method 1, but were heated and cooled during field diffusion in different ways. One half the cells were heated slowly ($\sim 15^\circ\text{C}/\text{min}$) from 400°C to 825°C and then quenched in liquid nitrogen. The other half were also heated slowly to 825°C, but then were allowed to cool slowly ($\sim 5^\circ\text{C}/\text{min}$) to 400°C. This group exhibited unusual recrystallization patterns, with the entire back covered by one large "star," whereas the usual structure is made of many small "stars" or a cloudy amorphous pattern with no clearly discernable "stars." After processing into completed solar cells, both groups showed very poor curve shape (fill factor $\sim .70$) and low E_{oc} (540-560 mV). The exact reason for such poor electrical output by both groups is not known.

2.4.2 Non-Vacuum Aluminum Field Source

Time constraints forced the work using evaporated aluminum to be terminated even though the objectives of this investigation had not been realized. However a non-vacuum method of depositing aluminum developed on another contract (NAS3-20029) had demonstrated consistently good results when used for the fabrication of ten ohm-cm BSF cells.

Prior to the actual production of the HESP field cells, a "quick look" was taken using this technique, and the results were so impressive that this method of forming the BSF was implemented into the production phase of the program. In this process the silicon wafers are first diffused to obtain a sheet resistance on the order of 100 to 120 ohms/square. The junction is then removed from the rear surface by chemical etching. Then an aluminum paste is screen printed onto the etched back and baked in air to drive off the organic binder. This leaves the surface coated with finely divided particles ($\sim 2-4 \mu\text{m}$, diameter) of aluminum which act as the acceptor source. The wafers are then heated to $\sim 800^\circ\text{C}$ for approximately

Process:

Junction then field

Field Diffusion @ 825°C for
15 minutes

TABLE 7
EFFECT OF THICKNESS OF DEPOSITED ALUMINUM
ON ELECTRICAL CHARACTERISTICS OF 2 OHM P+ CELLS

Thickness of Deposited Aluminum (μ)	E_{oc}	I_{sc}	I_{470mV}
$1\frac{1}{2}$	579	108	101
3-4	575	107.5	100
8	581	109.5	103
17	555	111	77

one minute to form the field region. The excess aluminum is removed using hydrochloric acid and then the wafer is processed normally.

This technique resulted in thin high efficiency cells ranging in thickness to as low as 0.10 mm (.004") and varying in bulk resistivity from two to one hundred ohm-cm. The electrical characteristics of these cells are provided in the section discussing pilot line production of HESP "hybrid" cells (2.9).

2.5 Contacts

The final version of the HESP cell consisted of a selectively etched surface in order to reduce reflection, and an extremely shallow junction which gave an optimized output in the radiation insensitive short wavelength region of the cell's response. Although junctions this shallow had been shown to be compatible with the standard titanium-palladium-silver contact system for chemically polished surfaces, the use of titanium appeared to cause some degradation in curve shape for textured surface cells.

One of our objectives had been to replace titanium as the bonding metal in order to develop a cell that would be more tolerant to high temperature excursions that might be experienced from a laser threat. This was the basis for our original investigation which examined nine alternate metals to titanium. The starting matrix consisted of chromium, tantalum, tungsten, nickel, niobium, zirconium, vanadium, palladium, and molybdenum.

The initial work concentrated on developing the necessary post deposition processes to form ohmic contact to silicon. Chromium was judged to be the best ohmic contact to bulk silicon. It had the additional advantage of not requiring a post deposition heat treatment involving high temperatures or a reducing atmosphere, thus allowing us to eliminate the separate "sintering" process required to form an ohmic contact to bulk silicon when titanium was used as the bonding metal.

Since the junction contact was being made to a degenerate (highly conducting) silicon surface, any of the candidate metals would make an adequate contact. In order to rank them for further evaluation, a crude screening test was developed to characterize the behavior of these metals with respect to high temperature performance. A heating assembly was fabricated which allowed metal-silicon structures to be heated to 600°C under vacuum (see Figure 14).

Silicon wafers 2×2 cm, 10 ohm-cm, were diffused to obtain a sheet resistivity of approximately 120 ohms/square, then back etched and contacted on the back with conventional Ti-Ag contacts which were subsequently sintered at 600°C in hydrogen to obtain ohmic contact. Front contacts were then deposited consisting of an initial layer, approximately 1000 \AA thick, of the test element, followed by a 2 micron layer of silver. The geometrical pattern of this front contact is simply a square slightly smaller than the wafer itself, as shown in Figure 15(a). After recording the dark forward and dark reverse I-V characteristic curves of each test diode fabricated in this manner, it is then baked at 600°C for 15 minutes in a vacuum. Test samples are then saw cut to eliminate extraneous edge effects leaving the diode structure illustrated in Figure 15(b). In this manner, only the effects of the contact material being tested will affect the I-V curves which are subsequently recorded.

Five metals, chromium, tantalum, niobium, molybdenum and tungsten, demonstrated acceptable performance using this screening method. Typical examples of temperature sensitive and insensitive metals are shown in Figures 16 through 19. An extremely significant observation was made with regard to the behavior of palladium. It was shown that this metal is extremely reactive with silicon. An investigation of the literature provided additional verification of our observations.⁽⁶⁾ Since palladium turned out to be necessary for passivating our final contact system, this observation has cast some doubt on the ability of the present HESP contact system to withstand a potential laser threat. This can be seen from Figure 20 which shows the effect of our screening test on a passivated tantalum-silver contact system.

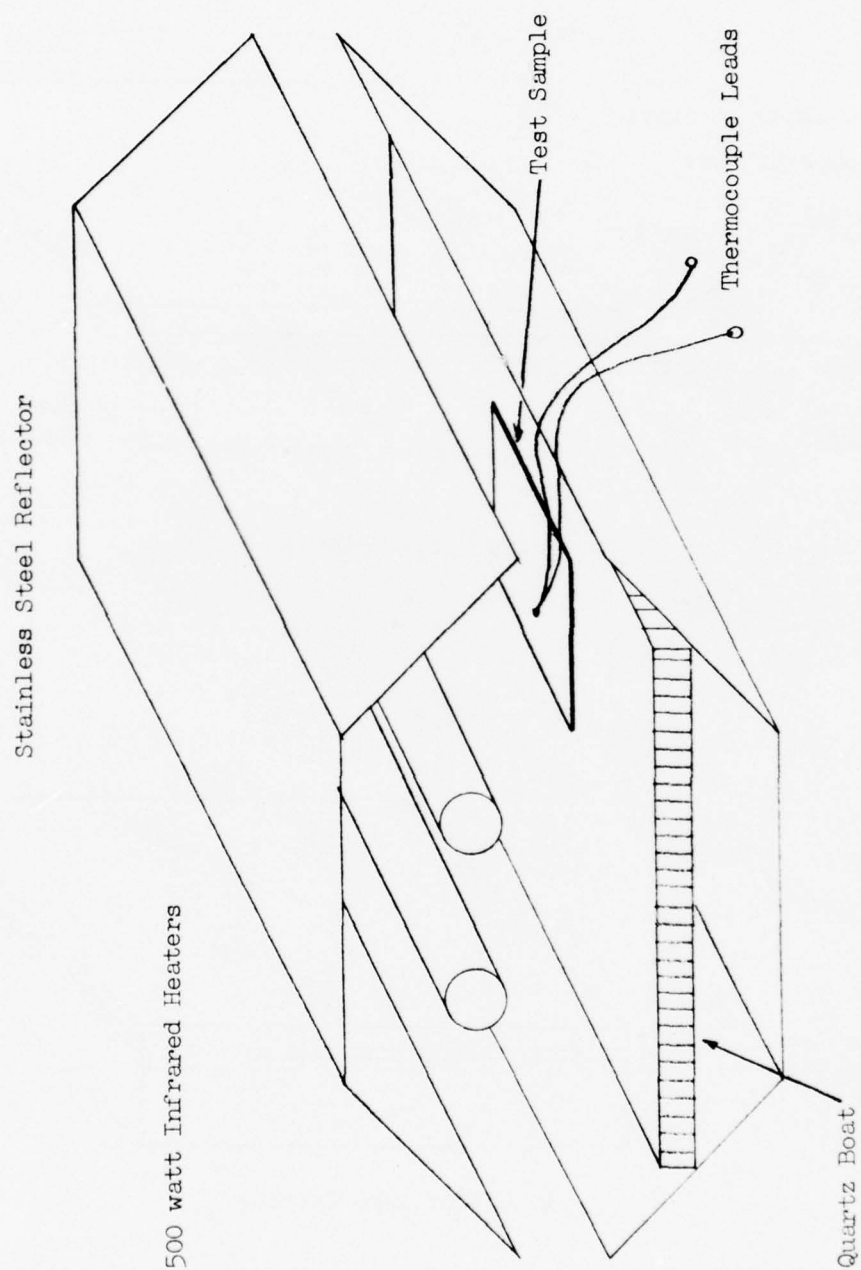
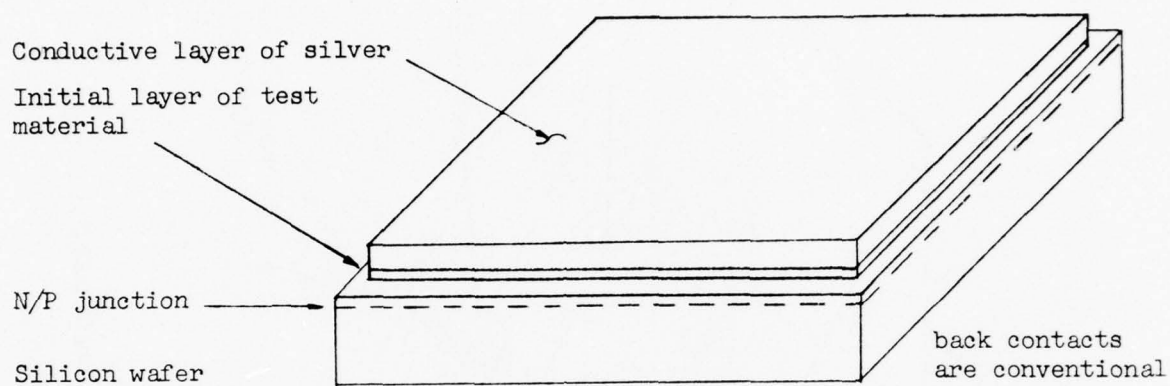
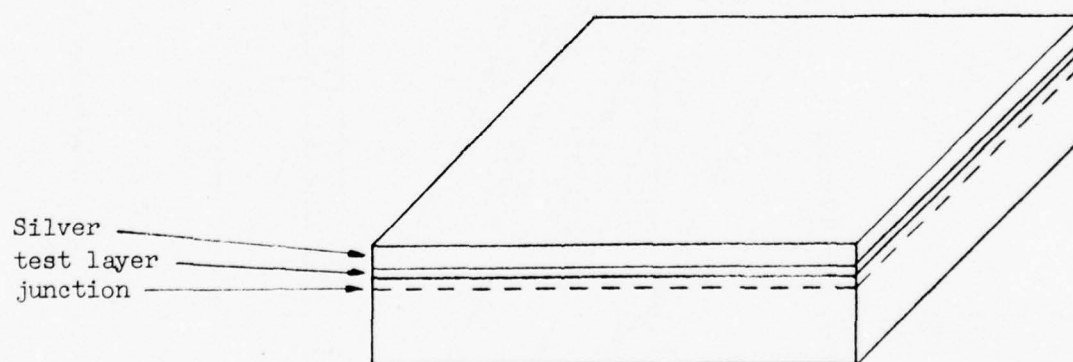


Figure 14. Heater Assembly Enclosed in Vacuum Chamber



a. Front Contact Configuration



b. After Edge Cutting

Figure 15. Test Sample Preparation

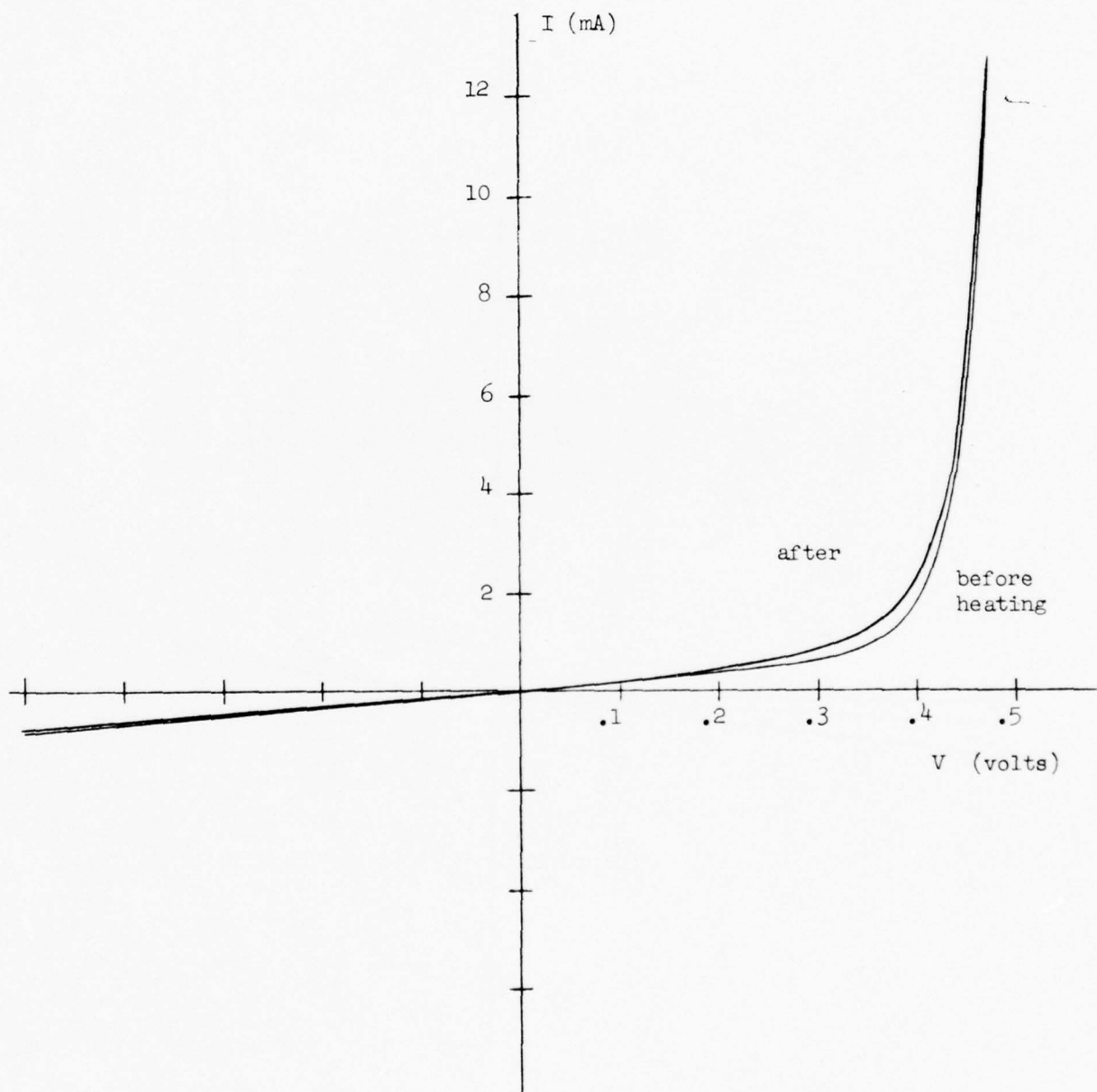


Figure 16. Tantalum-Silver Contacts Heated to 600°C in Vacuum

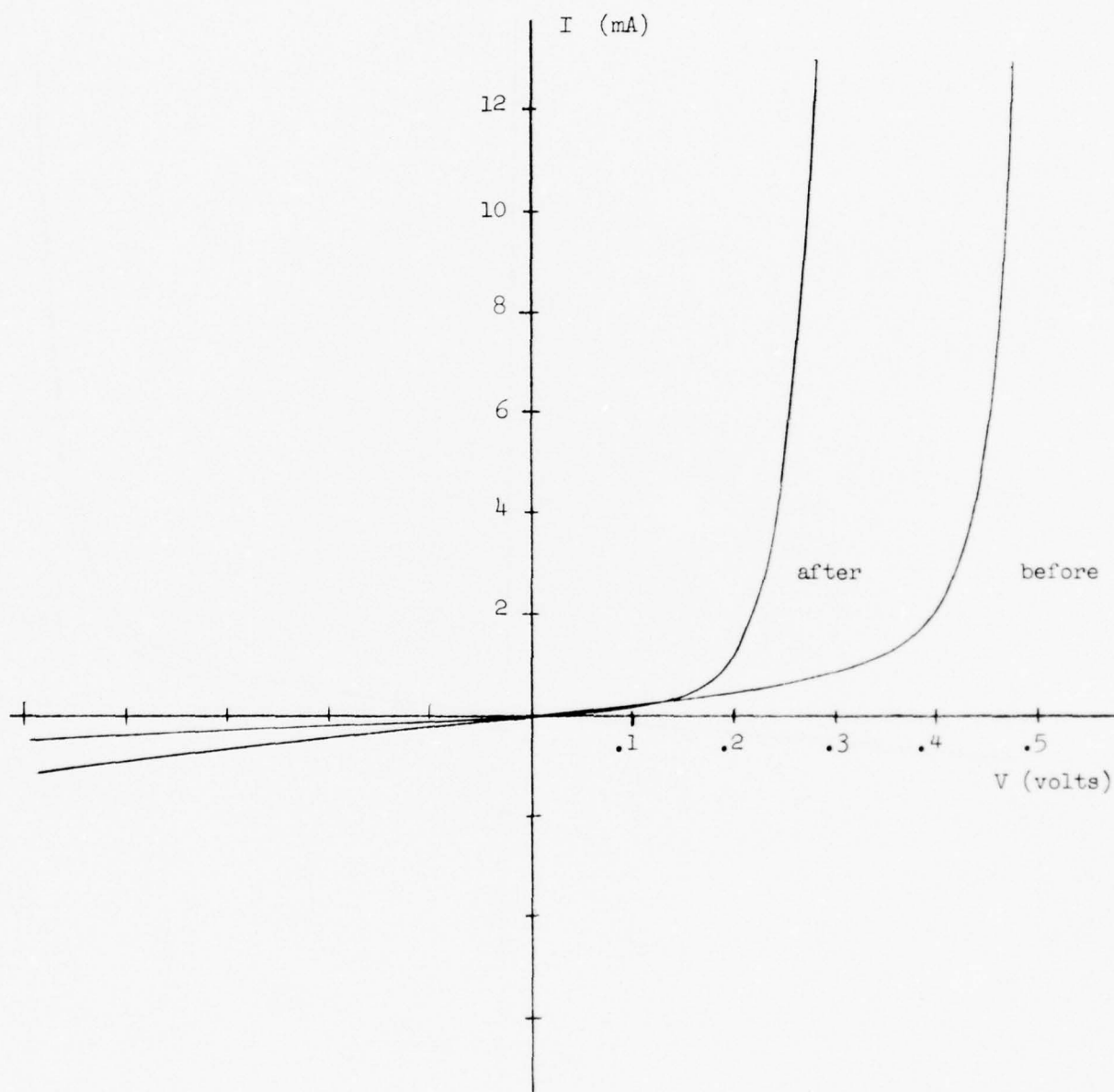


Figure 17. Vanadium-Silver Contacts Heated to 600°C in Vacuum

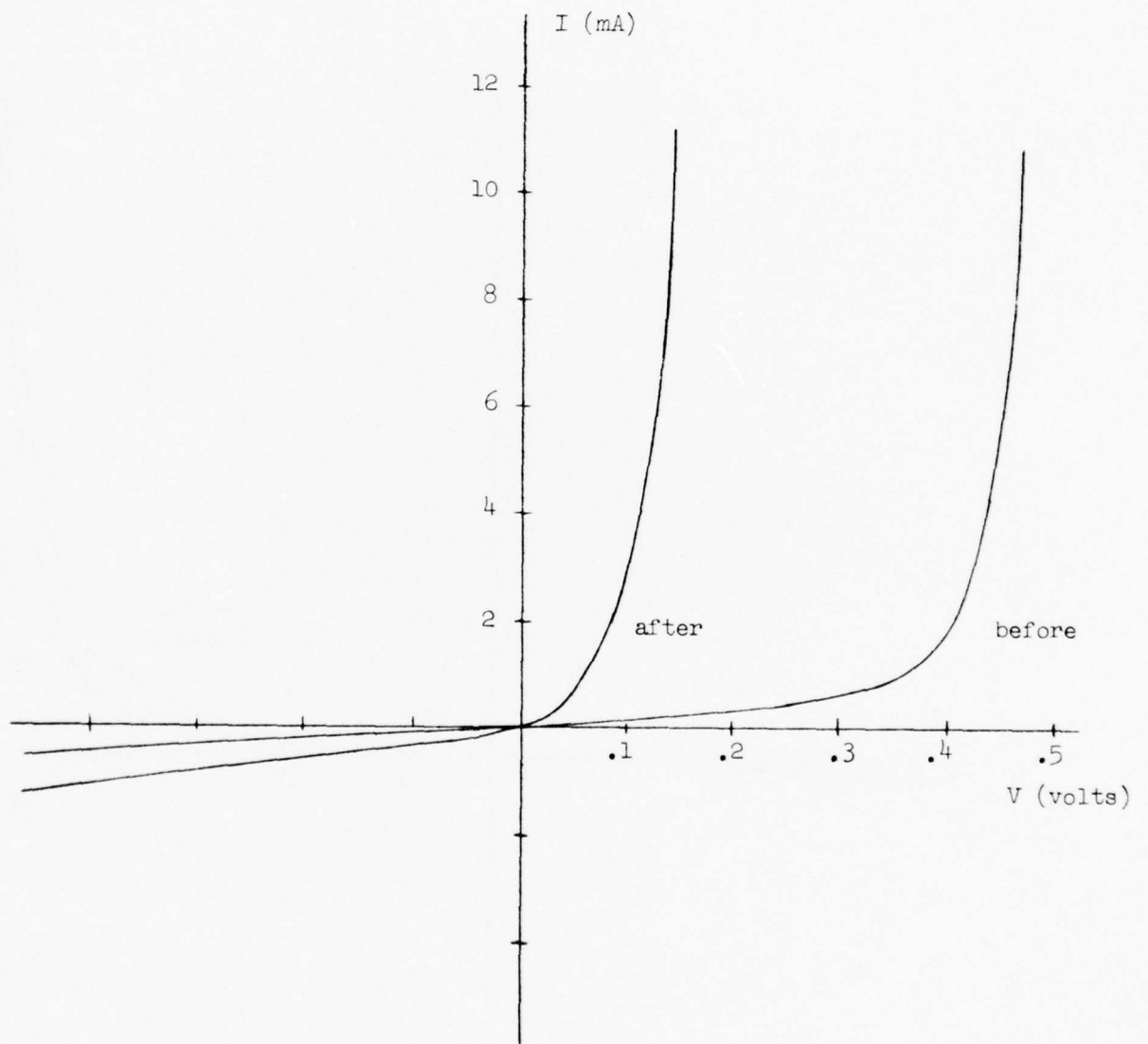


Figure 18. Zirconium-Silver Contacts Heated to 600°C in Vacuum

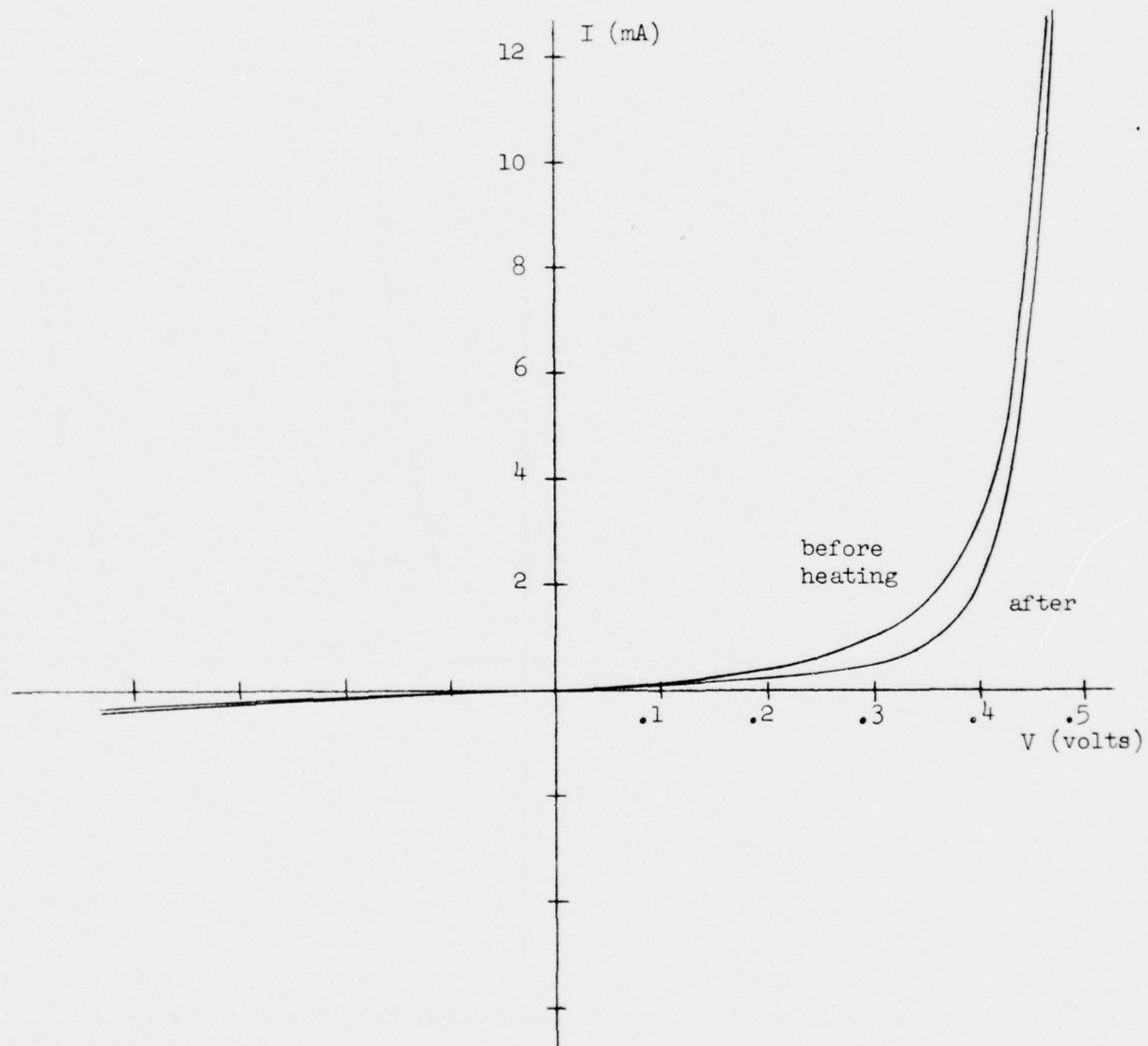


Figure 19. Niobium-Silver Contacts Heated to 600°C in Vacuum

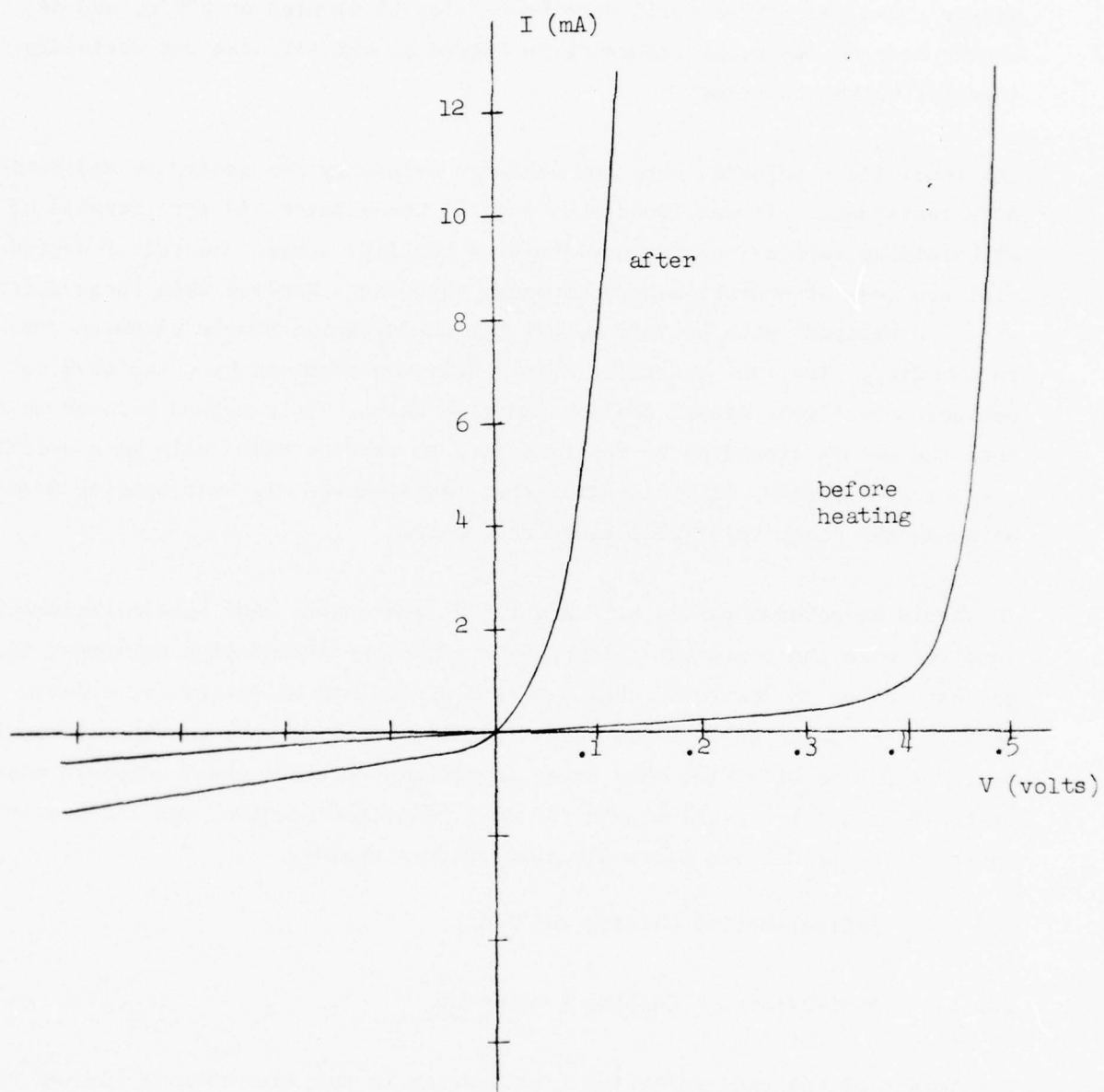


Figure 20. Tantalum-Palladium-Silver Contacts Heated to 600°C in Vacuum

Titanium was evaluated in this screening by comparing shallow junction cells made using tantalum-silver front contacts against cells made with titanium-silver contacts. These cells were heated for 15 minutes at 600°C, and as can be seen by comparing Figure 21 to Figure 22 the titanium was decidedly inferior to the tantalum.

The remaining candidates were now screened carefully for adherence and humidity resistance. It was found that none of these materials were capable of withstanding routine temperature-humidity testing, severe electrical degradation and loss of contact adherence being observed. However when these materials were "passivated" with palladium, all but the tungsten showed adequate resistance to humidity. The four remaining metals were now examined by using them to contact selectively etched shallow junction cells. This method allowed us to rank the metals according to their ability to produce HESP cells with optimized electrical outputs. It was decided that tantalum was the best bonding metal, although the other three performed adequately.

It should be pointed out in all candor that there were many subtle variables involved with the textured silicon surface and our evaporation equipment that may have acted to "perturb" what had been planned to be definitive experiments. The choice of tantalum was pragmatic, based on many months of experiments performed at a time when other parameters were not under complete control. Of the four metals tantalum gave the most consistent results, and its performance in the production phase did justify this choice.

2.6 Antireflection Coating and Filter

2.6.1 Antireflection Coating Evaluation

The impact of the antireflection (AR) coating is modified when it is used in conjunction with a textured surface. As was pointed out in Section 2.2 the total amount of reflection from a selectively etched silicon surface is on the order of twelve percent, and thus the amount of reflection reduction obtained from an AR coating is only in the order of eight to ten percent. In the case of

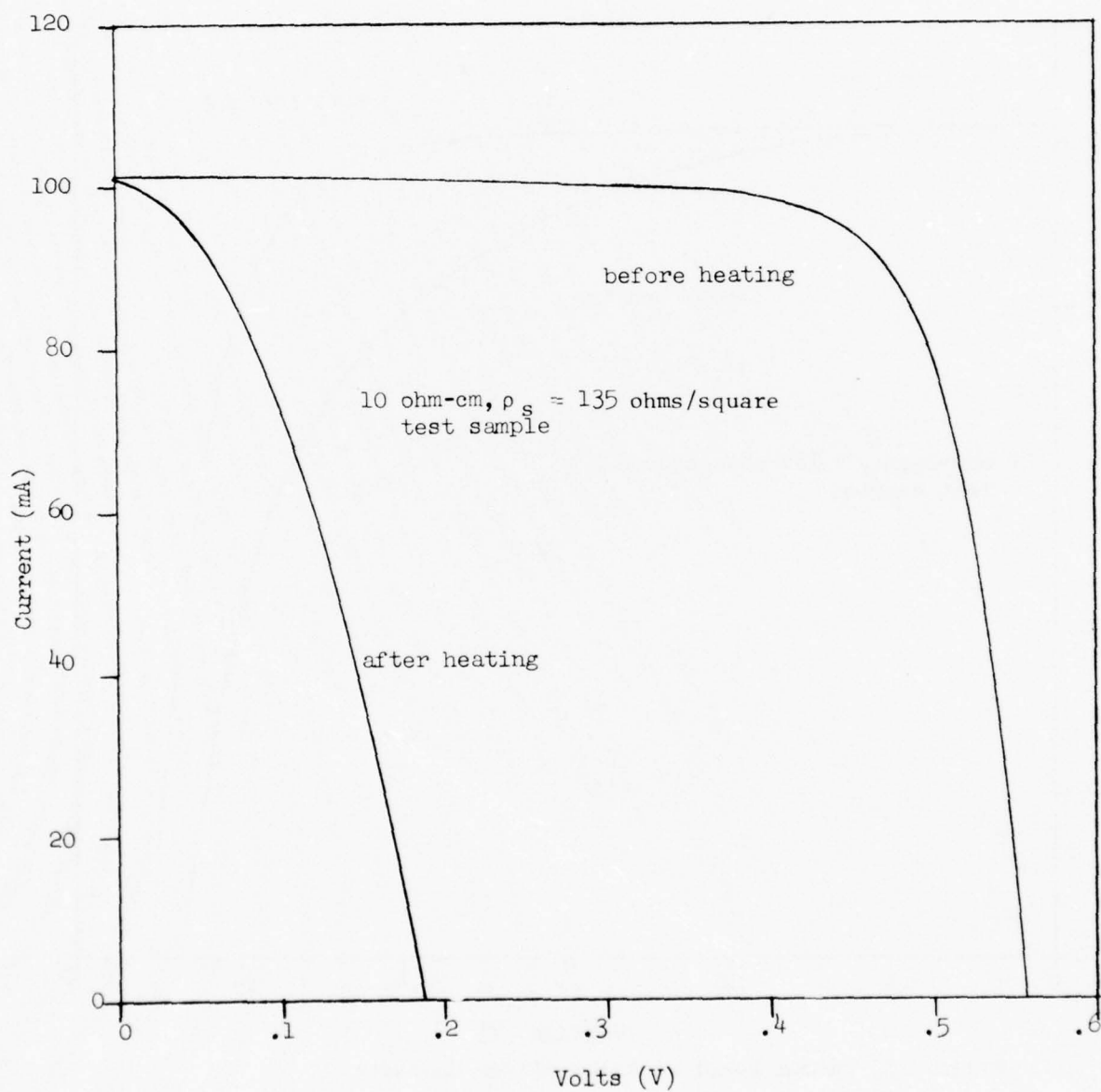


Figure 21. Vacuum Baked Titanium-Silver Contacts

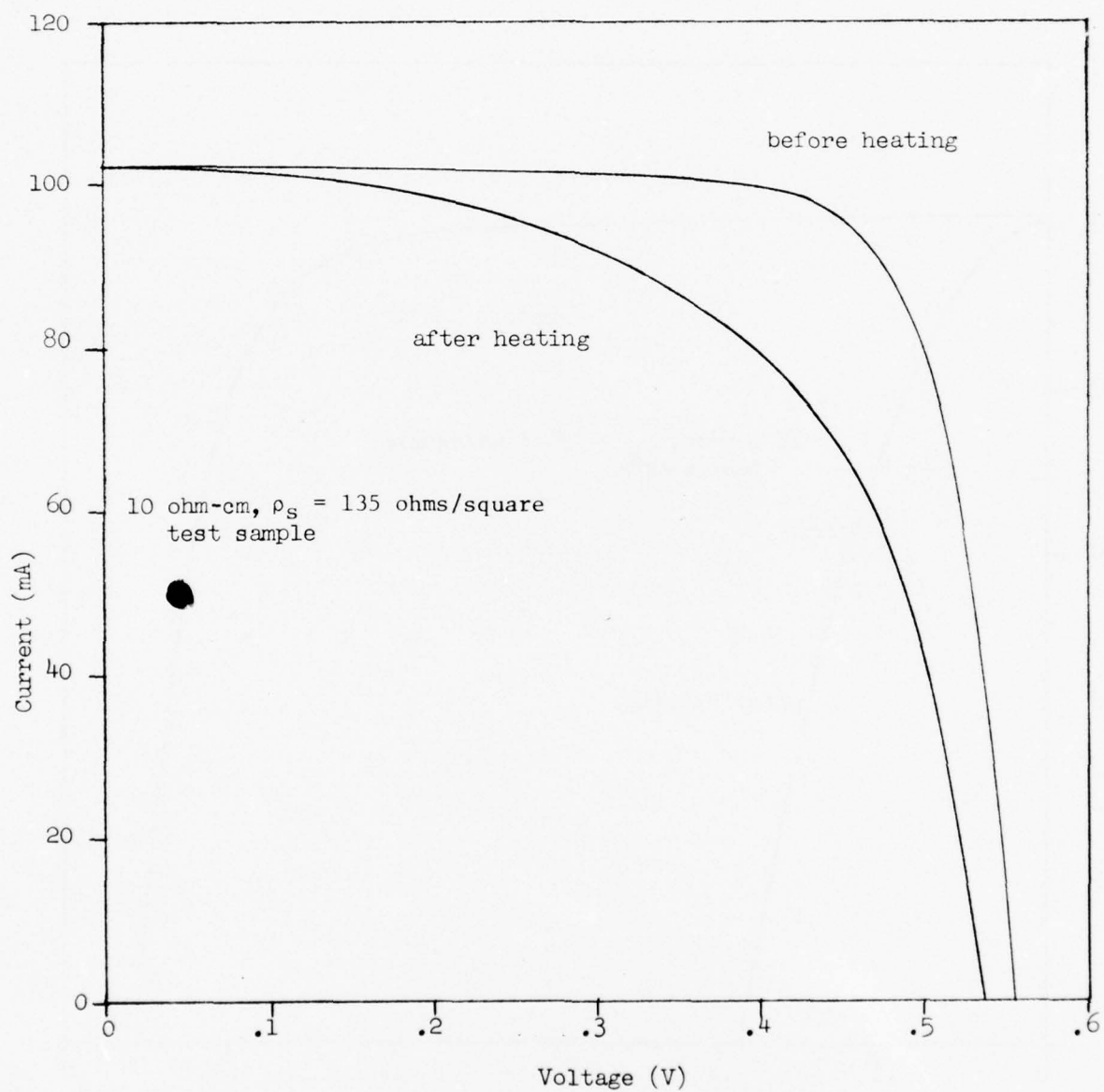


Figure 22. Vacuum Baked Tantalum-Silver Contacts

multiple light impingement it is extremely important that the coating has as high a value of transmission as is possible, since any absorption losses will have a double impact. Since the HESP cell is designed to be as radiation resistant as possible, it is critical that the short wavelength transmission of the AR coating be optimized.

Another very important property of the AR coating is the index of refraction which determines the amount of light lost by reflection when the coated cell is filtered. Crude calculations indicate that an index of refraction between 2.3 and 2.4 for the AR coating will minimize the reflection loss when the cell is filtered. Using optical transmission and refractive index as guidelines results in the conclusion that silicon "monoxide," which has been the standard AR coating for space cells, is not the proper choice. Not only does this material have a relatively low refractive index (1.8-1.9), but it displays significant absorption at wavelengths below 600 nm.

Two higher index AR coatings were evaluated during this program, titanium oxide (TiO_x) and tantalum pentoxide (Ta_2O_5). Both materials could be deposited with a high degree of control and both have been used to replace silicon "monoxide." By using electron beam deposition techniques TiO_x had been obtained that had an index between 2.15 and 2.20, while Ta_2O_5 deposited by the same method had an index between 2.10 and 2.15. Since the variation in refractive index between the two coatings would result in a nearly insignificant difference in output when the cell was filtered, the criteria for acceptance was determined by the optical transmission of these films, especially at very short wavelengths (<450 nm).

TiO_x possesses a natural cut-off at ~ 350 nm due to its bandgap and therefore at this wavelength it is approximately fifty percent absorbing. In contrast Ta_2O_5 transmits almost ninety percent of 350 nm light provided that it is heated in air for a few minutes at $\sim 350^\circ\text{C}$ after deposition. Therefore it was decided to employ the more optically transparent Ta_2O_5 as the HESP cell AR coating.

2.6.2 Coverglass

All space cells employ a protective cover, usually made from fused silica, to prevent low energy protons from severely degrading the cell's output. This cover is bonded to the silicon using a silicone based adhesive which has a refractive index equal to the cover material. There is a large amount of evidence based on ground test data indicating that certain regions of the solar ultraviolet spectrum can cause the adhesive to darken, thus reducing the amount of light transmitted to the cell. To avoid this an ultraviolet rejection filter is deposited on the cover and designed in such a way as to yield a precise cut-off point in the solar spectrum.

The radiation tolerance of silicon solar cells is in large part determined by the amount of short wavelength response that can be obtained. This was the stimulus for developing shallow junction, selectively etched cells. In order to retain the additional short wavelength response, it was necessary to replace the typical 400-410 nm UV cut-off filter with one having a cut-off at 350 nm. This filter is the standard for all advanced cells now being produced for space flight and therefore it was selected for use with the HESP cell.

2.7 Welding Evaluation

One of the main requirements of this program was that the HESP cell be capable of being interconnected without the use of solder. Therefore an investigation of the feasibility of using welded interconnects was initiated. Based on previous experience we decided to evaluate the possibility of using parallel gap welding techniques to weld silver plated molybdenum to the HESP cells. This interconnect material had many attractive properties such as good strength, and a thermal expansion coefficient nearly matching that of silicon.

Preliminary work aimed at establishing boundary conditions for this method of welding was begun using standard chemically polished production cells having relatively deep junctions and titanium-palladium-silver contacts.

Welding parameters such as electrode pressure, gap spacing, weld pulse time and voltage were defined for this type of cell using 37 to 50 μm thick molybdenum tabs plated with between 8 to 20 μm of silver.

Once our experience with this equipment was established, the studies were then extended to 0.010" thick cells having texturized surfaces. Since the textured etching portion of the program had not yet been optimized, the initial texturized cells provided particularly severe conditions for obtaining good reproducible bonds. The maximum strength obtained at first was only 225 grams, with an average 90° peel strength of only 50 grams. The worst electrical degradation was found to be just under 1% per weld, although in a few cases the total power actually improved, unfortunately a result that was associated with low pull strengths.

Activities then concentrated on increasing the amount of silver in the tab/cell contact area, and to obtain more constant surface characteristics by improving the texturizing etch processing. The use of commercially available electrodes having Hughes RWMA-2 shanks and molybdenum-carbide tips was adopted in order to minimize the electrode dressing needed and to reduce the tendency for "sticking" to the silver-plated tabs. Pull tests were also modified to conform with Solar Cell Specification MIL-C-83433, and were henceforth performed at a 45° angle, rather than at 90° .

Increasing the amount of silver in the tab/cell contact area by placing silver foil between the tab and the cell, or by the chemical deposition of additional silver on the molybdenum tab, did not prove to be successful in improving bond strengths. However, it was found that adding a second Ti-Ag metallization over the original deposition gave a substantial improvement in pull strengths. Average pull strengths of 175 grams were obtained, with power degradations of about 1% per weld.

Nearly all of the experiments described above were performed on the "N" contact. This is inherently the more difficult weld to make, since the

weld pad was only 0.033" wide, and the underlying junction can be damaged by improper welds, particularly when the junctions are shallow. The "P" contact welds were easier to make with comparable mechanical strengths to the "N" contact welds, and caused somewhat less electrical degradation of the cells. Some increase in the weld voltage was required however, because of the larger heat sink on the backs of the cells.

The work done until now turned out to be critically influenced by the surface texturing process as was demonstrated by the following test.

Experiments were carried out using more uniform texturized cells having single and double layers of contact metallization (4 and 8 microns). Once the weld parameters had been established fifty welds were made on each type and tested. There were two failures for the single metallized cells and one for the double metallized cells. Approximately half the welds made to the single metallized contacts separated at below 250 gms, but pulled small amounts of silicon, thereby qualifying as retest according to our specification. For the two layer contact cells the retest rate was roughly twenty-five percent of the welds. Welds passing the pull test displayed a narrow range of ultimate strength (400 to 600 grams) with nearly all failures resulting from cell fracture. The electrical degradation per weld averaged 0.3%, with the maximum power loss for a single weld being 1%. Since the requirement for electrical degradation allowed an average degradation of 0.25% per weld (4 welds per cell), these results were encouraging.

At this point it became apparent that the HESP contact system would not employ titanium and therefore our efforts switched to the chromium or tantalum-palladium-silver contact system. For the junction depths (0.10-0.15 μm) being considered, it was found that the electrical degradation was averaging slightly greater than two percent.

A wide variation in pull strength led us to tighten our evaporation schedules to be certain that a fixed amount of silver was being deposited for the cell contacts. Two groups of cells were then selected from a common group having

a sheet resistance of about 90 ohms per square. Front contacts were applied with the same chromium and palladium thicknesses but with the silver thickness adjusted to give total metal thicknesses of 3.5 and 5.0 microns. Interconnect tabs were prepared by evaporating Cr-Pd-Ag onto clean 0.001" molybdenum sheets which were then cut into tabs 0.070" wide. Here the silver thickness was controlled to give total tab metallization thicknesses of 6.0 and 11.0 microns. The results of these variations on weld strengths are shown in Table 8 . It can be seen that the failure rate was decreased by increasing either the cell or the tab silver thickness.

The effect of variations in the metallization thickness on the tab material was further investigated by electroplating 0.001" molybdenum sheet with silver thicknesses of 5, 10, and 15 microns. These sheets were then made into tabs and tested for weld strength using cells having Ta-Pd-Ag front metallization and Cr-Pd-Ag backs. As in the tests using evaporated metallization on the tabs, the percentage of welds passing the pull tests went up dramatically with increased metal thickness. One group of cells was found that had no failures and pull strengths in the 700-900 gram range. Weld strength thus appeared to be improved by either increasing the metallization thickness on the cell or on the tab, but seems to be more sensitive to the variations in tab metallization.

As mentioned previously the electrical requirements specified that the maximum electrical degradation for any one cell be less than 1.5% and that the average degradation be less than 1%. Cells from the same fabrication group were welded using tabs with a 10 micron silver plated metallization. The weld voltage was varied for these experiments and again it was observed that both the electrical degradation and the weld strength decreased for lower weld voltages. The results of these experiments are shown in Figures 23 and 24.

The effect of the cell sheet resistance was then investigated using cells with sheet resistances varying from 30 to 135 ohms per square. These were

TABLE 8

EFFECT OF TAB METALLIZATION ON WELD STRENGTH
AND FAILURE RATE FOR TWO CELL GROUPS

Cell Metallization Thickness	Results of Pull Tests	6 Micron Tab Metallization Thickness	11 Micron Tab Metallization Thickness
5.0 Microns	% Failure (Mean Strength in gms.)	12% (150)	0% (---)
	% Retest (Mean Strength in gms.)	25% (210)	40% (140)
	% Passing (Mean Strength in gms.)	63% (520)	60% (652)
3.5 Microns	% Failure (Mean Strength in gms.)	17% (100)	0% (---)
	% Retest (Mean Strength in gms.)	83% (154)	0% (---)
	% Passing (Mean Strength in gms.)	0% (---)	100% (692)

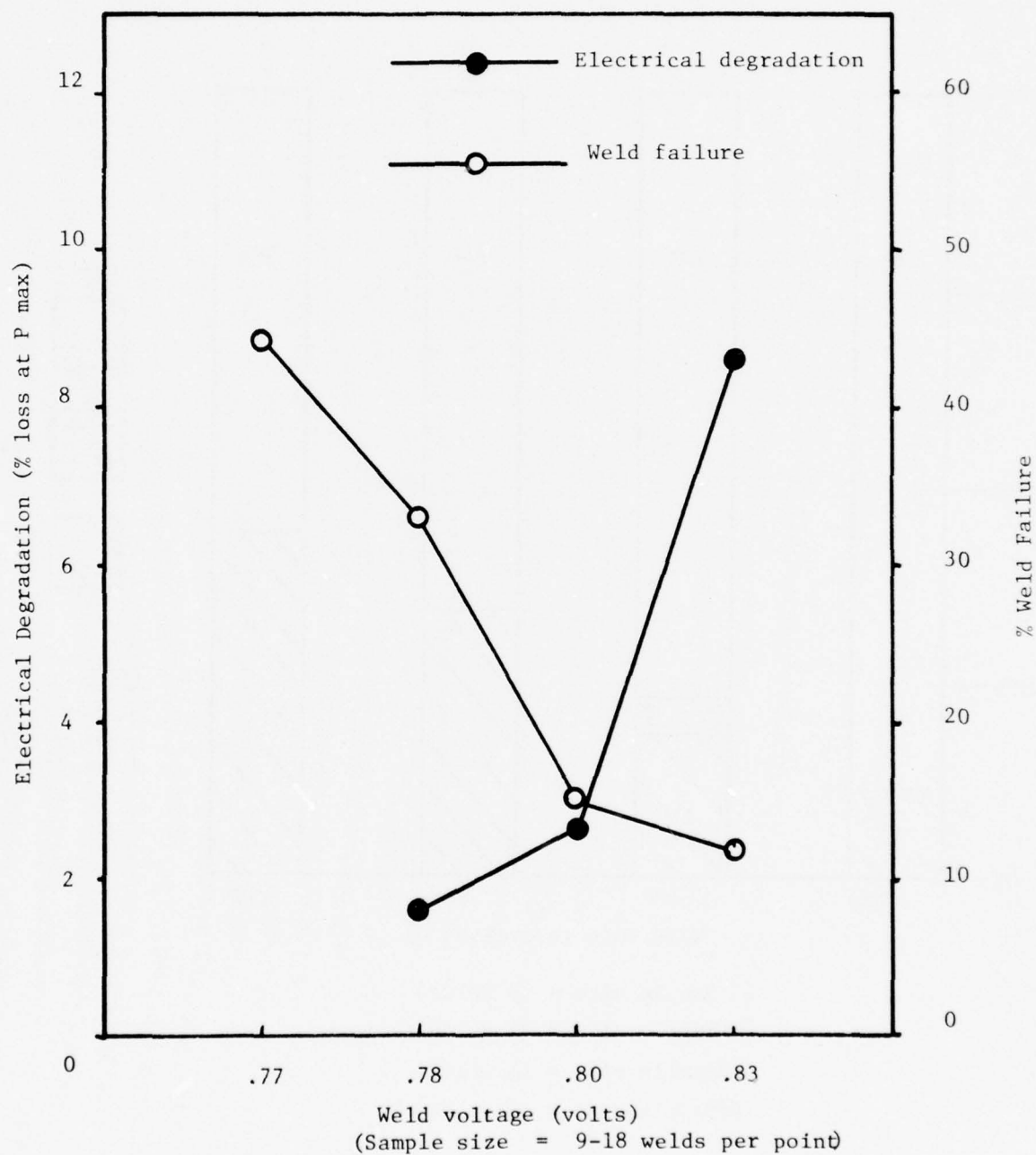


Figure 23. Trade-off of Strength vs. Electrical Degradation for Cells Welded with 10 μ Plated Tabs.

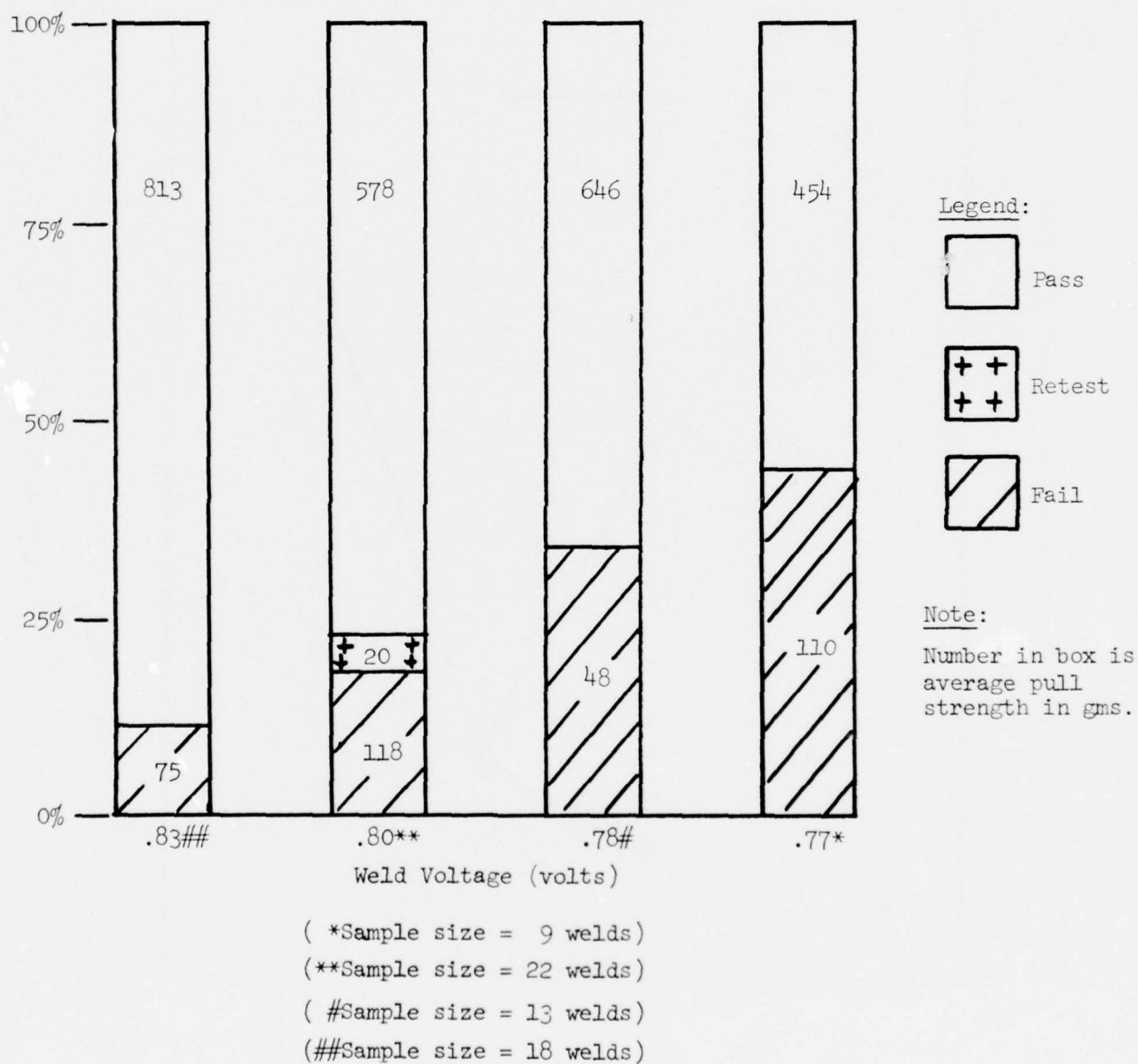


Figure 24. Effect of Decreasing Welding Voltage on Weld Strength and Failure Rate Using 10 μ m Plated Tabs

fabricated with Ta-Pd-Ag front contacts and Cr-Pd-Ag backs. Molybdenum tabs with 10 and 15 microns of evaporated silver were prepared and welded at three different weld voltages. The results for the 15 micron metallized tabs are shown in Figure 25. No 30 ohms/sq. cells were welded with the 15 micron metallized tabs, but with the 10 micron tabs (which had final results entirely similar to the 15 micron tabs) no degradation occurred.

It did not appear that any welding schedule showed promise of achieving welds with both high pull strength and low electrical degradation using silver plated molybdenum. The trend of the data indicated that the thickness of silver was the critical variable and therefore work began using interconnects of pure silver. These interconnects were of mesh form in thicknesses of both .001" and .002".

It was necessary to make significant changes in the welding parameters. The force was increased from 0.5 lb to 1.5 lb., the duration of the weld pulse was shortened to 70 msec, and gap separation was changed to .015". This last mentioned change was very important since it allowed us to minimize the total input energy which had been the major cause of the excessive electrical degradation. Welds made using the silver mesh had low individual pull strengths due to the very small weld area. However by making many welds the total pull strength of the mesh interconnect was brought up to between 500 and 600 grams without introducing unacceptable electrical degradation.

The weld voltage was found to be a function of the cell size, which side (front-back) was being welded, and whether the cell was filtered or uncovered. As the cell size increased the weld voltage had to be increased from 0.78 to 0.83 volts in order to obtain a high strength back contact weld. This can be understood by considering the fact that energy could be more easily dissipated over the back contact in the case of large area cells. The weld voltage for the front contact, which was small in all cases with respect to the back contact area, was optimized at 0.72 volts for all sizes. However when the cell was filtered the weld voltage for the front contact could be reduced to even lower values.

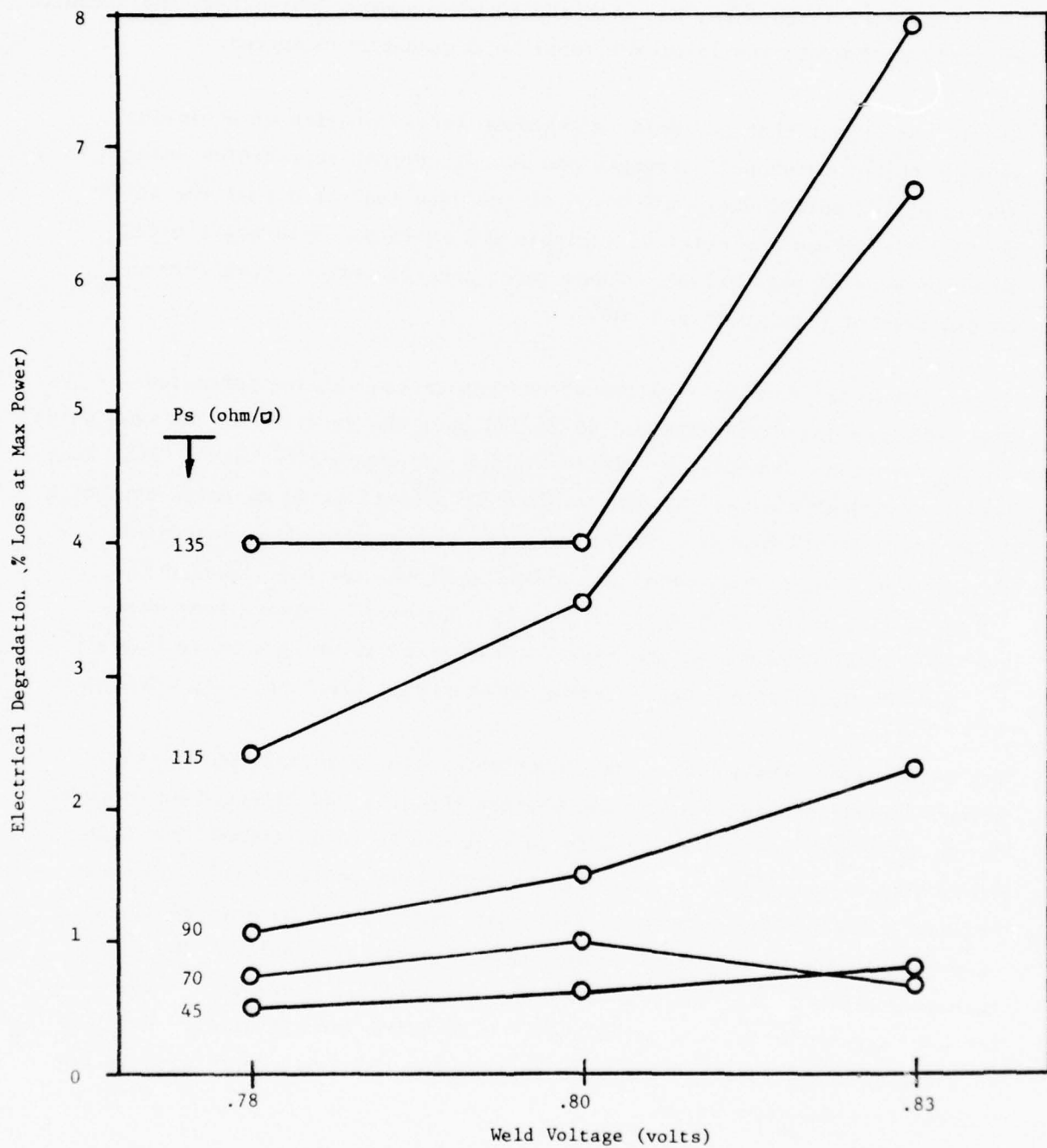


Figure 25. Degradation of Cells with Various Diffusion Depths
Using 15 μ Plated Tabs

The finalized silver interconnect was .001" mesh cut into a rectangular pattern 0.200" wide by 0.500" long. This interconnect was bonded by making three separate equally spaced welds. Prior to the welding, the mesh was baked in air at $\sim 350^{\circ}\text{C}$ for two minutes to drive off any unwanted surface film. Mesh which did not receive this treatment would not give reliable welds.

Cells with extremely shallow junctions ($\rho_s \sim 135$ ohms/square) were successfully interconnected using silver mesh. Four interconnects, requiring a total of twelve welds were attached to each cell for in-process pull tests. In no case was the amount of degradation greater than the allowable 1.5 percent maximum and the average amount of electrical degradation observed was well below the 1.0 percent requirement. More detailed information on welding test results is given in later sections of this report.

2.8 Process Integration

Combining the selective etch with an optimized diffusion was the first and most difficult step in process integration. Texturizing caused an enhanced energy absorption at all useful wavelengths, permitting an increase in short circuit current of about 6.5%. Shallow diffusions of approximately 130 ohms per square produced short circuit current gains of 8% over conventional diffusions. Unfortunately, when nonreflecting cells with shallow diffusions were contacted, drastic loss in curve shape was experienced. This loss in fill factor was directly attributable to shunting and not series resistance changes.

Four potential explanations for this behavior were postulated. These included handling damage, thin junction sections, and metallic contamination either from the sodium hydroxide etch or from the contact metallization itself. Initial investigations had shown the etched surface to be exceedingly sensitive to handling procedures. Surface tetrahedra were found to easily chip, allowing areas of P-type material to be exposed which could shunt the cell if covered by contact metal. Such fracturing could occur during ultrasonic cleaning operations and normal tweezer handling steps. As a consequence,

ultrasonic agitation prior to diffusion was instituted to remove any low strength tetrahedra, and a minimum of handling, using only narrow tipped metal tweezers, was prescribed for minimizing operator produced damage. Efforts to establish a firm correlation between etch type (size and number of tetrahedra) and handling sensitivity were inconclusive, so a sacrifice in double reflectivity for handling durability was not deemed warranted.

It was postulated that the presence of surface tetrahedra would result in a nonuniform diffusion cross section, the peaks of the pyramids being heavily doped and the interstices presenting extra thin junction cross sections. These thin sections would probably be highly sensitive to contact shunting. Samples of polished wafers with junction depths similar to what may have been present at the thinnest spot on texturized cells failed to confirm this mechanism for poor curve shape.

Since neither handling nor thin junction section seemed singularly responsible for fill factor loss, a hydrochloric acid cleaning sequence was instituted prior to diffusion. It was assumed that iron residue from the hydroxide texturizing etch might remain on the wafers causing the silicon to be contaminated. This treatment also failed to produce a consistent improvement in curve shape, although, by this time occasionally groups of excellent cells were being manufactured. This fact alone implicated the contact metals being used. Possibly trace impurities in the base metal layer were diffusing through the junction or the base metal was incapable of preventing the palladium passivation layer from migrating through the junction. Once tantalum was substituted for titanium on the front a high degree of consistency was introduced into fill factor. It is not possible to attribute any one change to this improvement. It can only be stated that an elusive combination of appropriate contact system and silicon surface condition resulted in ultimately obtaining consistently good curve shape.

The next step involved an empirical analysis of the optimum number of gridlines. Cells having sheet resistances of 120 ohms/square were contacted

with 8, 9, 10, 12, 16 and 18 grids per cm. Curve fill factors did not improve with more than twelve grids per cm, values of 0.79 to 0.80 being typical. Cells with higher sheet resistances (i.e. 200 ohms/square) showed twelve grids per cm to be ample, although shunting by the contact metal became a problem. Twenty-four gridlines per 2 cm x 2 cm cell was thus selected as optimum.

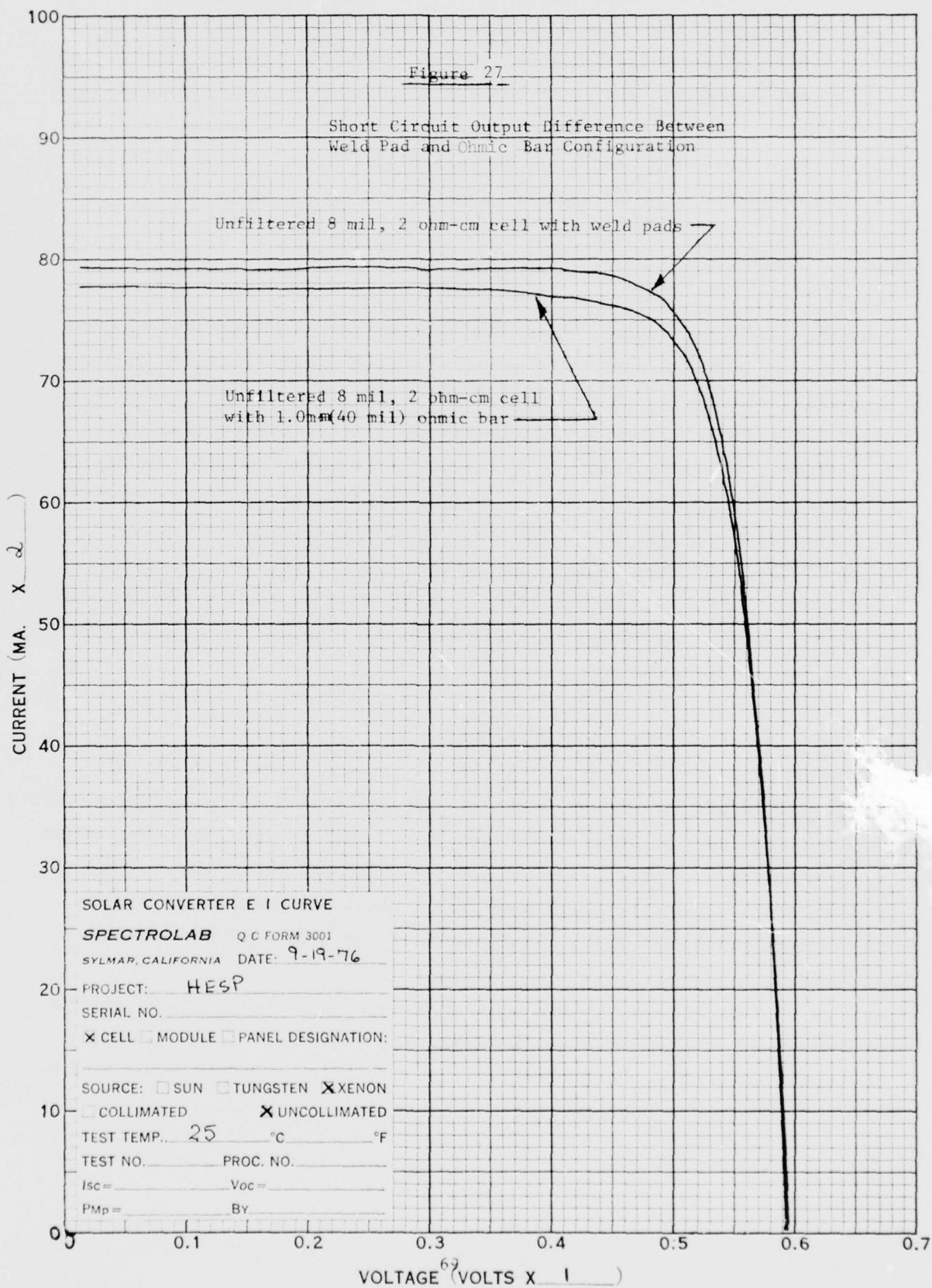
The state-of-the-art in bimetallic masking technology permitted 0.025mm (0.001") slots to be etched in the tooling used to obtain gridlines on our cells. However, the actual line dimension printed was approximately 0.037mm (0.0015"). The central section of the grid had a well defined plateau region extending the one mil mask width while the additional width was in the form of a fillet with disjoint fringes which can be seen in Figure 26. This "penumbra" was responsible for a significant loss in active area with no advantage by way of reduced series resistance.

Attempts were made to remove the penumbra using hydrochloric or nitric acid or a sodium cyanide solution. None were successful owing to the galvanic couple which forms to liberate hydrogen and cause anodic dissolution of the base metal. Such action resulted in peeling of the gridlines. To circumvent this problem an etch was developed using ammonium hydroxide and hydrogen peroxide. This solution causes the formation of silver oxide which is highly soluble in alkaline solvents. It was then possible to obtain a sharply defined gridline with no chemical residues which could potentially affect humidity sensitivity.

The original high efficiency cell concept included the use of weld pads rather than a conventional ohmic bar to increase active area. This idea was abandoned for three reasons. First, the coverglass would be expensive to shape. Second, the filter adhesive would be difficult to remove from the weld pad notches without irreversible cell output damage. The third and most pragmatic reason was the need for industry to retool if the ohmic bar were eliminated. Figure 27 provides a comparison between an unfiltered 8 mil, 2 ohm-cm cell with weld pads and one with a 1.0 mm (40 mil) ohmic bar. The ohmic bar cell was approximately two and one half percent lower in output than the original pad design.



Figure 26. Gridline Metallization Fringes



It had originally been planned to employ only one tooling configuration, the 2 x 6 cm size, and then dice the large cell into the smaller configurations using a high speed saw. This approach had worked successfully on conventionally etched cells, but the textured surface did not allow this concept to be employed. When diced the textured cells developed a severe reduction in output at load which could not be restored by edge etching. Therefore it was necessary to design separate tooling for each configuration.

2.9 Pilot Production

Once the development phase of the HESP program was concluded, formal documentation of all processes to be employed to produce the baseline cell was prepared. In addition to this a formal quality assurance plan was written which defined the various in-process and qualification tests that were to be performed to verify that the cell was being manufactured in conformance to the specification and to assure that the cells were capable of meeting the requirements of the specification. The original HESP specification was MIL-C-83443A, "Military Specification Cells, Solar, Silicon, General Application For." This was modified to bring it into conformance with the tentative Standardized Solar Cell Specification being prepared by a joint effort between NASA and DOD.

2.9.1 Manufacturing Control Document

The key to formal documentation was the preparation of a Manufacturing Control Document for the HESP solar cell assemblies. This is given as a supplement to this report. By definition the Manufacturing Control Document (MCD) is a description of all the steps used in the manufacture and test of units in order to provide that the requirements of the specification are met.

Included within the MCD are all applicable documents either used by Spectrolab or referenced in the HESP specification. A process flow chart showing all the steps involved in the manufacture and testing of the HESP assemblies makes

up another section of the MCD. A copy of all the lot travelers used in the production of the assemblies comprises another section of the MCD. Also included within this document is a complete HESP solar cell assembly drawing as well as a section that describes those requirements of the specification that may be certified rather than verified by testing. The final portion of the MCD contains the quality assurance instructions for performing and evaluating the results of the in-process verification tests as well as the qualification test requirements of the HESP specification. A copy of the MCD was submitted to the contracting agency on 1 October 1976.

2.9.2 HESP Assembly Fabrication Process - Baseline Cells

Figure 28 shows the process flow chart for the preparation of the silicon wafers used in the production of the baseline HESP solar cells. Three configurations were fabricated; 2 x 2 cm, 2 x 4 cm and 2 x 6 cm. Each configuration was made from nominal two ohm-cm crucible grown p-type silicon. The allowed resistivity range was from one to three ohm-cm. As will be discussed, this variation in resistivity seemed to have a significant impact on cell output, with the cells made from the lower end of this range having higher electrical outputs. The "as cut" silicon blanks were examined for mechanical defects such as chips, fractures and gross blade marks which would be caused by improper cutting techniques. Only those blanks which had passed this screening were accepted for use in the pilot production phase of the HESP program.

Figure 29 is a schematic representation of the processes used to fabricate completed solar cell assemblies for the HESP program. Since some of these process steps are considered company proprietary they will not be discussed in any great detail. Those wafers received from the Spectrolab Crystal and Mechanical Department were first etched in a thirty percent solution of sodium hydroxide in order to remove the sawing damage. This entails the removal of between .005" and .006" of silicon to ensure a damage free wafer. Although our etching studies had shown that the depth of damage was in the order of .001", previous experience in production had indicated that the "true" depth of damaged material was more in the order of .002" to .003" on a side. After the initial etch, one side of the blank was masked and then the blank was textured using a two percent sodium hydroxide solution modified

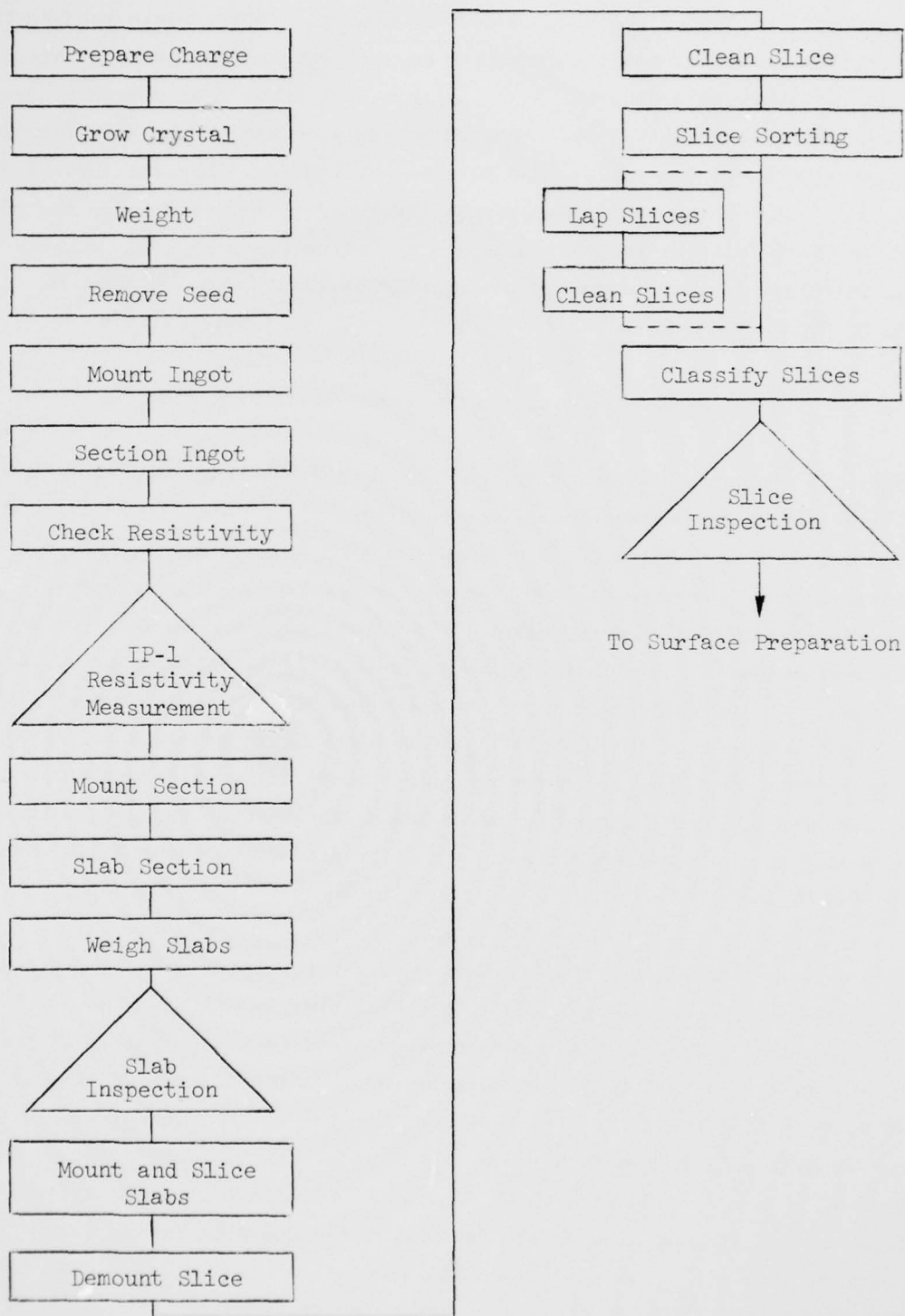


Figure 28. Crystal/Mechanical Processing

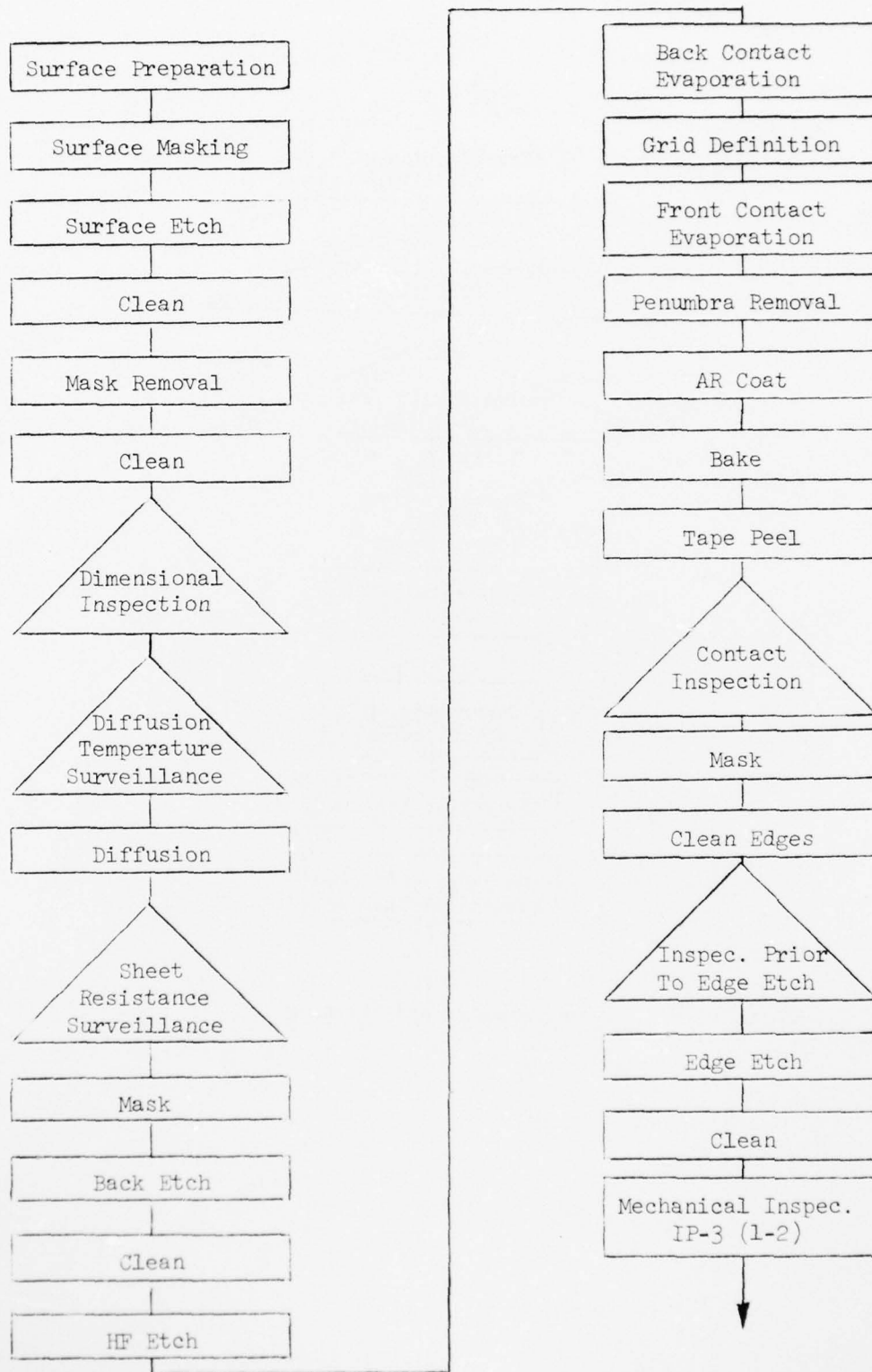


Figure 29. Diffusion and Final Processing

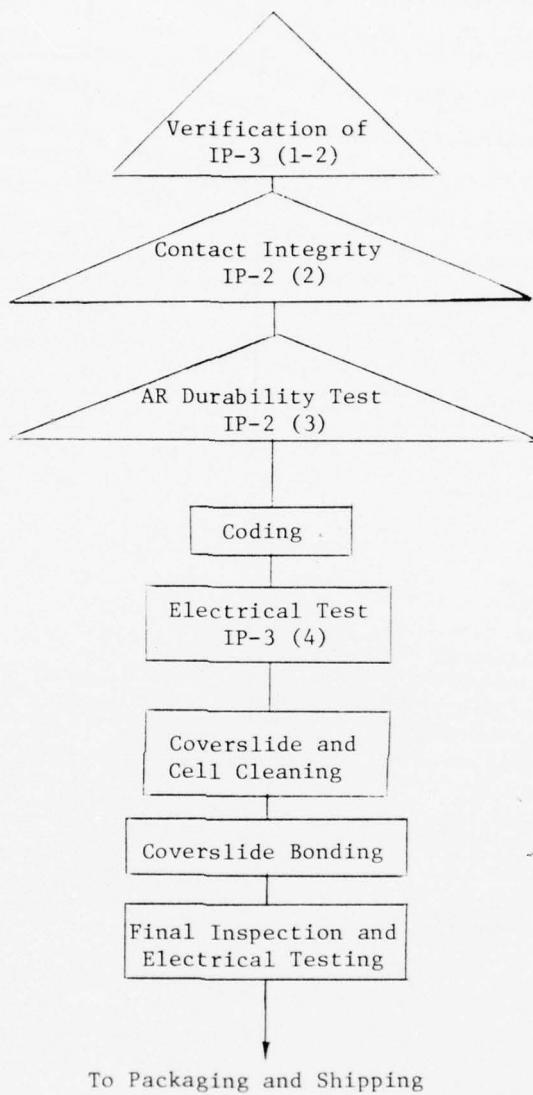


Figure 29. (Concluded)

with isopropyl alcohol. After removing the mask material and cleaning the blanks, they were checked for thickness and linear dimensions using the appropriate sampling plan.

The blanks were then diffused using phosphine gas as the dopant source. The target sheet resistance was between 100 and 140 ohms/square, corresponding to a junction depth on the order of 0.1 μm . After diffusion the blanks were sampled to ensure that the proper sheet resistance had been achieved. This was followed by back etching to remove the junction from the back side of the wafer. After cleaning the masking ink from the parts, a dilute solution of hydrofluoric acid was employed to remove the phosphorous diffusion glass on the front side just prior to loading the parts into the contact masks.

The contact depositions were done in the Spectrolab cell production coater, a two chamber Airco Temescal fast cycle vacuum coater which uses electron beam heating for metal deposition. The back contact was a three component layer consisting of $\sim 800 \text{ \AA}$ of chromium, followed by $\sim 500 \text{ \AA}$ of palladium, then 3.5 μm of silver. Before applying the front contacts the evaporation was terminated and the masks modified by a proprietary Spectrolab procedure in order to obtain optimized grid definition. After a second pump-down the front contact system consisting of $\sim 800 \text{ \AA}$ of tantalum, $\sim 400 \text{ \AA}$ of palladium and $\sim 5.0 \mu\text{m}$ of silver was deposited under a vacuum of below 1×10^{-5} Torr.

Upon removal from the evaporator, the cells were then treated in a solution which removes any unwanted overspray of silver on the gridlines. This procedure yields gridlines which are well defined with an average width of .001". The cells were then AR coated in the production programmable Airco Temescal fast cycle coater. After this step the cells are baked in air at $\sim 300^\circ\text{C}$ for 2 minutes to eliminate any short wavelength absorption. This process also ensures that the back contact is ohmic to the silicon. At this point all the baseline cells were tape tested using Scotch Brand #810 tape to test the contact adherence. Only one percent of the

2 x 2 cm configuration did not pass this test, which is an excellent showing. In the case of the 2 x 4 cm cell the loss at this test was well below one percent. The 2 x 6 cm cells had a four percent loss, but seventy-five percent of the total number of 2 x 6 cm cells that failed came from one evaporation lot in which the electron beam accidentally struck the graphite crucible, producing contaminated silver.

The final cell processing step was to edge etch the parts to eliminate any metal that may have been evaporated over the cell edge and to guarantee that there is no junction except at the top surface of the cell. After cleaning the masking ink from the cells, the lots are then inspected for mechanical imperfections such as chips, contact voids, stains and out of tolerance contact dimensions. Those cells passing this screening were then sampled to test for weldability and AR coating durability. Following this the parts were electrically tested and coded to retain lot identity. The cells were then filtered and given a final electrical test before packaging for shipment.

2.9.3 HESP Assembly Fabrication Process - Hybrid Cells

In addition to the baseline cell it was decided to produce a spectrum of HESP type cells in which the thickness and resistivity were varied. Table 9 lists those types that were evaluated along with the initial output power goal. These cells were to be in the 2 x 2 cm configuration and would use the baseline contact configuration consisting of twelve grids/cm and a .040" wide ohmic bar. Four types would be non-field cells while the other seven types would employ back surface fields. These cells would be characterized with respect to their radiation and radiometric properties. All but the .004" thick cells would be covered with 350 nm cut-on fused silica slides that were .009" thick.

TABLE 9
HESP HYBRID CELL MATRIX

Type	Thickness (mils)	Resistivity (ohm-cm)	BSF	Initial Power (mW)
1	12	2	Yes	79
2	12	10	No	72
3	8	2	Yes	78
4	8	10	Yes	78
5	8	30	Yes	78
6	8	100	Yes	75
7	8	2	No	75
8	8	10	No	70
9	4	10	No	57
10	4	100	Yes	70
11	4	10	Yes	68

The non-field cells were made using the same processing steps as for the baseline HESP cells. The field cells naturally required additional processing steps in order to incorporate the BSF effect. This processing was done as previously described in Section 2.4.2 of this report. The only other processing variation was the elimination of the tape peel test in the case of the very thin (.004") cells to avoid breakage. These cells did not undergo the normal mechanical inspection or the welding and AR durability tests since the basic process had already been qualified by the baseline HESP cell.

2.9.4 Production Test Results - Baseline HESP Cells

Table 10 is a statistical breakdown of the thirteen pilot production lots of 2 x 2 cm baseline HESP cells showing where the cells were lost during fabrication and test. The line loss data includes cell breakage and processing errors. As can be seen from this table lot E was responsible for nearly 60 percent of the total line loss. This occurred when the masking ink used in edge etching was improperly cured and the etch penetrated to many

TABLE 10
2 x 2 HESP PILOT PRODUCTION DATA

Lot	Starts	Line Loss	Tape Test	Mech. Insp.	In-Process Tests	Electrical	Yielded
A	26	0	1	11	3	1	10
B	27	1	0	3	6	4	13
C	48	0	0	3	11	0	34
D	48	0	0	4	3	9	32
E	88	31	0	4	13	7	33
F	95	0	0	5	9	12	69
G	95	0	0	5	6	17	67
H	96	7	3	8	1	33	44
I	96	6	1	4	1	36	48
J	96	8	1	6	8	40	33
K	96	0	2	4	0	35	55
L	96	2	2	6	0	44	42
M	96	0	0	5	11	6	74
	1003	55	10	68	72	244	554

of the cells. Mechanical inspection losses fell into four categories; (1) dimensional rejects such as cells with narrow or misaligned ohmic bars, (2) chips and nicks (3) contact voids and (4) miscellaneous such as stains, AR voids and the like. In-process testing losses were from the required contact integrity and AR coating durability tests. These losses are not realistic since mechanical rejects could, and for the other configurations were, used for these destructive tests. An electrical reject is defined as any cell with an output less than 17.5 mW/cm^2 when tested at 25°C .

Table 11 shows the electrical distribution of the cells tested. It can be seen that lots H through L had an extremely low electrical yield. An examination of the crystal lot travelers showed that the resistivity of the silicon used in these lots ranged up to the limit of 3 ohm-cm, while for the other lots the highest resistivity used was 2.6 ohm-cm. Since the load point for electrical testing was chosen to be 500 mV, relatively high resistivity material would have a severe impact since the test point would be beyond the maximum power point. In other words many of the reject cells may have delivered 17.5 mW/cm^2 at a load point lower than 500 mV.

The electrical yield from test based on a minimum cell output of 70 mW is 69.4 percent with an average power of 72.1 mW, equivalent to an AMO efficiency of 13.3 percent. To illustrate the impact on yield that higher average requirements would have, total yield based on 1003 starts as a function of average power desired is plotted in Figure 30. For a comparison of cost versus power requirements, an arbitrary price of unity is assigned to the maximum yield obtained and the price based entirely on yield is calculated for a twenty percent yield. In order to obtain approximately 1.5 percent more power, the cost per cell would rise by a factor of 2.25, an incredible penalty!

Table 12 presents the results of the in-process contact integrity screening. For this test four welds, two front and two rear, are made on a sample of cells from each production (evaporation) lot. In order to pass this test

TABLE 11
2 x 2 HESP ELECTRICAL DISTRIBUTION

Lot	Tested	I_L (mA) at 500 mV									
		<140	140-142	142-144	144-146	146-148	148-150	150-152			
A	11	1	5	5							
B	17	4	4	6	2	1					
C	34	0	1	12	6	7	4	4			
D	41	9	4	7	12	9					
E	40	7	7	10	10	4	1	1			
F	81	12	5	14	20	22	7	1			
G	84	17	12	17	26	7	5				
H	77	33	21	10	10	3					
I	84	36	5	15	21	5	2				
J	73	40	13	12	6	2					
K	90	35	20	23	9	2	1				
L	86	44	5	9	13	8	6	1			
M	80	6	11	14	33	12	4				
	798	244	113	154	168	82	30	7			

73.5
73.0
72.5
72.1
72.0

\bar{P}_{max}
(mW)

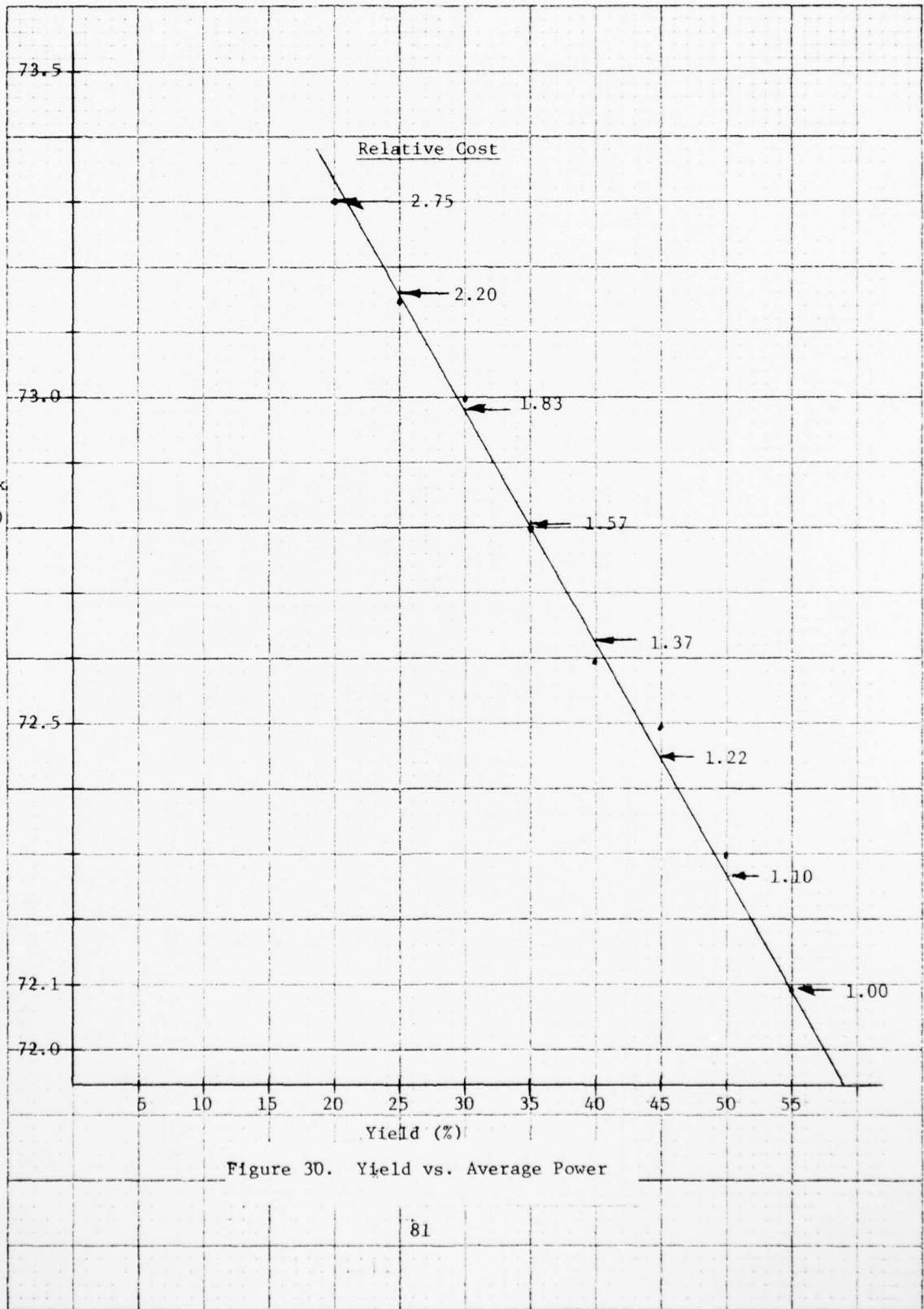


Figure 30. Yield vs. Average Power

TABLE 12
CONTACT INTEGRITY TEST RESULTS
(2 X 2 CM)

Lot	Electrical Change (%)	Front Contact (gms)	Range (gms)	Back Contact (gms)	Range (gms)
A	+0.3	567	700-450	708	800-650
B	0	438	550-250	750	800-700
C	-0.2	550	650-400	633	750-450
D	-0.1	525	650-450	750	800-700
E	-0.1	417	600-300	783	900-700
F	0	483	600-300	692	750-600
G	0	433	500-350	667	800-450
H	+0.8	592	700-500	642	800-500
I	+0.3	500	650-350	583	700-450
J	0	645	800-500	605	750-400
K	0	450	800-200*	508	650-350
K	-0.2	655	800-400	505	700-350
L	+0.1	508	600-350	492	700-300
M	0	395	600-20*	483	650-300
M	-0.1	620	800-250	448	700-275

*weld test failure (retested)

the average electrical degradation must be less than 1.0 percent with no single cell having greater than 1.5 percent loss at the appropriate test point. Each weld is then pulled to destruction with the requirement that no single weld have less than 250 gms pull strength. In the event of a failure, a larger sample is chosen and tested. Using the sampling plan of the MCD, acceptance was based on zero failures testing twelve individual welds, or one failure for a total of thirty-two welds. Of the 13 lots tested, two had to be retested at the more stringent level and they successfully passed. Included in this table are the average as well as the range of pull strengths obtained.

Similar data for the 2 x 4 and 2 x 6 HESP configurations is given in Tables 13 through 15. Both the electrical yield and the average output of these cells was once more influenced by the resistivity of the silicon used. The majority of the silicon used for the 2 x 4 cm cells had a resistivity between 1.6 and 1.9 ohm-cm, while the 2 x 6 cells came from silicon with a range of 2.6 to 2.9 ohm-cm. The average efficiency of the 2 x 4 cm cells was 13.65 percent as compared to 13.1 percent for the 2 x 6 cm parts. The electrical yield data based on a minimum cell efficiency of 12.9 percent (17.5 mW/cm^2) confirms this observation. The lower resistivity 2 x 4 cm cells had an electrical yield of 93.4 percent while the higher resistivity 2 x 6 cm cells only yielded 57.5 percent.

The yield data given in Table 13 shows a significant increase in line loss for the 2 x 6 cm cell configuration. This was caused by problems in edge etching. The extremely long edge was more difficult to clean prior to etching and this caused an increase in cell breakage. Another manifestation of this problem is reflected in the extremely high loss rate for the mechanical inspection phase. The majority of the 2 x 6 cm cells rejected at this point were chipped or had evidence of etch leakage which attacked the ohmic bar. In contrast the 2 x 4 cm configuration had acceptable line losses (less than 4 percent) but an extremely high reject rate in mechanical inspection. This was caused by an error in tooling which produced cells with ohmic bars located away from the edge. Since the cell was to be a zero gap design, this constituted a reject situation.

TABLE 13
HESP PILOT PRODUCTION DATA
2 X 4 AND 2 X 6

Lot	Starts	Line Loss	Tape Test	Mech. Insp.	In-Process Tests	Electrical	Yielded
(2 x 4) N	120	12	0	24	0	7	77
O	172	3	0	48	0	0	121
P	87	3	2	19	0	9	54
Q	98	2	0	29	0	2	65
R	98	3	0	20	0	9	66
	575	23	2	140	0	27	383
(2 x 6) S	163	19	5	27	1	49	62
T	96	18	1	8	0	16	53
U	72	7	17	20	0	24	4
V	96	1	0	22	0	37	36
W	96	3	0	16	0	26	51
	523	48	23	93	1	152	206

TABLE 14
2 X 4 AND 2 X 6 HESP ELECTRICAL DISTRIBUTION

Lot	Tested	I_L (mA) at 500 mV											
		<280	280-284	284-288	288-292	292-296	296-300	300-304	304-308	308-312			
N	84	7	12	14	17	24	10						
O	121	0	1	2	4	11	20	25	43	15			
P	63	9	10	5	13	16	10						
Q	67	2	1	3	10	18	23	10					
R	75	9	8	13	5	15	13	10	2				
(2 x 4)	410	27	32	37	49	84	76	45	45	15			
		<420	420-424	424-428	428-432	432-436	436-440	440-444	440-444	444-448			
S	111	49	22	12	16	7	4	0	1				
T	69	16	19	7	12	9	2	4					
U	28	24	3	1									
V	73	37	17	11	6	2							
W	77	26	24	15	8	3	1						
(2 x 6)	358	152	85	46	42	21	7	4	1				

AD-A043 382

SPECTROLAB INC SYLMAR CALIF
HIGH EFFICIENCY SOLAR PANEL (HESP). (U)
JUL 77 J SCOTT-MONCK, C GAY, P STELLA, F UNO

F/G 10/2

UNCLASSIFIED

AFAPL-TR-77-36

F33615-75-C-2028
NL

2 OF 2
AD
A043382

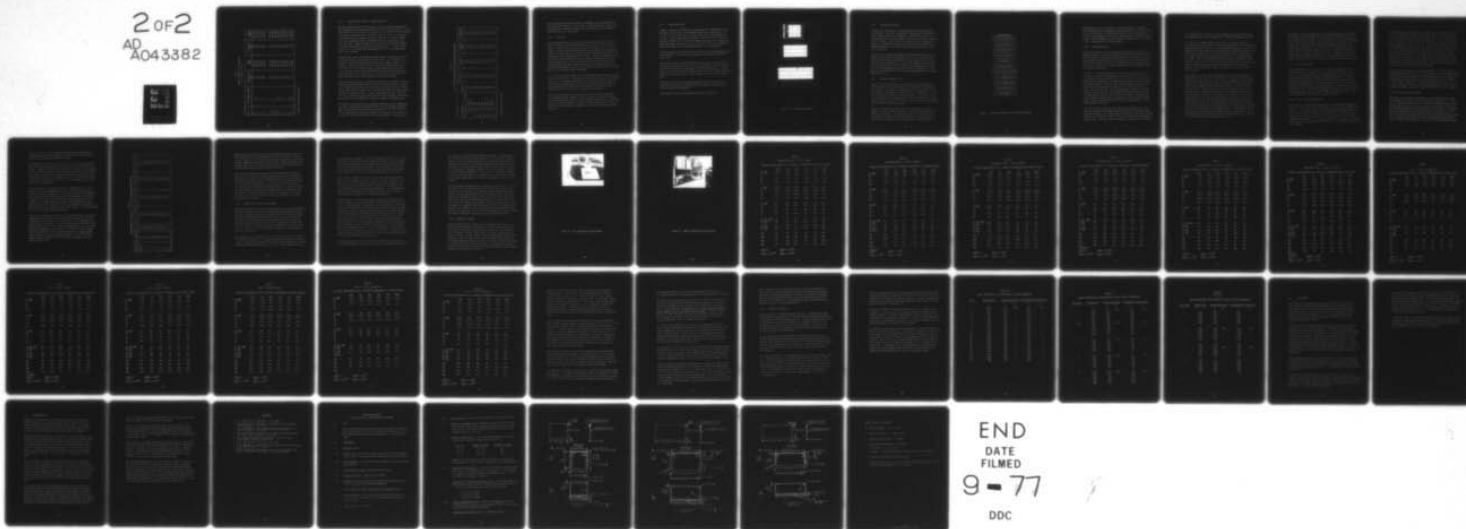


TABLE 15
CONTACT INTEGRITY TEST RESULTS
(2 X 4 AND 2 x 6 CM)

Lot	Electrical Change (%)	Front Contact (gms)	Range (gms)	Back Contact (gms)	Range (gms)
N	0	558	650-450	700	900-500
O	-0.1	517	600-450	508	600-400
P	0	583	700-500	567	700-300
Q	0	483	600-400	583	650-550
R	0	600	650-550	550	600-500
S-1	0	658	750-600	492	700-300
S-2	0	667	800-500	767	900-700
S-3	0	725	800-550	683	700-600
S-4	-0.5	658	800-450	633	800-500
T	-0.2	617	700-550	675	700-600
U	0	483	600-400	467	650-200*
U	0	480	650-400	498	600-275
W	+0.1	575	700-450	525	700-400
X	-0.1	550	600-500	533	600-500

*weld test failure (retested)

2.9.5 Production Test Results - Hybrid HESP Cells

The hybrid HESP cells were not subjected to the same thorough examinations and in-process tests as the baseline parts, but lot travelers were kept. From these travelers it was possible to calculate a line loss value, and by assuming a mechanical inspection reject rate equal to that of the 2 x 2 cm baseline cell a projected total mechanical yield was obtained. In order to compare one cell type against another, an arbitrary yield of fifty percent from start was taken. Using this figure it was possible to provide the minimum cell power output and the average power for the entire lot. This is given in Table 16. As another basis for comparison the 2 x 2 cm baseline HESP cell is also included.

The mechanical yield on the HESP hybrids shows that for non-BSF cells there is little difference between .008" and .012" cells. At .004" there is a significant reduction in mechanical yield due to a higher incidence of cell breakage. However the nearly 70 percent yield does indicate that even a very thin cell can be fabricated under present manufacturing conditions. In all honesty it must be admitted that filtering and interconnecting techniques suitable for thin cells have yet to be developed, but these results would argue that future efforts along these lines are warranted.

Field cells show a reduction in mechanical yield which is directly attributed to the additional processing steps required to form the BSF effect. However these results once more point out that there is relatively little difference between .008" and .012" thick cells. Once more the .004" cell shows a drastic reduction in mechanical yield. It must be concluded that thin field cells are not yet ready for mass production, but the power performance demonstrated here should act as a stimulus for further work aimed at increasing yield.

The output of the various cells is extremely important since it demonstrates the impact of texturizing and the BSF effect on the relationship between power and resistivity as a function of thickness. In the case of nonfield cells, comparing cells varying in thickness by a factor of three shows that the gain in initial output power is only fourteen percent. The field cell

TABLE 16
2 X 2 HYBRID HESP ELECTRICAL SYNTHESIS (UNFILTERED)

Cell Type	Starts	Mech. Yield (%)	Min. Cell (mW)	Avg. Power (mW)	Efficiency (%)
Baseline (2 Ω -cm, .011")	1003	79.0	70.0	72.3	13.4
2 Ω -cm, .012" P+	234	73.5	73.0	75.5	14.0
2 Ω -cm, .008" P+	323	77.5	74.0	76.9	14.2
2 Ω -cm, .008"	238	84.5	70.0	71.7	13.2
10 Ω -cm, .012"	319	85.5	67.7	69.7	12.9
10 Ω -cm, .008"	220	86.5	65.8	67.2	12.4
10 Ω -cm, .004"	443	69.5	59.0	60.9	11.3
100 Ω -cm, .008" P+	212	70.5	73.0	74.4	13.7
30 Ω -cm, .008" P+	286	71.5	74.0	75.6	14.0
10 Ω -cm, .008" P+	389	68.5	72.4	76.2	14.1
10 Ω -cm, .004" P+	398	31.0	70.0*	74.5*	13.8*

*Based on 25% Total Yield

matrix indicates that there is almost no dependence on either thickness or resistivity with respect to initial power. However when these various cells are subjected to radiation a distinction can be made as will be discussed in Section 2.10.3 of this report.

2.9.6 Filtering

All baseline HESP cells as well as all the hybrid HESP cells greater than .004" in thickness were filtered using .009" fused silica covers having a MgF_2 AR coating on the front surface and a 350 nm cut-on filter on the rear surface. Although the filtering operation was performed using standard procedures, the sensitivity of the textured surface required much greater care in handling to avoid degrading the cell output. There was a definite correlation between power appreciation and the personnel involved in the various filtering operations. The key steps that had the most influence were the first and final cleaning. These processes required removal of the excess R63-489 bonding adhesive and if not done with care the edges would be damaged and the cell curve shape would be degraded.

If all steps were done properly the cell would show an appreciation in output from one to two percent. However many cells showed no gain or a loss ranging from one to three percent, especially for the first few hundred cells that were filtered. Measurements of short circuit current before and after filtering showed gains of from one to three percent, but this was offset by reductions in curve fill factor of from two to five percent.

The only other problem that was observed in the filtering operation was excess adhesive bubble formation. This was traced to the sharp definition of the gridlines which resulted from the penumbra removal etch. An alternate method of curing the adhesive solved this problem although many of the 2 x 6 HESP cells have what would be considered to be unacceptable adhesive bubble formation.

2.9.7 Module Fabrication

A number of modules were fabricated to demonstrate the compatability of the developed cells with basic panel assembly techniques. Three each of 2 cm x 2 cm, 2 cm x 4 cm and 2 cm x 6 cm cells (with covers) were assembled in circuits of three parallel by three series. For the 2 cm x 2 cm cells the substrates consisted of .5 inch thick aluminum honeycomb, with .1 inch thick epoxy glass sheet used for the 2 cm x 4 cm and 2 cm x 6 cm cell assemblies. Micaply was bonded to the aluminum honeycomb for circuit isolation.

Cell interconnections were made using 1 mil thick .2 inch wide (approximately) silver mesh tabs, with circuit end terminations formed from 1 mil thick silver sheet.

Two tabs were used for series connections on the 2 cm x 2 cm and 2 cm x 4 cm cell modules and three for the 2 cm x 6 cm cell modules. The P-P parallel-ing interconnections used a single mesh tab between adjacent cells in all modules. Tab stress loops were formed between cells in the series and parallel directions to minimize stress. Each cell bond consisted of three separate welds.

Although formal module electrical performance tests were not required, "quick look" measurements indicated that the assembly techniques did not incur any significant degradation.

A photograph of typical finished modules is shown in Figure 31.

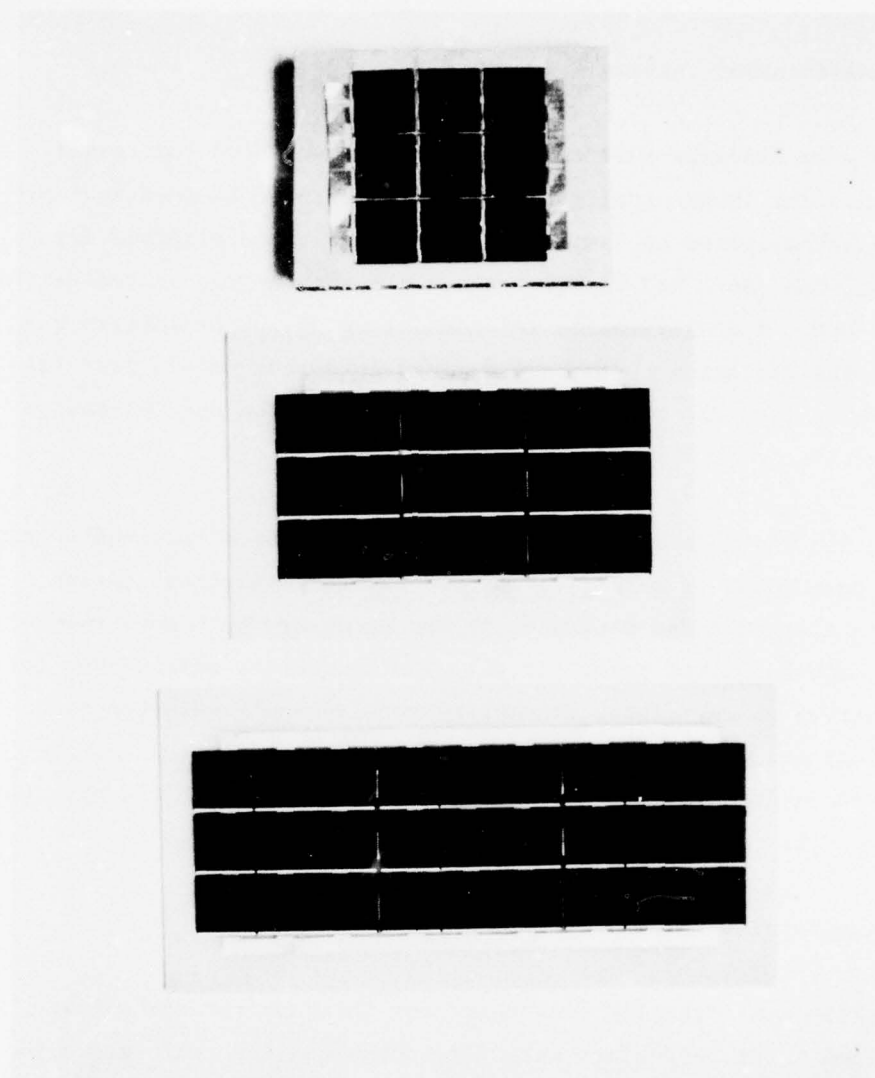


Figure 31. Assembled Sample Modules

2.10 Qualification Testing

The HESP 2 x 2 cm baseline cell configuration was selected for formal qualification. The larger configurations, manufactured by identical processes would be qualified by similarity. In order to be eligible for qualification, the parts had to have passed all the in-process verification tests of the MCD. A qualification lot consisting of 300 assemblies was formed. The qualification tests were divided into four categories; (1) temperature-humidity, (2) thermal cycling, (3) radiation and (4) radio-metric properties.

Sample selection was made according to MIL-STD-105D which required twenty samples for each phase of qualification. Since the radiation testing employed both electrons and neutrons, it was necessary to choose twenty samples for each radiation test. In all, 100 assemblies were chosen for the qualification phase. These assemblies were randomly selected from each electrical grouping such that the electrical distribution of these samples was representative of the electrical distribution of the original qualification lot.

2.10.1 Temperature-Humidity Test

Figure 31 is the qualification flow chart for the temperature-humidity testing portion. The assemblies were first examined for conformance to the electrical and mechanical requirements of the specification. Tabs were welded to each sample followed by testing for conformance to the electrical degradation allowance of the specification. The results of this test were excellent, the average output of the welded assemblies actually showed a slight increase of 0.25 percent with the greatest single assembly degradation observed being 1.3 percent.

The welded assemblies were then placed in an environmental chamber programmed to provide a minimum temperature of 45°C and a minimum relative humidity of 90 percent. After 30 days of exposure to these conditions, the samples were removed, once more examined for mechanical defects and then electrically tested. The average degradation in performance was

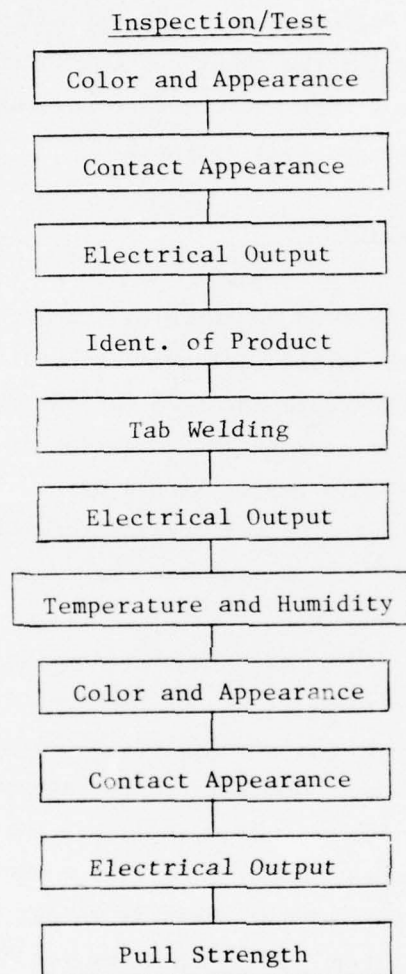


Figure 32. Temperature-Humidity Qualification Flow Chart

0.20 percent, with one cell showing 1.6 percent degradation. Therefore the HESP assemblies had successfully passed this phase of qualification since one reject was allowed. Following this the welded contact integrity was verified. Pull strengths for the front contact averages 545 gms with a range of 350 to 700 gms obtained. The back contacts averaged 615 gms with a range of 500 to 750 gms observed for pull strength.

2.10.2 Temperature Cycling

The results of this test were not meaningful since the weld tab proved to be improperly designed for the artificial cycling conditions experienced by the welded assemblies. The procedure employed for the cycling was a poor choice since extraneous influences such as the formation of ice crystals severely influenced the results of this test. Before discussing the details of this test, the test steps prior to thermal cycling as well as those planned after cycling will be discussed.

The sample of assemblies (20 parts) was screened for conformance to all the mechanical and electrical requirements of the specification. The acceptance number for these tests was one reject, the same as for the temperature-humidity qualification phase. Assembly weight averaged 513 mg, well below the allowable maximum of 575 mg. This indicated that the samples were well within the allowed thickness tolerance of $.011 \pm .001$ " for silicon and $.009 \pm .002$ " for the filter. Total assembly weight is made up of silicon, contacts, adhesive and filter. Allowing 12 mg for the contacts and 20 mg for adhesive leaves 481 mg. Since the filter is usually on the high side of the tolerance specification, an assumption of 230 mg was made for glass weight. Thus the weight of the silicon, 251 mg, corresponds to an average cell thickness of 10.5 mils.

After this series of inspections and tests, tabs were welded to the assemblies and these parts underwent verification testing for electrical performance after welding. The average change in electrical output showed a slight increase of 0.15 percent, similar to the results obtained in the temperature-humidity phase. The twenty samples ranged from a degradation of 0.7 percent

to an enhancement of 0.3 percent. The assemblies were then thermal cycled from liquid nitrogen (-195°C) temperature to $+100^{\circ}\text{C}$ under ambient conditions.

For this test the welded assemblies were placed on screens which were in turn held within a wire basket. The basket was immersed in a Dewar containing liquid nitrogen, held there until the thermocouple attached to a sensing cell registered the proper temperature, then removed and immediately placed inside an oven set at 140°C until the sensing cell reached 100°C . After approximately two hundred cycles some tabs from the top layer of assemblies began to separate. The test was terminated and a new holder configuration was designed to prevent the tabs from encountering the wire mesh of the basket. Even with the new method of holding the welded assemblies, tabs continued to separate. It was decided to complete the 1000 cycles in order to obtain electrical data.

Upon completion of 1000 cycles the assemblies were once more examined for mechanical defects then electrically tested. The change in electrical performance was slightly positive, with an average improvement of 0.40 percent with the worst single assembly degrading by slightly less than one percent. However those assemblies still possessing tabs (six) all failed the pull strength test. An examination of the failed tabs indicated that the mesh had been severely deformed between welds in the perpendicular direction. This deformation was directly attributable to the formation of ice crystals beneath the mesh. The constant stress from the ice acted to separate the mesh from the contacts. The failure mechanism on cell fronts was in many cases a tearing of the mesh leaving the welds still attached to the contacts. On the back contact there was no delamination of the evaporated silver contact from the silicon nor did any residual mesh remain. It would appear that the failure was at the weld interface between the mesh and the contact. This is in keeping with the observed failure modes encountered during lot acceptance tests in which the mesh is pulled from the silicon.

Although the thermal cycling phase of this qualification must be classified as a failure, it is not certain that the results are meaningful in view of the problem with ice formation. It is obvious that in the space environment such an event could not occur. However attempting to perform this test under vacuum would be extremely costly and time consuming and therefore these results must stand as they are. The failure of the tabs may have been completely induced by the test conditions or may be indicative of potential failure modes that might be encountered in space. Techniques to avoid the latter possibility might involve the use of an expanded silver mesh or a "T" shaped stress relief loop to alleviate both intercell and interweld stresses.

2.10.3 Radiation Testing

The hybrid HESP cells were included in this phase of qualification. The planned test matrix for both the electron and neutron radiations called for twenty 2 x 2 cm baseline HESP cells and one hundred and ten HESP hybrids representing ten samples from each designation (see Table 9). However problems in obtaining type 10 hybrid cells (.004" 100 ohm-cm BSF) caused a reduction in these matrices to an initial sample size of 125 cells for the electron tests and 124 cells for the neutron tests. After the first electron radiation (3×10^{14} electrons/cm²) additional type 10 cells became available and they were substituted for a small number of other hybrid types. There were no additional cells used for the neutron testing.

2.10.3.1 Electron Radiation Testing

The assemblies and cells were irradiated at 1 MeV using the JPL Dynamitron facility. Prior to the initial test complete I-V curves for all samples were taken at six temperatures between -20 and +100°C under AMO conditions (135.3 mW/cm²) using a Spectrosun^R Mark III solar simulator. Pertinent data such as short circuit current, open circuit voltage, maximum power, voltage at maximum power and curve fill factor was obtained for each sample. A detailed description of the apparatus and the technique used is provided in Section 2.10.4 of this report.

At JPL the assemblies were mounted to aluminum plates using Apiezon grease in order to obtain good thermal contact. The plates in turn were attached to a water cooled block within the test chamber and the cell temperature was held at between 25 and 30°C during the irradiation. The tests were conducted under a vacuum better than 1×10^{-5} Torr. Each plate held eighteen samples and seven plates were used for the test. For the first test a fluence rate of 3×10^{11} e/cm²/sec was employed. The samples were removed from the plate after testing and returned to Spectrolab for electrical testing over the same range of temperatures. Prior to the retest all samples were held at 60°C for forty-eight hours to fully anneal them. It has been observed that storage at room temperature for a period of thirty days will induce a significant amount of radiation damage recovery. It has also been shown that one to two days at 60°C will provide the same result.

After retesting the samples, a second irradiation of 7×10^{14} e/cm² was performed using a fluence rate of 3×10^{11} e/cm²/sec. The cells and assemblies were retested using the previously described method and then returned to JPL for the final test which resulted in the parts receiving a total fluence of 1×10^{16} 1 MeV electrons/cm². For the final test the fluence rate was 1×10^{12} e/cm²/sec. After the two day annealing period the final electrical tests were performed. This data is given in Section 2.10.4 of this report.

2.10.3.2 Neutron Radiation Testing

Those parts to be irradiated with neutrons were initially measured at AMO (135.3 mW/cm²) using the Spectrosun^R Mark III solar simulator. I-V curves for each sample were taken at 25°C. The HESP cell assemblies plus the eleven Hybrid assembly groups were then irradiated with fission spectrum neutrons at the Northrup Research and Technology Center's TRIGA Reactor. The experiments were conducted within the Northrup Reactor Dry Exposure Room. The neutron fluence levels were measured with two button dosimeters placed between the six assembly holder boards, which were arranged in an arc equidistant from the exposure room window area. The cell to shielding distance varied

from 14" to 12.5". The post-irradiation measurements for radiation and contamination check of the assemblies were taken with a USM-4 and SP-11 probe and a gas proportional automatic counter.

The assemblies were initially taped to 5" x 7" x $\frac{1}{2}$ " thick styrofoam boards using Scotch brand mending tape. The .004" thick cells were placed into "pockets" formed with masking and mending tapes. However after irradiation with 9.0×10^{10} neutrons/cm² it was found that the adhesive of the mending tape separated from the backing material and adhered to the glass filter. Cleaning the surface of these assemblies proved very difficult, therefore on subsequent irradiations, the "pocket" type of attachment to the boards was used for all assemblies.

After irradiation, all cells were "cooled" at Northrup until the specific activity of a typical assembly reached $1-7 \times 10^{-4}$ microcurie per gram, thereby considered nonradioactive. At this level the cells and assemblies were returned to Spectrolab and placed into a preheated oven at 60°C for a minimum of 48 hours. At the end of this anneal period, the cells and assemblies were electrically checked under 1 Sun AMO conditions, 25°C, then replaced into the "pockets" on the styrofoam boards and returned to Northrup for the next irradiation until a total fluence of 1×10^{13} neutrons/cm² of 1 MeV equivalent energy was attained.

Table 17 is a summary of the results of the neutron testing. The original program goal for the HESP cell was an output of 70 mW for the 2 x 2 cm configuration after a fluence of 1×10^{11} n/cm². The revised goal due to the decrease in active area of the cell should have been ~ 68.3 mW. Power outputs ranging from 71.5 to 61.7 mW were obtained, with eight cell groups equaling or exceeding the revised goal. At 1×10^{12} n/cm² the original and revised goals were 51 mW and 49.8 mW respectively. Outputs ranged from 59.3 mW to 55.2 mW for the groups tested. For 1×10^{13} n/cm² the samples delivered from 41.4 mW to 45.5 mW, well in excess of even the original goal of 35 mW.

TABLE 17
MAXIMUM POWER AS A FUNCTION OF 1 MeV FISSION SPECTRUM NEUTRON FLUENCE

Cell Type	No. Samples	$\phi = 0$	$\phi = 9 \times 10^{10} \text{ n/cm}^2$	$\phi \times 10^{12} \text{ n/cm}^2$	$\phi = 7 \times 10^{12} \text{ n/cm}^2$	$\phi = 1 \times 10^{13} \text{ n/cm}^2$
Baseline	20	72.8	68.0	57.0	44.5	43.3
1	10	77.5	67.9	55.2	42.5	41.4
2	10	70.6	67.4	57.1	45.7	44.8
3	10	78.7	71.2	57.7	44.9	43.8
4	10	78.0	71.5	58.3	46.3	45.5
5	10	77.7	70.1	56.9	45.3	44.5
6	10	76.1	68.2	55.7	43.7	42.8
7	10	72.5	68.2	56.6	43.6	42.2
8	10	67.6	65.3	57.1	45.1	43.9
9	10	62.6	61.7	57.3	46.8	45.2
10	5	73.4	70.1	58.2	44.7	42.5
11	10	75.5	71.3	59.3	47.0	45.4

These excellent results conflict with the expected performance based on the electron test data. The conversion factor relating neutrons to electrons is on the order of 2×10^3 electrons per neutron. Applying this correction and then comparing the equivalent electron results shows a significant discrepancy between the actual data and what would be expected on the basis of the conversion factor relating neutrons to electrons.

Since this large difference between theory and measurement was apparent before the test series was concluded, annealing effects were investigated. What was to have been the final irradiation resulted in a total fluence of 7×10^{12} rather than the desired 1×10^{13} n/cm². After an additional dose of 3×10^{12} n/cm² to complete the test, the samples were tested prior to the two-day "bake" at 60°C, then retested afterward. An increase in power output of from 1.9 to 4.2 percent was observed after the annealing cycle, not enough to explain the variation observed. Thus we can only conclude that there was an error in dosimetry or that the conversion factor which was applied is not correct.

2.10.4 Temperature Coefficient Measurements

Although technically not a part of the HESP qualification, these measurements were made in conjunction with the electron radiation testing phase and for the sake of program consistency are included within the qualification phase. The data was obtained by measuring the I-V power curve of each cell subjected to electron radiation testing and from these curves collating the important electrical properties of the cell. Measurements were made prior to the irradiation test series, then after each fluence level so that four sets of I-V curves, taken at six different temperatures, were generated for each cell in the test.

The equipment used for measuring the I-V characteristic curves at six different temperatures consisted of a standard gas pressure actuated test fixture having a vacuum hold-down, mounted within a thick-walled aluminum test chamber. The chamber measured approximately 10" x 10" x 4" (inside dimensions) and

was fitted with a hinged lid. The lid was constructed with a 4" x 4" opening directly over the cell location on the test fixture. The test chamber had provision for placing a quartz window over this opening, however this was not used during these investigations. The chamber was so constructed as to be gas tight, with all electrical, vacuum, gas, and liquid nitrogen fed through the rear wall of the enclosure using appropriate fittings.

Since the quartz window was not used in these measurements, dry nitrogen was fed into the chamber, providing a positive pressure environment. The gas was so fed into the chamber as to form a curtain of flowing nitrogen across the top of the fixture in order to prevent frost build-up on the test sample during the low temperature measurements. This arrangement also allowed cells or assemblies to be readily placed in the test fixture or removed without any necessity for raising the hinged lid.

An insulated gas line was connected from a liquid nitrogen storage tank to the test chamber, and provision was made to electrically control the flow of the nitrogen by means of a manually switched solenoid valve. The liquid nitrogen was conducted through the base plate of the test fixture and then exhausted into the room using a sound reducing muffler. Two small cylindrical heating elements were imbedded in the base block of the test fixture, which were connected in parallel and driven by a variable AC power input. The base plate of the test fixture was a thick plate of solid copper to which were attached two iron-constantan thermocouples. These thermocouples were fed through gas tight fittings in the side wall of the test chamber. During these experiments only one of these thermocouples was used, namely the one that was located closest to the cell under test. During the initial setup procedures it was found that the readings at various temperatures for the two thermocouples were almost identical.

Locating markings on the table below the solar simulator assured that the test chamber, whenever used, would be always in the same geometrical location.

The standard cell used to assure identical intensity of illumination was also located by means of fiducial marks on the lid of the test chamber. Figure 32 shows the chamber setup for cell testing with the standard cell monitoring the intensity. Correlation checks were run during the setup operations to establish the 25°C short circuit current values for a test cell, designated a "secondary standard," in the test chamber, as compared to the 1037 primary standard cell. New values for the primary standard cell were then established for its location on the lid of the test chamber by comparing readings against the "secondary standard" cell in the test chamber.

Copper-constantan thermocouples were soldered to each of three test cells, one 0.004" thick, one 0.008" thick, and one 0.012" thick. These cells were each in turn placed in the test fixture and the heater and liquid nitrogen controls manipulated to hold the temperature of the cell at the various test temperatures, namely -20°C, +5°C, +25°C, +50°C, +75°C, and +100°C. For each case the thermocouple readings for the base block of the test fixture were measured and recorded. Once this had been done it was now possible to adjust the base block temperature to a given value corresponding to the thickness of the cell under test and be reasonably certain that the cell was within 0.5°C of the desired temperature. Figure 33 shows the complete temperature testing setup used for these measurements.

2.10.4.1 Analysis of Results

Tables 18 through 29 are a summary of the temperature data taken on the baseline and hybrid HESP cell designs as a function of electron fluence. The amount of information contained in these tables is quite substantial and it is beyond the scope of this report to attempt to explain all the results in detail. Unless otherwise noted each item of data represents the average of a ten cell sample in the case of the HESP hybrid cell types. The baseline HESP data came from a twenty cell sample. Rather than attempt to reduce the data into a particular format, it was decided to present it in raw form in order that any interested parties could put it into a format germane to their particular interests.

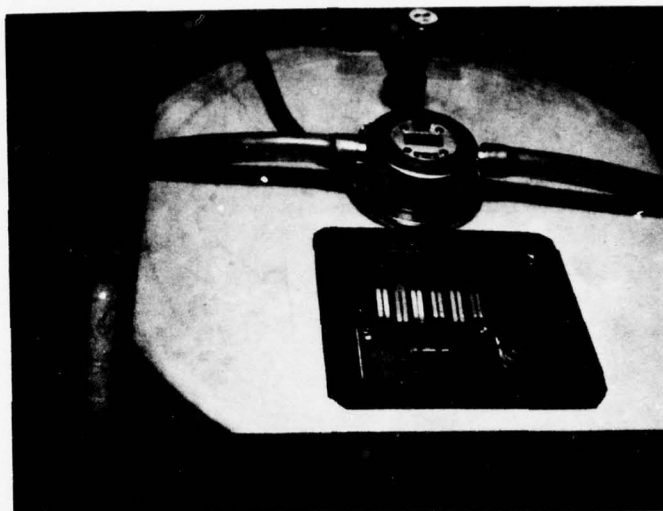


Figure 33. Cell Temperature Testing Chamber

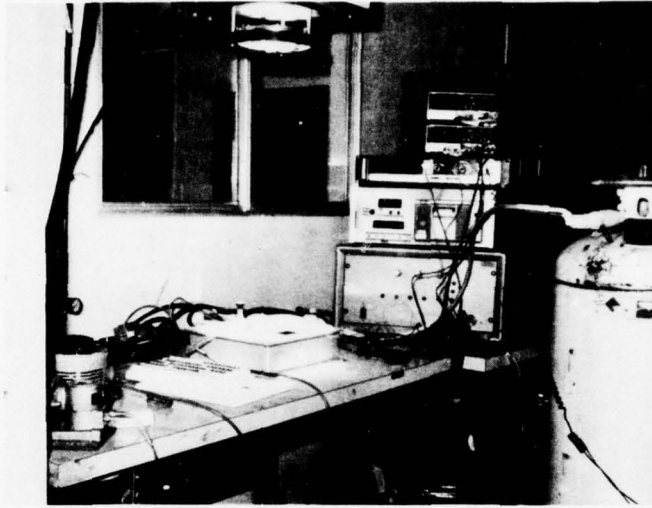


Figure 34. Complete Temperature Testing Set-Up

TABLE 18

BASELINE HESP CELL .279 MM 2 OHM-CM

ELECTRICAL CHARACTERISTICS AS A FUNCTION OF TEMPERATURE AND ELECTRON FLUENCE

	-20	+5	+25	+50	+75	+100
P_o (mW)	82.6	78.6	73.3	65.2	57.3	48.3
P_1	67.7	64.1	60.5	54.5	48.1	41.3
P_2	60.5	57.7	53.9	48.8	43.3	36.8
P_3	44.4	42.2	39.6	35.9	31.6	26.6
I_o (mA)	155.8	158.7	159.9	161.9	164.1	166.7
I_1	132.2	136.0	139.4	144.1	147.8	153.3
I_2	121.4	125.2	128.3	133.5	137.9	143.0
I_3	95.2	99.7	104.4	109.6	114.7	119.9
V_o (mV)	669	626	586	530	477	416
V_1	658	599	556	500	448	393
V_2	641	587	541	484	432	375
V_3	602	542	494	443	390	335
$V_o (P_o)$ (mV)	570	534	498	441	390	332
$V_1 (P_1)$	548	505	469	413	364	315
$V_2 (P_2)$	535	496	455	399	350	294
$V_3 (P_3)$	498	456	411	362	311	258
FF_o	.792	.791	.783	.760	.733	.696
FF_1	.778	.788	.780	.756	.726	.685
FF_2	.777	.786	.778	.755	.726	.683
FF_3	.773	.780	.769	.741	.706	.663

$$\begin{array}{ll}
 X_o/\emptyset = 0 & X_2/\emptyset = 1 \times 10^{15} \\
 X_1/\emptyset = 3 \times 10^{14} & X_3/\emptyset = 1 \times 10^{16}
 \end{array}$$

TABLE 19

HESP HYBRID TYPE 1 .30 MM 2 OHM-CM P+

ELECTRICAL CHARACTERISTICS AS A FUNCTION OF TEMPERATURE AND ELECTRON FLUENCE

	-20	+5	+25	+50	+75	+100
P_o (mW)	90.6	84.1	78.2	69.8	62.1	53.0
P_1	68.1	62.9	59.0	53.2	46.9	40.7
P_2^*	60.7	55.9	52.6	47.1	42.1	35.8
P_3^*	44.0	40.7	38.2	34.6	30.5	25.4
I_o (mA)	160.2	163.5	165.2	167.0	169.3	170.9
I_1	129.1	133.3	136.9	141.7	145.3	151.1
I_2^*	119.1	122.7	126.9	131.2	136.1	141.5
I_3^*	93.3	97.6	102.8	107.7	113.2	118.7
V_o (mV)	705	650	607	551	501	443
V_1	659	598	555	497	446	391
V_2^*	642	581	537	479	429	370
V_3^*	599	537	490	436	383	326
$V_o(P_o)$ (mV)	621	566	520	461	412	355
$V_1(P_1)$	579	516	471	413	363	314
$V_2(P_2)^*$	560	500	454	395	346	292
$V_3(P_3)^*$	520	458	409	356	306	251
FF_o	.802	.792	.780	.758	.733	.700
FF_1	.800	.790	.777	.756	.725	.689
FF_2^*	.794	.784	.771	.750	.721	.684
FF_3^*	.788	.777	.760	.735	.703	.657

*8 samples

$$X_o/\phi = 0$$

$$X_2/\phi = 1 \times 10^{15}$$

$$X_1/\phi = 3 \times 10^{14}$$

$$X_3/\phi = 1 \times 10^{16}$$

TABLE 20

HESP HYBRID TYPE 2 .30 MM 10 OHM-CM

ELECTRICAL CHARACTERISTICS AS A FUNCTION OF TEMPERATURE AND ELECTRON FLUENCE

	-20	+5	+25	+50	+75	+100
P_o (mW)	83.1	77.1	70.5	60.8	51.6	41.5
P_1	69.5	65.1	60.5	53.2	45.9	36.7
P_2	62.5	58.3	54.2	47.7	40.8	32.8
P_3	47.0	44.5	41.2	36.7	29.3	24.1
I_o (mA)	156.3	159.3	161.3	162.6	164.9	166.8
I_1	137.7	143.4	147.6	153.1	156.5	160.0
I_2	127.2	132.6	138.3	143.2	147.9	152.7
I_3	105.1	112.1	118.6	124.2	129.2	133.7
V_o (mV)	645	599	555	495	434	371
V_1	638	573	530	470	416	354
V_2	620	558	511	453	398	338
V_3	578	514	465	413	357	299
$V_o (P_o)$ (mV)	562	516	470	410	350	291
$V_1 (P_1)$	532	483	441	382	330	272
$V_2 (P_2)$	519	468	423	366	311	254
$V_3 (P_3)$	479	427	377	328	263	214
FF_o	.824	.808	.788	.756	.722	.671
FF_1	.791	.792	.774	.739	.705	.647
FF_2	.792	.788	.768	.735	.693	.636
FF_3	.775	.773	.746	.714	.635	.603

$$X_o/\emptyset = 0$$

$$X_2/\emptyset = 1 \times 10^{15}$$

$$X_1/\emptyset = 3 \times 10^{14}$$

$$X_3/\emptyset = 1 \times 10^{16}$$

TABLE 21

HESP HYBRID TYPE 3 .20 MM 2 OHM-CM P+

ELECTRICAL CHARACTERISTICS AS A FUNCTION OF TEMPERATURE AND ELECTRON FLUENCE

	-20	+5	+25	+50	+75	+100
P ₀ (mW)	91.2	84.9	78.9	70.9	63.0	54.9
P ₁	71.7	66.4	61.3	55.9	49.6	43.1
P ₂	62.8	58.3	53.1	49.2	43.5	37.8
P ₃ *	44.3	41.5	40.1	35.4	31.3	26.4
I ₀ (mA)	159.9	162.3	163.8	165.3	166.7	168.4
I ₁	131.8	136.9	139.7	143.8	148.5	152.9
I ₂	120.9	124.9	128.1	133.1	137.5	142.2
I ₃ *	94.4	98.0	106.8	108.7	115.2	120.9
V ₀ (mV)	703	652	610	559	508	457
V ₁	670	605	558	508	451	401
V ₂	642	586	534	487	433	381
V ₃ *	595	541	490	441	385	330
V ₀ (P ₀) (mV)	618	566	524	469	419	367
V ₁ (P ₁)	590	526	478	424	369	320
V ₂ (P ₂)	564	506	454	407	352	299
V ₃ (P ₃) *	515	462	411	360	308	258
FF ₀	.812	.802	.790	.767	.744	.713
FF ₁	.812	.802	.786	.766	.740	.704
FF ₂	.809	.796	.776	.759	.732	.697
FF ₃ *	.789	.783	.766	.738	.706	.662

*9 samples

$$X_0/\emptyset = 0 \quad X_2/\emptyset = 1 \times 10^{15}$$

$$X_1/\emptyset = 3 \times 10^{14} \quad X_3/\emptyset = 1 \times 10^{16}$$

TABLE 22

HESP HYBRID TYPE 4 .20 MM 10 OHM-CM P+

ELECTRICAL CHARACTERISTICS AS A FUNCTION OF TEMPERATURE AND ELECTRON FLUENCE

	-20	+5	+25	+50	+75	+100
P_o (mW)	93.5	85.8	79.0	70.5	62.5	53.7
P_1	72.4	66.6	62.0	56.2	49.3	41.8
P_2	64.6	59.9	54.6	49.9	43.7	36.6
P_3	47.2	45.0	42.4	37.6	32.8	26.8
I_o (mA)	164.1	166.0	167.7	168.7	170.1	171.8
I_1	138.9	144.9	149.7	154.9	159.3	163.1
I_2	128.4	134.0	139.3	144.4	148.8	152.7
I_3	105.8	112.0	120.1	124.6	129.7	134.3
V_o (mV)	696	645	602	551	503	450
V_1	637	577	531	481	429	379
V_2	619	559	508	462	411	358
V_3	566	514	465	417	368	313
$V_o (P_o)$ (mV)	609	554	510	458	410	357
$V_1 (P_1)$	562	496	448	395	348	298
$V_2 (P_2)$	541	482	428	378	331	272
$V_3 (P_3)$	485	433	385	335	288	240
FF_o	.819	.801	.783	.760	.730	.696
FF_1	.818	.797	.780	.754	.723	.676
FF_2	.813	.799	.772	.743	.715	.669
FF_3	.788	.781	.756	.724	.688	.636

$$\begin{array}{ll}
 X_o/\emptyset = 0 & X_2/\emptyset = 1 \times 10^{15} \\
 X_1/\emptyset = 3 \times 10^{14} & X_3/\emptyset = 1 \times 10^{16}
 \end{array}$$

TABLE 23

HESP HYBRID TYPE 5 .20 MM 30 OHM-CM P+

ELECTRICAL CHARACTERISTICS AS A FUNCTION OF TEMPERATURE AND ELECTRON FLUENCE

	-20	+5	+25	+50	+75	+100
P_o (mW)	93.8	85.4	78.1	69.6	61.2	52.3
P_1	71.8	66.0	60.3	53.3	45.2	36.8
P_2	64.8	59.1	53.7	47.2	39.4	30.8
P_3 *	49.6	44.5	40.0	34.0	27.4	20.0
I_o (mA)	164.7	166.7	168.0	169.4	170.8	172.2
I_1	142.6	150.3	155.3	160.1	164.0	167.3
I_2	132.7	140.2	145.4	151.5	155.1	158.2
I_3 *	117.8	124.6	130.4	134.0	137.8	140.9
V_o (mV)	700	648	605	552	503	451
V_1	618	558	511	458	404	353
V_2	603	540	489	435	380	321
V_3 *	549	487	437	384	328	267
$V_o (P_o)$ (mV)	610	553	511	456	408	354
$V_1 (P_1)$	535	472	422	366	316	265
$V_2 (P_2)$	519	455	402	343	295	227
$V_3 (P_3)$ *	453	388	337	290	237	188
FF_o	.814	.790	.768	.744	.712	.673
FF_1	.815	.787	.760	.727	.682	.624
FF_2	.810	.782	.755	.720	.668	.605
FF_3 *	.768	.734	.702	.660	.605	.532

*9 samples

$$X_o/\phi = 0 \quad X_2/\phi = 1 \times 10^{15}$$

$$X_1/\phi = 3 \times 10^{14} \quad X_3/\phi = 1 \times 10^{16}$$

TABLE 24

TYPE 6 .20 MM 100 OHM-CM P+

ELECTRICAL CHARACTERISTICS AS A FUNCTION OF TEMPERATURE AND ELECTRON FLUENCE

	-20	+5	+25	+50	+75	+100
P_o (mW)	91.8	82.8	75.8	67.1	58.6	49.6
P_1	72.7	65.7	59.8	51.1	43.0	33.7
P_2	64.5	58.9	52.8	45.3	36.7	27.7
P_3						
I_o (mA)	164.4	166.2	168.1	169.7	171.2	172.8
I_1	145.9	152.9	158.1	162.0	165.8	168.1
I_2	135.8	144.9	149.2	154.7	157.7	160.0
I_3						
V_o (mV)	691	638	595	542	492	437
V_1	615	553	506	449	397	344
V_2	595	531	481	425	367	305
V_3						
V_o (P_o) (mV)	599	541	497	444	393	341
V_1 (P_1)	530	463	511	353	299	250
V_2 (P_2)	507	439	386	325	274	207
V_3 (P_3)						
FF_o	.809	.781	.758	.730	.696	.656
FF_1	.810	.778	.747	.702	.654	.582
FF_2	.799	.767	.736	.691	.635	.568
FF_3						
$X_o/\phi = 0$						
$X_1/\phi = 3 \times 10^{14}$						
$X_2/\phi = 1 \times 10^{15}$						
$X_3/\phi = 1 \times 10^{16}$						

TABLE 25

TYPE 7 .20 MM 2 OHM-CM

ELECTRICAL CHARACTERISTICS AS A FUNCTION OF TEMPERATURE AND ELECTRON FLUENCE

	-20	+5	+25	+50	+75	+100
P ₀ (mW)	80.4	77.2	72.7	65.6	57.5	49.5
P ₁	67.3	64.7	61.5	55.1	48.7	42.5
P ₂	58.7	56.3	53.7	48.8	42.9	36.8
P ₃ *	39.5	37.4	37.9	33.0	29.6	25.0
I ₀ (mA)	152.1	154.2	156.0	158.2	159.6	162.0
I ₁	130.7	133.9	137.8	140.8	144.4	149.8
I ₂	117.0	120.7	124.4	128.8	133.0	136.7
I ₃ *	88.2	92.0	98.2	101.8	107.2	113.3
V ₀ (mV)	665	630	591	539	485	429
V ₁	674	616	570	511	460	406
V ₂	661	599	552	498	442	387
V ₃ *	610	547	502	449	394	339
V ₀ (P ₀) (mV)	568	536	502	450	397	343
V ₁ (P ₁)	555	523	482	428	376	324
V ₂ (P ₂)	538	509	468	409	362	304
V ₃ (P ₃) *	480	436	418	355	308	260
FF ₀	.795	.795	.739	.771	.743	.711
FF ₁	.764	.784	.783	.766	.733	.699
FF ₂	.759	.779	.783	.761	.730	.696
FF ₃ *	.734	.739	.767	.717	.700	.649

*9 samples

$$X_0/\emptyset = 0 \quad X_2/\emptyset = 1 \times 10^{15}$$

$$X_1/\emptyset = 3 \times 10^{14} \quad X_3/\emptyset = 1 \times 10^{16}$$

TABLE 26

TYPE 8 .20 MM 10 OHM-CM

ELECTRICAL CHARACTERISTICS AS A FUNCTION OF TEMPERATURE AND ELECTRON FLUENCE

	-20	+5	+25	+50	+75	+100
P_o (mW)	81.1	74.4	67.6	59.5	50.1	41.1
P_1	70.2	65.5	60.6	53.5	45.6	38.2
P_2	62.5	58.6	54.3	48.6	41.9	34.3
P_3	46.2	43.7	41.4	36.5	31.2	24.6
I_o (mA)	151.5	153.5	155.5	157.9	159.0	161.3
I_1	136.1	141.3	145.4	149.6	153.9	157.2
I_2	125.6	131.4	136.0	141.5	146.5	149.7
I_3	101.9	108.5	116.1	122.3	128.2	132.7
V_o (mV)	646	597	551	494	436	373
V_1	642	580	532	473	421	362
V_2	628	562	514	460	405	345
V_3	581	518	470	415	359	300
$V_o (P_o)$ (mV)	563	515	468	510	352	292
$V_1 (P_1)$	545	494	448	390	334	285
$V_2 (P_2)$	527	480	431	374	323	261
$V_3 (P_3)$	483	433	387	330	279	226
FF_o	.830	.812	.789	.763	.724	.683
FF_1	.804	.800	.783	.756	.706	.671
FF_2	.792	.794	.778	.748	.706	.665
FF_3	.780	.777	.758	.719	.678	.618
$x_o/\phi = 0$	$x_2/\phi = 1 \times 10^{15}$					
$x_1/\phi = 3 \times 10^{14}$	$x_3/\phi = 1 \times 10^{16}$					

TABLE 27

TYPE 9 .10 MM 10 OHM-CM

ELECTRICAL CHARACTERISTICS AS A FUNCTION OF TEMPERATURE AND ELECTRON FLUENCE

	-20	+5	+25	+50	+75	+100
P_o (mW)	77.1	70.2	63.8	55.0	46.3	36.9
P_1	70.4	65.0	59.8	52.2	44.4	35.6
P_2	63.2	59.4	54.9	48.8	41.5	33.4
P_3	48.1	45.3	42.0	37.0	31.0	23.6
I_o (mA)	143.9	146.8	149.4	150.3	152.6	154.9
I_1	135.1	139.9	144.5	147.1	149.8	152.4
I_2	125.2	131.8	137.3	142.0	145.7	148.9
I_3	105.1	112.6	119.1	125.5	130.4	134.8
V_o (mV)	640	586	537	477	416	351
V_1	637	576	526	469	413	348
V_2	625	561	511	456	399	336
V_3	579	514	464	409	353	288
$V_o (P_o)$ (mV)	561	505	454	397	337	273
$V_1 (P_1)$	549	494	446	392	336	264
$V_2 (P_2)$	531	479	433	379	326	258
$V_3 (P_3)$	492	434	380	339	285	227
FF_o	.838	.816	.796	.767	.730	.679
FF_1	.818	.807	.788	.756	.719	.672
FF_2	.807	.802	.783	.753	.713	.667
FF_3	.790	.782	.760	.719	.672	.607

$$\begin{array}{ll}
 X_o/\phi = 0 & X_2/\phi = 1 \times 10^{15} \\
 X_1/\phi = 3 \times 10^{14} & X_3/\phi = 1 \times 10^{16}
 \end{array}$$

TABLE 28

TYPE 10 .10 MM 100 OHM-CM P+

ELECTRICAL CHARACTERISTICS AS A FUNCTION OF TEMPERATURE AND ELECTRON FLUENCE

	-20	+5	+25	+50	+75	+100
P_o (mW)	95.7	80.5	73.4	68.8	56.3	47.5
P_1	74.9	68.7	62.6	54.0	44.9	35.8
P_2	67.8	61.9	56.0	47.9	38.5	29.8
P_3						
I_o (mA)	156.9	160.5	162.0	162.7	165.6	168.0
I_1	148.3	155.5	159.4	161.1	163.3	164.9
I_2	140.2	149.0	153.4	156.9	158.9	161.7
I_3						
V_o (mV)	692	638	593	549	485	428
V_1	619	561	516	464	411	355
V_2	595	532	486	431	374	310
V_3						
$V_o (P_o)$ (mV)	652	542	491	438	386	333
$V_1 (P_1)$	536	475	429	375	325	258
$V_2 (P_2)$	513	445	399	349	289	218
$V_3 (P_3)$						
FF_o	.881	.786	.764	.720	.701	.661
FF_1	.816	.787	.761	.722	.669	.612
FF_2	.813	.782	.751	.708	.647	.593
FF_3						
$X_o/\phi = 0$						
$X_1/\phi = 3 \times 10^{14}$						
$X_2/\phi = 1 \times 10^{15}$						
$X_3/\phi = 1 \times 10^{16}$						

TABLE 29
TYPE 11 .10 MM 10 OHM-CM P+

ELECTRICAL CHARACTERISTICS AS A FUNCTION OF TEMPERATURE AND ELECTRON FLUENCE

	-20	+5	+25	+50	+75	+100
P ₀ (mW)	98.4	83.1	76.0	67.2	59.1	50.4
P ₁	74.5	68.8	64.1	57.6	50.4	42.2
P ₂	65.7	60.8	56.5	51.0	43.9	36.3
P ₃	49.8	46.3	42.9	38.1	31.9	25.0
I ₀ (mA)	158.0	160.4	161.6	162.1	164.5	166.9
I ₁	140.5	145.9	152.2	156.2	160.1	162.5
I ₂	128.4	135.6	141.2	147.5	151.1	155.9
I ₃	107.3	115.4	122.1	127.9	132.6	137.5
V ₀ (mV)	702	644	599	545	492	435
V ₁	642	581	536	486	435	380
V ₂	620	560	512	460	407	349
V ₃	575	511	464	410	354	291
V ₀ (P ₀) (mV)	669	556	508	454	401	344
V ₁ (P ₁)	563	499	452	400	350	294
V ₂ (P ₂)	544	480	434	380	326	269
V ₃ (P ₃)	497	434	381	330	281	220
FF ₀	.888	.804	.786	.761	.731	.694
FF ₁	.826	.807	.786	.759	.724	.683
FF ₂	.825	.801	.782	.752	.714	.667
FF ₃	.807	.786	.758	.725	.681	.624

$$\begin{array}{ll}
 X_0/\emptyset = 0 & X_2/\emptyset = 1 \times 10^{15} \\
 X_1/\emptyset = 3 \times 10^{14} & X_3/\emptyset = 1 \times 10^{16}
 \end{array}$$

A number of observations were made while accumulating this information which are worthy of some comment. After irradiating the cell matrix to $3 \times 10^{14} \text{ e/cm}^2$, an anomalous effect involving the open circuit voltage and curve fill factor of many cell types was noted. At measurement temperatures of -20°C and in some cases at $+5^\circ\text{C}$ the open circuit voltage showed little or no change after irradiation. In fact some cells actually had higher values of V_{oc} . In addition the curve fill factor of the cell degraded substantially, showing evidence of increased series resistance. These effects were only observed in cells which did not have a back surface field.

There is evidence in the literature stating that at very low temperatures and low levels of light intensity silicon solar cells show this effect because of a non-ohmic condition in the back contact termed the Schottky-barrier defect.⁽⁷⁾ However there has been little data reported on the effect of radiation on the low temperature performance of silicon solar cells. Of interest, this effect seems to be either reduced or totally eliminated as the cells are subjected to increased fluences of electrons. The impact of this phenomenon on the temperature coefficient of open circuit voltage is significant. The change in voltage with temperature is not linear over the range investigated in this program.

Curve fill factor data as a function of temperature is also influenced by this radiation induced phenomenon. The general trend of fill factor data shows a decreasing fill factor with increasing temperature and increasing electron fluence. This trend is not always obeyed in those nonfield cell groups that exhibit the Schottky barrier defect after radiation. Above $+5^\circ\text{C}$ the fill factor trend for all cell groups is fairly well behaved.

The temperature coefficient of short circuit current is significantly changed after exposure to electrons, increasing by a factor of from two to four after $1 \times 10^{16} \text{ e/cm}^2$. The majority of this increase occurs at or before a fluence of $3 \times 10^{14} \text{ e/cm}^2$. There is a variation in temperature coefficient between

field and nonfield cells, but a precise analysis has not been done due to the complicated nature of the mathematical function relating these two variables.

The effect of electron radiation on the various cell types indicates that the use of back surface fields can yield devices with superior post irradiation electrical performance if the thickness and bulk resistivity are properly chosen. At 25°C the type 11 hybrid, which is a .004", 10 ohm-cm field cell, had the highest output at all three electron fluences. The type 4 hybrid, which is an .008" 10 ohm-cm field cell, also showed well in these tests. Of even greater significance, the performance of these two cell types at elevated temperatures (75°C) was equally outstanding.

At $3 \times 10^{14} \text{ e/cm}^2$, equivalent to seven years in synchronous orbit, there was very little difference in power output at 25°C between two and ten ohm-cm cells, although the field cell versions of both resistivities were better than the nonfield types. At 75°C, which is a fairly normal operating temperature for many panels, there was a distinct difference in power output. Two ohm-cm cells and ten ohm-cm field cells delivered at least five percent more power than the nonfield ten ohm-cm cells.

In the case of $1 \times 10^{15} \text{ e/cm}^2$, at 25°C the ten ohm-cm cell types yield slightly more power than the two ohm-cm cells. However at 75°C the two ohm-cm nonfield cells are once more superior to the ten ohm-cm nonfield cells, and equivalent to the ten ohm-cm field cells. At $1 \times 10^{16} \text{ e/cm}^2$ the ten ohm-cm cells show a distinct advantage in power at 25°C, but the difference is minimal at 75°C.

The field cells made from higher than normal bulk resistivities such as 30 and 100 ohm-cm exhibited relatively poor performance to higher operating temperatures but were competitive at 25°C for fluence levels up to $1 \times 10^{15} \text{ e/cm}^2$. At $1 \times 10^{16} \text{ e/cm}^2$ the .2mm, 100 ohm-cm field cells suffered a catastrophic collapse of curve shape, making any data analysis meaningless. This is attributed to a nearly complete loss of the field enhancement which causes the cell to revert to a normal mode of operation where its bulk resistance now adversely effects the cell curve shape.

Based on this very cursory review of the data it can be concluded that no single cell now in current production can meet all the varying requirements of thermal and radiation performance that would be considered by designers. However, the outstanding performance of the very thin silicon cell offers some hope that a "universal" cell may become available provided some further attention is given to the processing details.

2.10.5 Radiometric Properties

Twenty baseline 2 x 2 cm HESP assemblies as well as a representative sample of HESP hybrid cells were delivered to the TRW Defense and Space Systems Group for measurements of their thermal properties. The data obtained from this test included spectral directional reflectance at wavelengths from 0.29 to 2.5 microns and total infrared reflectance for all samples. The spectral directional reflectance of a subgroup of cells (10 samples) was obtained over the region between 2.0 and 26 microns.

The spectral directional reflectance of all samples was measured using a Beckman DK2A Spectrophotometer with an Edwards-type integrating sphere reflectometer. This information was then numerically integrated over the Thekaekara (air mass zero) solar spectrum to yield values of solar reflectance, $\bar{\rho}_s$. Subtraction of solar reflectance values from unity yielded values of solar absorptance, $\bar{\alpha}_s$.

The spectral reflectance of the subgroup was measured in the wavelength region 2.0 to 26 microns using a Gier Dunkle Heated Cavity Reflectometer. These results were then numerically integrated over the Planckian (80°F) black body emission spectrum to yield the total reflectance of the cells to a room temperature black body source. Subtraction of these values from unity provided values of the absorptance of the cells to energy from a room temperature black body source which is equal to the normal emittance of the cells at room temperature.

The total infrared reflectance was measured using a Gier Dunkle Model DB100 Infrared Reflectometer. Subtraction of these reflectance values from unity yielded values of normal room temperature emittance. Values of hemispherical emittance was determined from the normal emittance using theoretically and empirically derived correlations. (8)

Table 30 is a summary of the data obtained for the 2 x 2 cm HESP baseline assemblies. It can be seen that the thermal properties of this group are extremely uniform. The B test column indicates a special measurement made using a heated cavity absolute reflectometer. Table 31 provides the thermal properties of the HESP hybrid assemblies. Since Types 9 through 11 were not filtered, meaningful information can be presented.

The hybrid cell data shows that with one exception, the Type 1R assemblies, there is no significant difference in absorptance or emittance for the various hybrid types. The 1R assemblies show a reduction in absorptance which is attributable to the use of a thin layer of aluminum at the rear surface of the cell. This acts to reflect long wavelength light back out through the front surface of the cell, rather than allowing it to be absorbed at the back contact. The emittance values are determined by the coverglass properties, since all assemblies used fused silica coverglass there was no significant difference observed in emittance from group to group.

TABLE 30

SOLAR ABSORPTANCE AND EMITTANCE OF HESP ASSEMBLIES

<u>Cell</u>	<u>Absorptance</u>	<u>Normal Emittance</u>		<u>Hemispherical Emittance</u>	
		A	B	A	B
1	.946	.819	.808	.786	.776
2	.945	.818	-	.785	-
3	.946	.816	-	.783	-
4	.946	.817	-	.784	-
5	.946	.815	-	.781	-
6	.948	.817	-	.789	-
7	.948	.817	-	.784	-
8	.945	.818	-	.785	-
9	.948	.820	-	.787	-
10	.944	.820	-	.787	-
11	.947	.816	-	.783	-
12	.944	.820	-	.787	-
13	.948	.818	-	.785	-
14	.948	.816	-	.783	-
15	.948	.815	-	.782	-
16	.948	.814	-	.781	-
17	.945	.817	-	.784	-
18	.947	.818	-	.788	-
19	.948	.816	-	.783	-
20	.946	.815	-	.782	-

TABLE 31

SOLAR ABSORPTANCE AND EMITTANCE OF HESP HYBRID ASSEMBLIES

<u>Cell Type</u>	<u>Absorptance</u>	<u>Normal Emittance</u>		<u>Hemispherical Emittance</u>	
		A	B	A	B
1	.949	.817	.806	.784	.774
	.948	.817		.784	
	.947	.814		.780	
	.947	.817		.784	
	.947	.810		.778	
1 (R)	.925	.813	.794	.780	.762
	.920	.820		.787	
	.925	.820		.787	
	.928	.819		.786	
	.929	.817		.784	
2	.950	.817	.795	.784	.763
	.950	.818		.785	
	.949	.819		.786	
	.946	.821		.788	
	.946	.820		.787	
3	.947	.820	.795	.787	.763
	.949	.821		.788	
	.946	.819		.786	
	.945	.819		.786	
	.945	.818		.785	
4	.947	.816	.802	.783	.770
	.949	.817		.784	
	.950	.819		.786	
	.949	.820		.787	
	.948	.817		.784	

TABLE 31

(Cont'd)

SOLAR ABSORPTANCE AND EMITTANCE OF HESP HYBRID ASSEMBLIES

<u>Cell Type</u>	<u>Absorptance</u>	<u>Normal Emittance</u>		<u>Hemispherical Emittance</u>	
		A	B	A	B
5	.951	.816		.783	
	.949	.820		.787	
	.944	.817		.784	
	.945	.818		.785	
	.948	.821		.788	
6	.946	.820	.802	.787	.770
	.948	.816		.783	
	.945	.817		.784	
	.947	.818		.785	
	.947	.816		.783	
7	.942	.818		.785	
	.947	.821	.798	.788	.766
	.946	.822		.789	
	.949	.818		.785	
	.947	.820		.787	
8	.947	.817		.784	
	.947	.816		.783	
	.949	.820		.787	
	.948	.820		.787	
	.944	.817		.784	

3.0 CONCLUSIONS

As a result of this program there now exists a family of cell types which offer extremely high initial AMO conversion efficiencies (greater than 14.0 percent) and in many cases superior radiation (neutron and electron) resistance. These cell types basically divide into shallow junction only and back surface field designations. Cells as thin as .004" have been successfully fabricated in a manufacturing environment with acceptable (greater than 50 percent) yields.

The baseline HESP cell which incorporates a shallow junction, a selectively etched surface, a new contact system and a high index AR coating (Ta_2O_5) was produced in three configurations (2 x 2, 2 x 4 and 2 x 6 cm) under formal documentation and control. This demonstrates that the HESP cell is now ready for full scale production as a power source for future Air Force missions. In addition to the baseline HESP cell, there were eleven other cell types which also were manufactured under basically the same conditions. Of these, at least six are now ready for full scale production in either 2 x 2 or 2 x 4 cm configuration. Two other types (.004" and .004" P+) show great promise and hopefully more work will be done in the future to bring them to production ready status.

It was demonstrated conclusively that the HESP cell could be interconnected by parallel gap resistance welding provided the proper interconnect material, in this case silver, was used. Reliable, high strength bonds could be formed in routine fashion with minimal effect (< 0.5 percent) on the electrical output of the cell.

The results of the formal qualification tests indicate that this cell is capable of meeting the rigorous requirements for space qualification. Although the thermal cycling test results were negative, an analysis of the test failure showed that an improperly designed interconnect, and not anything in the cell construction, was responsible for this problem.

The radiation testing phase showed that low resistivity (2 ohm-cm) float zone silicon was susceptible to photon redegradation and thus crucible grown silicon was used for the HESP cells. Almost every type of HESP cell met or exceeded the neutron radiation goals of this program which was quite surprising. The electron radiation goals were nearly achieved by the Type 11 HESP hybrid device, a .004" 10 ohm-cm BSF cell. The remaining cell types failed to meet the goals by no more than ten percent, a good performance considering that float zone silicon could not be used.

A large body of data concerning the radiometric properties of these cells was accumulated. Temperature coefficient data as a function of electron fluence was also obtained. This is perhaps the most complete characterization of the latest state-of-the-art cells that has ever been done.

Although significant progress was made in developing a space qualified high efficiency cell, there are still many aspects of both cell and cell related technology that could be optimized. We feel that it is possible to develop space qualified cells that will deliver better than 21 mW/cm^2 and which can be mass produced using existing production equipment.

Although the presently available low resistivity float zone silicon is not suitable for use on space flight programs, it is possible that higher resistivity (ten ohm-cm) will not show the photon redegradation effect. There is information which indicates that using an acceptor dopant other than boron will eliminate the redegradation problem. If this is true it may be possible to gain additional end-of-life power by using either alternately doped or higher resistivity float zone silicon. This should be investigated.

The present HESP cell probably is optimized with respect to junction and selective etching technology and future work in these areas will probably yield very little improvement in cell output. The present contact configuration does offer potential for improvement in both cell output and reliability. We would strongly recommend a serious effort aimed at using a weld pad configuration coupled with complete coverage of the front surface of the cell by the protective filter after the front surface interconnects have been made.

The junction contact of tantalum-palladium-silver is quite satisfactory, but the observation that a low temperature barrier defect can be formed at the rear contact after exposure to electron radiation argues for further work on the back contact metallization system. One combination that would probably be suitable for welding is the aluminum-silver system. The tantalum based front contact offers a unique situation which would allow an "in situ" AR coating to be deposited which would probably possess superior optical

properties (refractive index and transmission) to the present electron beam deposited coating. This activity should be pursued.

The results of the thermal cycling test point out another area of technology that could benefit from further work, namely interconnect design. The silver mesh interconnect should be designed so that it incorporates a stress relieving loop. This new design should be rigorously evaluated using vacuum thermal cycling.

Our experience in filtering the HESP cells indicates that the conventional method of bonding and especially cleaning the excess adhesive from the cell should be re-evaluated. The textured surface of this cell is extremely sensitive to handling and electrical degradation in the order of 1 to 2 percent can easily occur. Improvements in the filtering process would eliminate these losses, thus providing additional power.

The outstanding performance of the thin (.004) back surface field cells in both initial and end-of-life power output warrants further development. We are not at all certain that the field process has been optimized and further work might yield a significant increase in output power. The peripheral technology for these cells, such as welding and filtering techniques should also be developed. Another potentially fruitful area would be to investigate the implementation of a back reflector which should act to both increase output and lower the absorptivity of the textured cell.

REFERENCES

1. R. L. Statler, Proc. 1968 IECEC, p. 122 (1968)
2. R. L. Statler, Proc. Int. Conf. on Photovoltaic Power Generation, Hamburg, Germany, p. 369 (1974)
3. J. R. Carter and H. V. Tada, Solar Cell Radiation Handbook, JPL Contract 953362, p. 3-35, (1973)
4. D. J. Curtin and R. W. Cool, Proc. Int. Conf. on Photovoltaic Power Generation, Hamburg, Germany, p. 32, (1974)
5. R. L. Crabb, Proc. Ninth IEEE Photovoltaic Specialists Conf., Silver Spring, Maryland, p. 329, (1972)
6. K. N. Tau, App. Phys. Lttrs, 27, p. 221 (1975)
7. P. A. Payne and E. L. Ralph, Proc. Eighth IEEE Photovoltaic Specialists Conf., Seattle, Wash. p. 135 (1970)
8. E. R. G. Eckert and R. M. Drake, Jr., Heat and Mass Transfer, 2nd Edition, Mc Graw-Hill Book Company, Inc., New York (1959)

SPECIFICATION SHEET
TYPE-D HESP PHASE I SILICON SOLAR CELL ASSEMBLY

1.0 SCOPE

1.1 This specification sheet covers all quantitative parameters referenced by the General Specification for Silicon Solar Cell Assemblies for HESP Type weldable silicon solar cell assemblies to be used for space flight.

2.0 REQUIREMENTS

2.1 Materials (3.2.2)

2.1.1 Silicon: Boron doped, single crystal p-type with resistivity between 1 and 3 ohm-cm. Crystal orientation 100 side for front etched surface.

2.1.2 Contact Materials: Top contact evaporated TaPdAg, back contact evaporated Cr(Pd)Ag.

2.1.3 Anti-Reflection Coating: Tantalum pentoxide (Ta_2O_5).

2.1.4 Coverglass Adhesive: General Electric R63-489.

2.1.5 Coverglass: Corning Glassworks 7940 fused silica with 350 nm cut-on filter in accordance with OCLI SPEC #6024000-03.

2.2 Contact Thickness, Surface Finish, and Critical Areas (3.3.5.1)

2.2.1 Contact Thickness: The thickness of the contact system required in 2.1.2 shall be no less than 4 μm in the designated areas shown in attached figure.

2.2.2 Surface Finish: Not applicable

2.2.3 Critical Areas: Critical areas are as shown in the attached figure.

2.3 Dimensions and Weight (3.3.3): Assembly dimensions shall be as shown in the attached figure. The assembly weight shall not exceed 52 gm/100 cells for 2 x 2 cm cells, 104 gm/100 cells for 2 x 4 cm cells or 156 gm/100 cells for 2 x 6 cells.

2.4 Electrical Output (3.4.1): The minimum cell current and lot minimum average current measured at 500 mV shall be as follows:

<u>CELL SIZE</u>	<u>MINIMUM I MA GROUP</u>	<u>MINIMUM I MA AVERAGE</u>
2 x 2 cm	136 - 138	150
2 x 4 cm	272 - 276	300
2 x 6 cm	408 - 414	450

Assemblies shall be sorted into groups according to current output differentiated by $.5 \text{ ma/cm}^2$ current categories for all configurations.

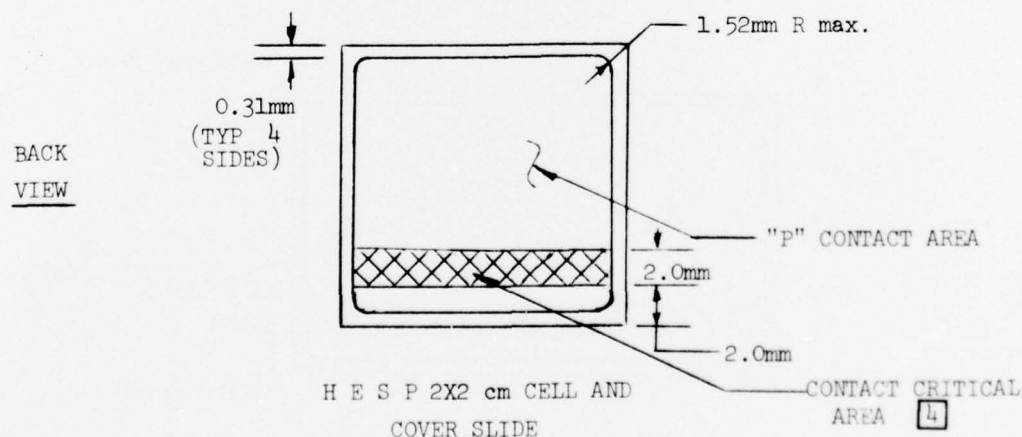
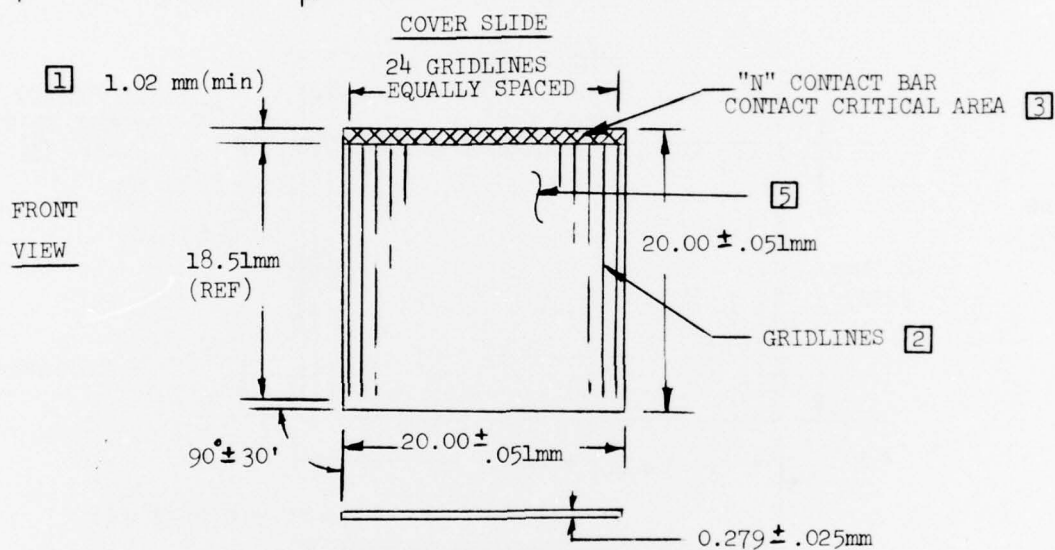
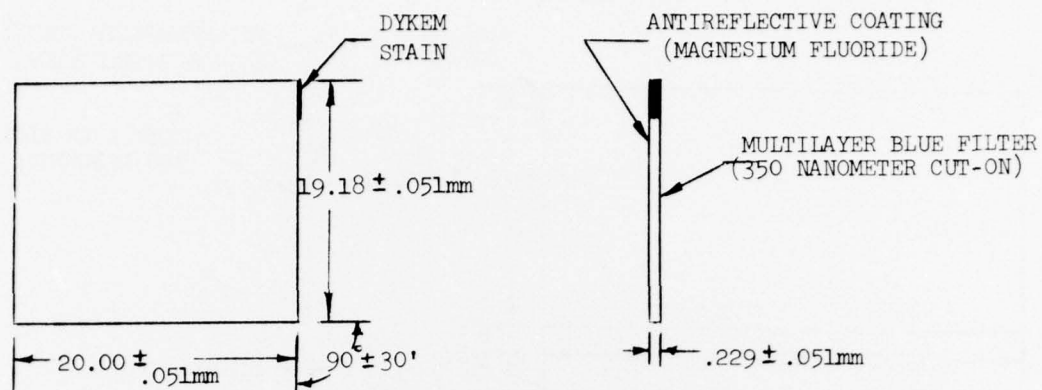
2.5 Temperature Cycling (3.4.4): Cycling shall be done in a vacuum of 10^{-4} Torr or lower. Two hundred and fifty cycles between -190°C and $+150^{\circ}\text{C}$ at a maximum rate of 25°C per minute. Assemblies to dwell at -190°C and $+150^{\circ}\text{C}$ for a minimum of 10 minutes.

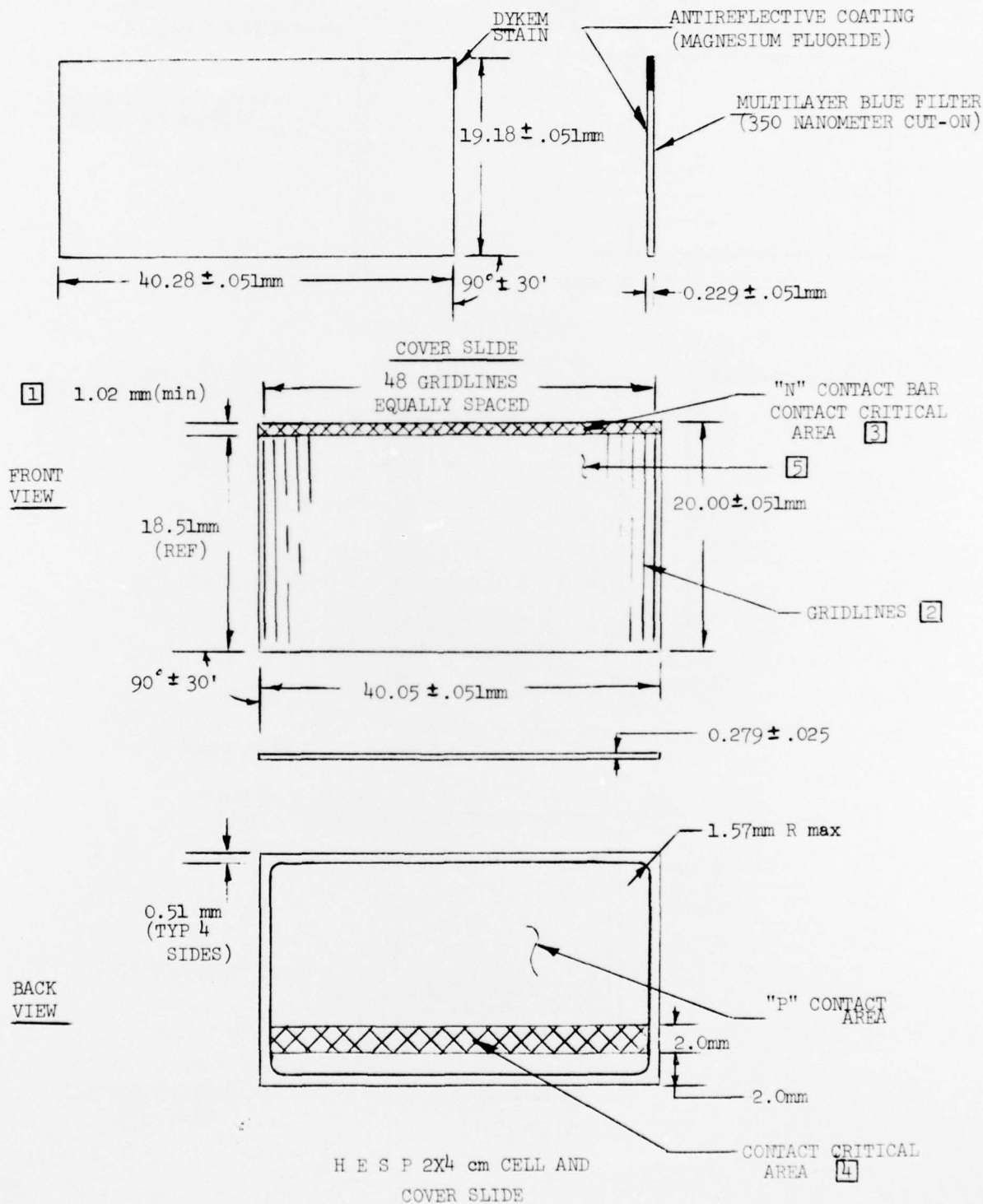
2.6 Charged Particle Radiation Resistance (3.4.6): The average output of these assemblies when exposed to a normal incident particle fluence of 1×10^{15} 1 MeV electrons/cm² shall be as follows at 455 mV.

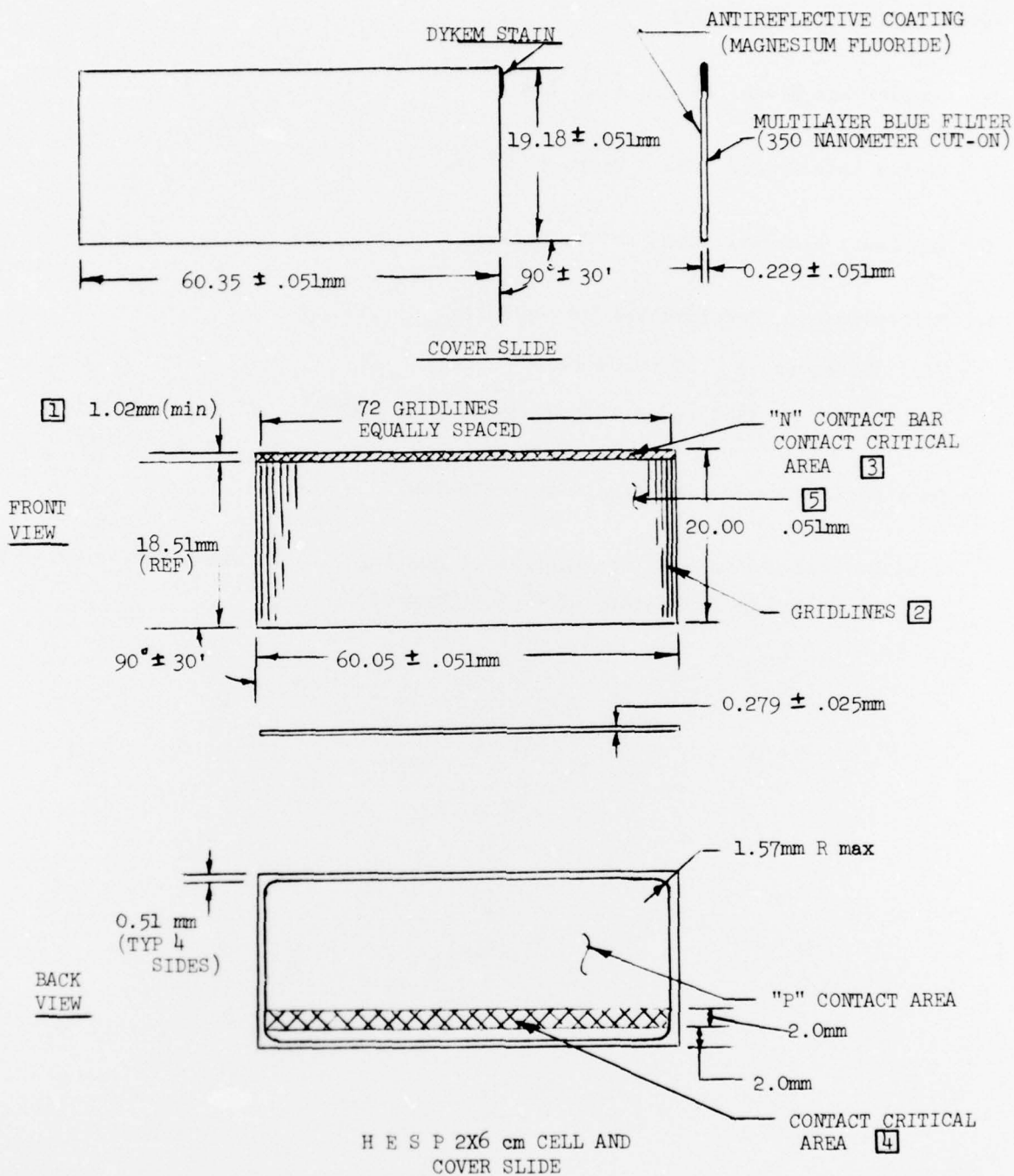
2 x 2 cm cell, 120 mA
2 x 4 cm cell, 240 mA
2 x 6 cm cell, 360 mA

2.6.1 Particle Irradiation (4.5.11): After the irradiation of 2.6, the assemblies shall be stored at room temperature ($15-30^{\circ}\text{C}$) for at least 6 days before final electrical testing.

2.7 Identification of Product (3.3.2): No marking required.







NOTES: (HESP 2 x 2 cm CELL)

1. Contact Bar Width = $1.0 \pm \begin{smallmatrix} .1 \\ 0 \end{smallmatrix}$ mm.

2. Twelve (12) Grids/ cm Width = .04 mm.

3. Top Contact Metalization = Ta(Pd)Ag.

4. Bottom Contact Metalization = Cr(Pd)Ag.

Cell Thickness = $.28 \pm .02$ mm.

Coverglass = 7940 Fused Silica with 350 nm cut-on; $.23 \pm .02$ mm thick.

5. Anti-Reflective Coating (Tantalum Pentoxide).

6. Finished Assemblies Shall be Capable of Seating Flat Within a Cavity 20.45 mm x 20.45 mm and an Angularity of $0^{\circ} \pm 2$ Minutes.